PilotSTRATEGY

Deliverable 2.10

Report of Reactive Transport Modelling for 3 Areas

Release Status:

Author: Frédéric Mathurin, Patrícia Moita, Andrew Kilpatrick, Paula Afonso, Mário Abel Gonçalves, Carlos Ribeiro, Júlio Carneiro & Sylvain Stephant

Edited by Mark Wilkinson

Date: February 2026
Filename and Version: PilotSTRATEGY D2.10 v1
Project ID Number: 101022664

PilotSTRATEGY (H2020- Topic LC-SC3-NZE-6-2020 - RIA)

1. Document History

1.1 Location

This document is stored in the following location:

Filename	PilotSTRATEGY D2.10 v1
Location	

1.2 Revision History

This document has been through the following revisions:

Version No.	Revision Date	Filename/Location stored:	Brief Summary of Changes

1.3 Authorisation

This document requires the following approvals:

AUTHORISATION	Name	Signature	Date
WP Leader	Mark Wilkinson	MW	26 February 2026
Project Coordinator	Isaline Gravaud	IG	27 February 2026

1.4 Distribution

This document has been distributed to:

Name	Title	Version Issued	Date of Issue
Public		V1	27/02/2026

The PilotSTRATEGY project has received funding from the European Union's Horizon 2020 research and innovation programme under grant agreement No. 101022664

Mathurin F., Moita P., Kilpatrick A., Afonso P., Abel Gonçalves M., Ribeiro C., Carneiro J., Stephant S., 2026. Report of Reactive Transport Modelling for 3 Areas. Deliverable D2.10. EU H2020 PilotSTRATEGY project 101022664, report, pp86

Disclaimer

The information and views set out in this report are those of the author(s) and do not necessarily reflect the official opinion of the European Union. Neither the European Union institutions and bodies nor any person acting on their behalf may be held responsible for the use which may be made of the information contained therein.

The PilotSTRATEGY project has received funding from the European Union's Horizon 2020 research and innovation programme under grant agreement No. 101022664

2. Executive summary

As part of the PilotSTRATEGY project batch reaction experiments were carried out on reservoir and caprock samples from target sites in France, Portugal, and Spain, as reported in PilotSTRATEGY Deliverable 2.9. The original experiments were undertaken to assess the reactions likely to occur when the rocks were exposed to dissolved CO_2 during storage operations at realistic temperatures and pressures. The rocks include clastic sediments (sandstones, shales) and carbonates (limestones, marls). For this report, modelling was undertaken both to check the reliability in using such modelling to predict the reaction in multi-mineral systems and to clarify the reactions taking place within the experiments and hence in CO_2 storage sites.

For the clastic rocks, the results highlighted the generally low levels of reactivity between the rock samples and the brines carrying dissolved CO_2. The only notable reaction observed was the dissolution of minor primary carbonate, with minimal dissolution of silicates/aluminosilicates and other minerals, and little evidence for secondary precipitation to a degree which might have a meaningful impact on reservoir properties, i.e. porosity and permeability. For the carbonates, the reactions were dominated by the dissolution and precipitation of carbonate minerals (calcite, dolomite, ankerite) and the dissolution of gypsum.

In all cases where carbonate minerals were present, the modelling reliably predicted the significant and rapid dissolution of these minerals. All models overpredicted the release of calcium compared to the experiments. It may be that reactive surface area was more limited than assumed or that reactions were limited by transport, although the experiments were well stirred. An alternative explanation is that degassing of the samples during removal from the pressurised reaction vessels allowed CO_2 to escape, causing the precipitation of secondary calcite. This is supported by modelled versus pH measurements, with systematic differences in all experiments except for those with low (atmospheric) CO_2 pressures.

In some cases, primary minerals had to be added to the modelled experiments to supply elements that were not otherwise present in the initial rock mineralogy. For example, for the Portuguese reservoir, the presence of dolomite was modelled, although this phase had not been detected by XRD, to explain the magnesium levels in the experiments. The model results appear to support this assumption, as the predicted magnesium release was similar to that observed in the experiments, for both rate and overall magnitude.

Comparisons between modelled and experimental results for non-carbonate primary minerals are more varied. Model results appear to accurately predict the gradual release of Al and K from the feldspar present in the Spanish reservoir sample, for example, while silica release was significantly underpredicted in this model and that of the Portuguese reservoir sample experiment. Similarly, for the models of the Spanish caprock and Portuguese reservoir rock, Al release matched relatively poorly to the measured results from the experiments.

A major issue in this work (and other comparable studies) is a lack of understanding of mineral reactive surface areas and how they change over the course of time. While assumptions can be made based on geometry or likely bulk surface area, for mixed mineral systems where different phases may have a wide range of specific surface areas (i.e. surface area per weight of sample), there is significant uncertainty. This work demonstrates such discrepancies are also due to the compositional complexity

The PilotSTRATEGY project has received funding from the European Union's Horizon 2020 research and innovation programme under grant agreement No. 101022664

of such systems, where mineral phases almost never reflect the pure end-members often used as model assemblages and effects such as incongruent dissolution, adsorption and desorption processes and the reactivity of trace phases (e.g. dolomite) or impurities is very difficult to account for.

This work highlights the utility of geochemical modelling in the prediction of major chemical reactions, both in terms of magnitude and direction, for mineral assemblages subject to conditions relevant to geological sequestration of CO_2, where rapid dissolution of carbonates and longer-term dissolution of some aluminosilicate phases were modelled with reasonable accuracy. However, in detail, the results also highlight some of the shortcomings and issues when applying such models to complex mixed mineral systems.

The PilotSTRATEGY project has received funding from the European Union's Horizon 2020 research and innovation programme under grant agreement No. 101022664

Table of Contents

The PilotSTRATEGY project has received funding from the European Union's Horizon 2020 research and innovation programme under grant agreement No. 101022664

The PilotSTRATEGY project has received funding from the European Union's Horizon 2020 research and innovation programme under grant agreement No. 101022664

3. Introduction

As part of the PilotSTRATEGY project batch reaction experiments were carried out on reservoir and caprock samples from target sites in France, Portugal, and Spain, as reported on as part of Deliverable 2.9. This report describes geochemical modelling undertaken using the aqueous geochemical modelling software PHREEQC (Parkhurst and Appelo, 2013) which enables the simulation of complex interactions between dissolved gases, aqueous solutions, and mineral assemblages in a batch configuration.

The models incorporated detailed aqueous speciation, mineral assemblages, and kinetic rate laws derived from Transition State Theory following Palandri and Kharaka (2004) for France and Spain, with kinetic parameters accounting for pH-dependent effects on dissolution rates sourced mostly from Palandri and Kharaka (2004). The Portuguese modelling uses only the rates available in the PHREEQC.dat database.

The objective of the modelling was not to apply the experimental results to a full-scale reactive transport reservoir model (reservoir modelling will be carried out as part of WP3, Simulation, of the PilotSTRATEGY project) but to:

a) Better understand the experimental results and confirm the likely reactions occurring;
b) To provide important context for the experimental results such that their relevance to full scale systems can be better understood.

This report will outline the modelling approach and conceptualisation taken and present the results. The modelling files used are provided in the supplementary material.

The PilotSTRATEGY project has received funding from the European Union's Horizon 2020 research and innovation programme under grant agreement No. 101022664

4. Portugal

4.1 Model conceptualisation and set-up

4.1.1 Equilibrium Model of Experiments: Caprocks

The simulations carried out in PHREEQC (Parkhurst and Appelo, 2013), using the PHREEQC.dat database, aimed to reproduce the experimental results obtained by the University of Edinburgh (UEDIN), investigating the interaction between a brine and Portuguese cap rock (CD-DARN-15) under CO_2 over-pressure.

Modelling was carried out on a single sample from the caprock. The particular sample, essentially composed of quartz (SiO_2) and calcite ($CaCO_3$), was modelled using dissolution kinetics in order to assess its reactivity over the experimental period. The mineralogical composition of the caprock sample was previously determined by X-ray diffraction (XRD), and the proportion of each phase was used to calculate the initial amount, in moles, of each mineral in the model. Quartz and calcite were designated as the main reactive phases, representing 12.7% (0.0105 moles) and 87.3% (0.0435 moles) of the total mass of 5g of the sample, respectively.

The brine used in the experiment was a NaCl solution with a salinity of 55.6 g/L. This was subjected to a period of pre-equilibration with the caprock material, prior to the addition of CO_2 to the experiment. The chemical composition of the solution fluid was measured (Table 4.1) before the introduction of CO_2 and used as the initial condition in the PHREEQC model. For the simulation, 158.25 mL of brine were added at a temperature of 40°C. For the control simulation with N_2, the initial chemical composition of the fluid is shown in Table 4.2.

For the caprock model, the presence of dolomite ($CaMg(CO_3)_2$) was assumed as an equilibrium phase in the solution, implying that it would be dissolved until thermodynamic equilibrium with the system is reached, since the experimental data indicates the release of magnesium (Mg) into the solution over time.

CO_2 was injected into the reactor on the 14th day of the experiment, immediately following collection of a fluid sample. CO_2 was assumed to behave as an ideal gas, and added to the simulation at a temperature of 40°C and a pressure of 100 bar, in order to maintain consistency with the experimental work. To reproduce the experimentally measured pH values, it was necessary to simulate a decompression step and partial loss of CO_2 during sampling and pH measurement. Although this approach does not represent a state of strict physical equilibrium with either the reactor conditions or the atmosphere, it allows us to approximate the chemical state of the solution at the actual moment of measurement, which is strongly conditioned by the kinetics of CO_2 degassing.

The PilotSTRATEGY project has received funding from the European Union's Horizon 2020 research and innovation programme under grant agreement No. 101022664

Properties	Fluid characteristics	Unit
Gas	CO_2	-
Temperature	40	°C
pH	6.67	-
pe	-0.935	-
Density	1	g/cm³
Water mass	0.15825	kg
Al	0.260	
Ba	0.020	
Ca	27.564	
Cu	0.090	
Fe	2.055	

Table 4.1: Chemical composition of the injected solution fluid used as input in the CO2 cap rock simulation.

Properties	Fluid characteristics	Unit
Gas	N_2	-
Temperature	40	°C
pH	9.25	-
pe	2.625	-
Density	1	g/cm³
Water mass	0.176	kg
Al	0.355	
Ba	0.002	
Ca	24.731	
Fe	0	
K	5.629	
Li	0.0160	ppm
Mg	0.455	
Na	20046.914	
S	5.689	
Si	0.773	
Sr	0.198	

Table 4.2: Chemical composition of the injected solution fluid used as input in the N2 cap rock simulation.

4.1.2 Equilibrium Model of Experiments: Reservoir rocks

Two experiments carried out using a Portuguese reservoir sample (CD-CRR-10) were also modelled, again using the PHREEQC.dat database. The mineralogical composition of the sample from the reservoir sample was determined by XRD and includes predominantly quartz (SiO_2), representing 91.1% (0.0758 moles) and potassium feldspar ($KAlSi_3O_8$) with 8.9% (0.0016 moles) of the total mass of 5 g of sample, and the proportion of each phase was used to calculate the initial amount in moles of each mineral. The presence of 0.5% calcite ($CaCO_3$) was also assumed, corresponding to 0.00025 moles. Although calcite had not been detected in the XRD analysis, this addition is required to fit the modelled to the experimental results. As XRD has a detection limit of c. 2%, the existence of calcite below this value is perfectly possible.

As for the caprock experiment, the chemical composition of the brine was measured (Table 4.4) before the introduction of CO_2 and used as the initial condition in PHREEQC, with a brine volume of 168.95 mL at a temperature of 40°C. In the control system with N_2, the brine had a volume of 174.55 mL and composition in Table 4.4.

The PilotSTRATEGY project has received funding from the European Union's Horizon 2020 research and innovation programme under grant agreement No. 101022664

Properties	Fluid characteristics	Unit
Gas	CO_2	-
Temperature	40	°C
pH	7.44	-
pe	3.513	-
Density	1	g/cm³
Water mass	0.16895	kg
Al	0.252	ppm
Ba	0.074	
Ca	25.941	
Cd	0.002	
Cu	0.030	
Fe	0.120	
K	25.520	
Li	0.009	
Mg	1.320	
Mn	0.032	
Na	21812.988	
P	0.058	
S	6.664	
Si	2.288	
Sr	0.257	
Zn	0.003	

Table 4.3: Chemical composition of the solution fluid used as input for the CO2-reservoir rock simulation

Properties	Fluid characteristics	Unit
Gas	N_2	-
Temperature	40	°C
pH	6.9	-
pe	3.764	-
Density	1	g/cm³
Water mass	0.17455	kg
Al	3.3635	ppm
Ba	0.192	
Ca	23.473	
Cr	2.951	
Fe	20.804	
K	25.919	
Li	0.026	
Mg	4.256	
Mn	0.414	
Na	22339.012	
S	6.063	
Si	16.110	
Sr	0.343	
Zn	0.043	

Table 4.4: Chemical composition of the solution fluid used as input for the Nitrogen-reservoir rock simulation

For the simulation of the system with CO_2 from the reservoir sample, the presence of dolomite ($CaMg(CO_3)_2$) was assumed as an equilibrium phase in the solution, which allowed it to dissolve according to the thermodynamic conditions of the system, since the experimental results indicated the release of Mg into the solution in this system. However, this equilibrium phase was not included in the model of the control system with N_2, as the experimental results did not indicate the need for it.

Similar to the experimental conditions of the caprock sample, the CO_2 injection parameters of pressure and temperature were maintained. A decompression stage associated with partial CO_2 loss during sampling was also considered in order to approximate the chemical state of the brine at the actual time of measurement. This approach does not aim to reproduce a strict physical equilibrium state, but rather to capture the effect of CO_2 degassing on the pH values and chemical composition observed experimentally during sampling.

4.1.3 Incorporation of kinetics

The default rate equations available for quartz, calcite, and K-feldspar in the phreeqc.dat database were used, though dolomite is not included. For quartz, the dissolution rate was corrected according to the salinity of the fluid used, bearing in mind that the PHREEQC limits this parameter to a maximum of 35 ppt, and it is calculated on the basis of the sodium concentration.

The rate equations require the specific surface area of each mineral present in the samples (Table 4.5 - caprock; Table 4.6 - reservoir). This was estimated using the recommended procedure in the PHREEQC database, by measuring the grain size of each mineral and applying a geometric formulation, assuming that minerals are spherical grains. The first step is to determine the number of moles of the

The PilotSTRATEGY project has received funding from the European Union's Horizon 2020 research and innovation programme under grant agreement No. 101022664

mineral (n) based on the density (ρ) and molecular weight (M), assuming that the particles are spherical in shape (radius r). The number of moles in a grain is given by the equation:

$$n = \frac{4\rho}{3M}\pi r^3 \quad \text{(Eq. 4.1)}$$

The specific surface area (S) is obtained by dividing the surface area of the particle by the number of moles of mineral, thus indicating the area available for reaction per quantity of mineral.

$$S = \frac{4\pi r^2}{n} \quad \text{(Eq. 4.2)}$$

The last input parameter for the modelling was the time in seconds at which the samples were collected in the experiment. Each time step used the chemical concentrations resulting from the previous step as the initial condition for the next. This step is essential for kinetic simulations, as it allows the chemical evolution of the solution over time to be calculated in a cumulative and reliable way.

Mineral	*Formula*	*Moles*	*Mineral volume fraction (in 100 %)*	*Particle size*	*Density (ρ)*	*Molar Mass (M)*
Quartz	SiO_2	0.0105	12.7	125 - 250 µm	2.65 g/cm³	60.08 g/mol
Calcite	$CaCO_3$	0.0435	87.3	125 - 250 µm	2.71 g/cm³	100.09 g/mol
Dolomite	$CaMg(CO_3)_2$	-	-	-		

Table 4.5: Mineral phases of the caprock sample used as input for modelling.

Mineral	*Formula*	*Moles*	*Mineral volume Fraction (in 100 %)*	*Particle size*	*Density (ρ)*	*Molar Mass (M)*
K-feldspar	$KAlSi_3O_8$	0.0016	8.9	125 - 250 µm	2,56 g/cm³	278,33 g/mol
Quartz	SiO_2	0.0758	91.1	125 - 250 µm	2.65 g/cm³	60.08 g/mol
Calcite	$CaCO_3$	0.00025	0.5	125 - 250 µm	2.71 g/cm³	100.09 g/mol
Dolomite	$CaMg(CO_3)_2$	-	-	-		

Table 4.6: Mineral phases of the reservoir rock used as input for the modelling

The PilotSTRATEGY project has received funding from the European Union's Horizon 2020 research and innovation programme under grant agreement No. 101022664

4.2 Results

4.2.1 Caprock

The results of the simulation of the caprock sample (CD-DARN-15) with the introduction of CO_2 compared to the results of the nitrogen control simulation are presented in terms of the evolution of pH and the concentrations of the main cations.

Figure 4.1 shows the evolution of pH over time for the caprock sample, comparing the experimental data obtained in the laboratory experiments (1162 - CO_2 and 1163 - N_2) with the results of the simulations. In experiment 1162 the pH measured after the introduction of CO_2 on the 14th experimental day shows a reduction from 6.67 to values close to 6.3. After this initial decrease, the pH remains relatively stable over time. This behaviour is compatible with the dissolution of CO_2, which causes acidification, although possible buffering processes linked to the dissolution of carbonates may limit the drop in pH. In contrast, the simulated pH shows a more acidic behaviour, with a reduction from the initial 6.67 to values close to 5, where it remains constant over time. This discrepancy can be explained by the fact that the experimental pH measurements were carried out at atmospheric pressure, which means that an unknown quantity of the dissolved CO_2 escaped from the solution, reducing the concentration of carbonic acid and consequently increasing the pH. The pH values with N_2 are visibly higher, both measured and simulated. This behaviour is typical of a low-reactive system, with no significant sources of acidification, which suggests that the initial alkaline solution was little altered by interactions with the caprock sample. Both the experimental and modelling results suggest that the presence of N_2 did not induce significant chemical changes in the system.

As reported in deliverable D2.9, the fluid samples from the experiment carried out with the caprock samples in the presence of CO_2 show high levels of calcium. Figure 4.2 shows the concentration of calcium in the brine over time in the experiments compared with the modelling results in PHREEQC for the CO_2 (1162 - CO_2) and N_2 (1163 - N_2) systems.

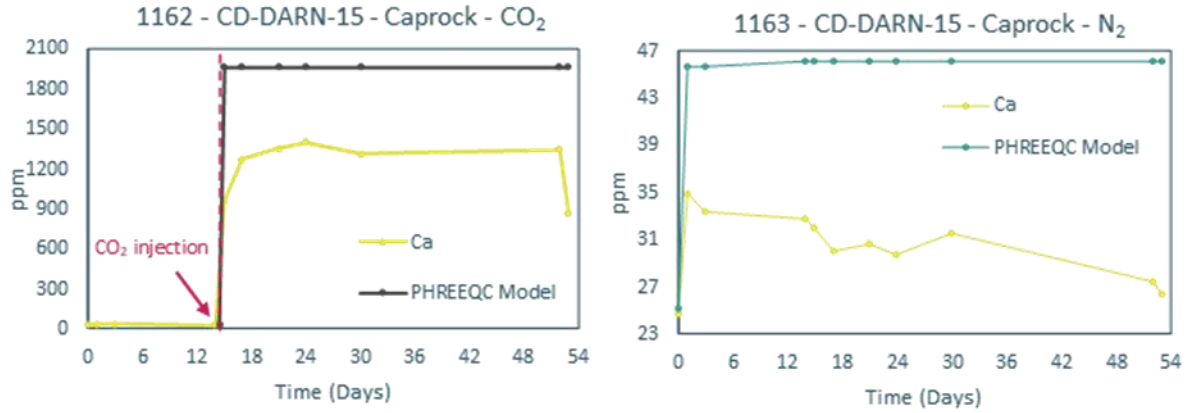

Fig 4.2: Comparison of Ca measured values with modelled values for the caprock with CO_2 and N_2.

In the experiment, the calcium concentration showed a significant increase with the introduction of CO_2 on day 14, reaching values on the order of 1200 ppm and further climbing to 1400 ppm over the following days, values that remained relatively stable until the end of the test, where on the last day there was a drop in values. This decrease may be associated with the depressurisation of the chamber at the end of the experiment, which may have led to the reprecipitation of carbonates due to the release of CO_2, a factor that was not included in the modelling. In the simulation, a similar behaviour is observed in terms of the general trend, but the calcium concentration quickly reaches values of

The PilotSTRATEGY project has received funding from the European Union's Horizon 2020 research and innovation programme under grant agreement No. 101022664

around 2000 ppm after the introduction of CO_2 into the chamber. For the N_2 control, the Ca concentration is lower in both the measured and simulated values. This result is consistent with the pH in the N_2 system, where there is no significant acidification. The absence of CO_2 prevents the formation of carbonic acid, which limits the dissolution of calcium-bearing minerals and in some cases can even favour precipitation.

The differences between modelled and experimental data, especially in the CO_2 system, may be related to the kinetic control of mineral dissolution in the experiment, in contrast to PHREEQC, which assumes chemical equilibrium. The mineral dissolution observed in the experimental results is possibly influenced by the reactivity of the surface of the minerals. In addition, PHREEQC is not the ideal software for high-pressure simulations, the thermodynamic constants used in the model are largely derived from data obtained at ambient pressure therefore requiring proper thermodynamic model functions to extrapolate data for pressurised experimental systems.

The concentrations of the other elements are lower when compared to Ca. For Si concentrations in the system with CO_2 (Figure 4.3), the measured values show an increase when CO_2 is added, reaching values close to 2.5 ppm and assuming a subsequent stabilisation with minimal fluctuations. This behaviour suggests that the dissolution of Si is not being controlled by kinetic factors, but by the equilibrium of mainly amorphous or more soluble phases that rapidly dissolve into solution. The modelled values show a similar trend, but with slightly higher values around 3.2 ppm. This difference suggests that the model is not correctly representing the phases that control Si dissolution experimentally, since the dissolution kinetics of quartz alone are not sufficient to explain the observed trend. The presence of amorphous phases, ultra-fines, or more soluble silicate minerals in the sample may also explain the stabilisation of the silicon in the experimental solution, which is not included in the model. In the system with N_2, the silicon concentration remained practically constant throughout the experiment, indicating that there was no significant dissolution of silicates in the absence of CO_2. This result reinforces the idea, described above, that the acidification of the solution by CO_2 promotes a more significant dissolution of the silicate minerals present in the caprock sample. However, the results of the PHREEQC modelling show a significant increase initially, followed by stabilisation until the end of the run. This difference suggests that the model is controlled by the thermodynamics of the solution, and that it is overestimating the dissolution of the less representative minerals in the rock, thus causing a much higher Si concentration than that recorded experimentally.

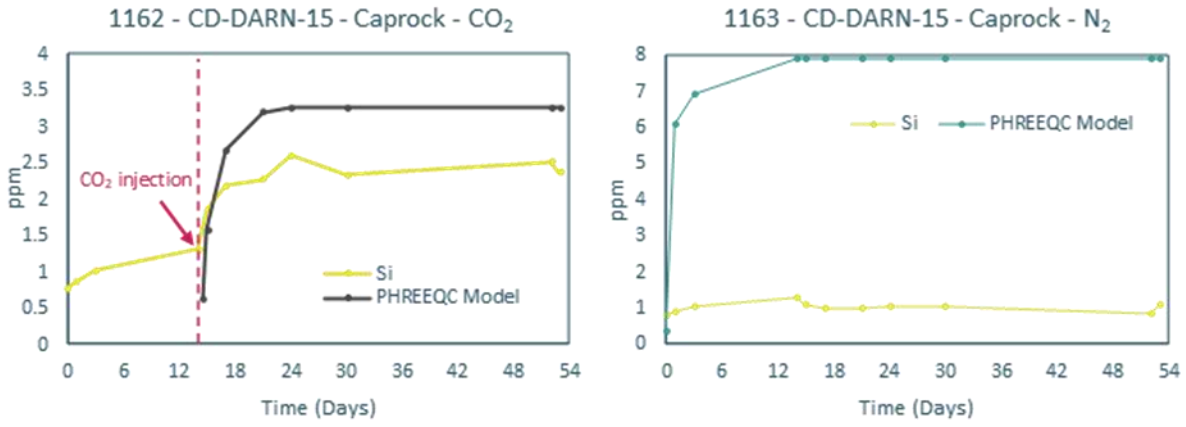

Fig 4.3: Comparison of Si measured values with modelled values for the caprock with CO_2 and N_2.

The PilotSTRATEGY project has received funding from the European Union's Horizon 2020 research and innovation programme under grant agreement No. 101022664

The behaviour of Al is different (Figure 4.4), with a drop in concentration when CO_2 is added to the reactor. This suggests that the precipitation of aluminosilicates or aluminium hydroxides controls the availability of aluminium in the solution. In the N_2 control fluctuations of low amplitude may be due to the difficulty of analysing low concentrations of Al with model reproducing the general trend of Al in the solution.

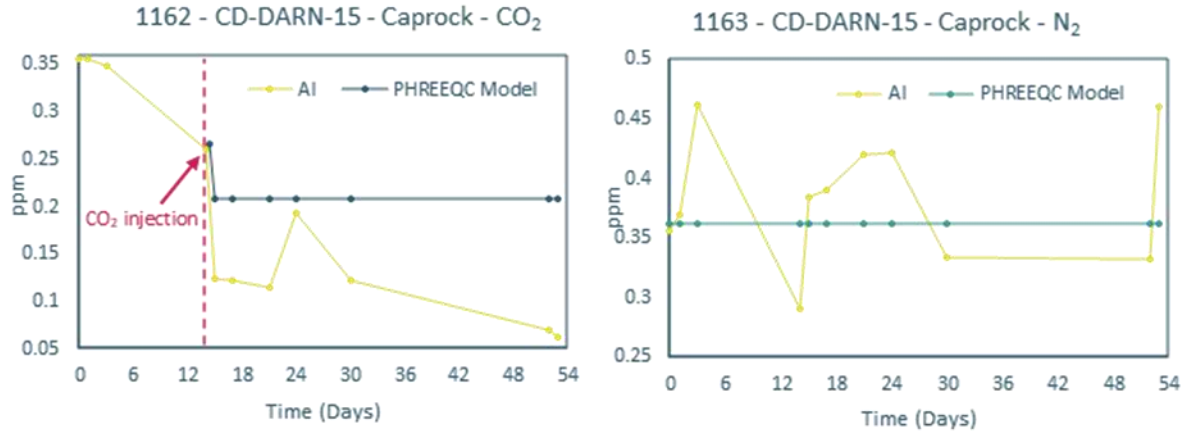

Fig 4.4: Comparison of Si measured values with modelled values for the caprock with CO_2 and N_2.

Figure 4.5 shows a significant increase in the concentration of Mg when the CO_2 was introduced, which suggests that a mineral phase containing Mg was dissolved in response to the acidification introduced by the dissolution of CO_2 in the solution. The inclusion of dolomite in the system at equilibrium in the modelling made it possible to reproduce the measured Mg values, which suggests that this element may be being released by the dissolution of either minor dolomite (below 1%) or another mineral phase rich in Mg, such as magnesian calcite, or clay minerals containing Mg. However, since no mineral phase has been identified analytically to release the magnesium into the solution, its origin is unproven.

For the control system with N_2, the measured Mg concentration values show small variations, while the modelling predicts a constant Mg behaviour. However, the amplitudes of the variations recorded are relatively small, which may indicate that the model reasonably represents the experimental results. In the control system the absence of CO_2, and hence a higher and more stable pH, limits the dissolution of carbonates and, consequently, the release of Mg under the conditions of the simulation.

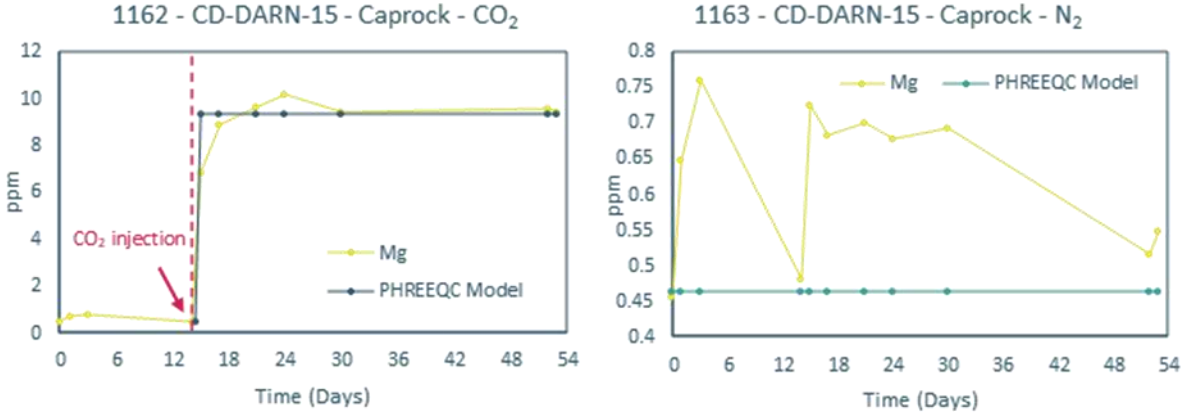

Fig 4.5: Comparison of Mg measured values with modelled values for the caprock with CO_2 and N_2.

The PilotSTRATEGY project has received funding from the European Union's Horizon 2020 research and innovation programme under grant agreement No. 101022664

The behaviour of K (Figure 4.6) in both the CO_2 system and the nitrogen control suggests that its mobility is mainly controlled by pH and the dissolution and precipitation of silicate and clay minerals. In the CO_2 system, initial acidification promotes a significant release of K, followed by stabilisation, probably due to the reprecipitation of secondary phases. In the system with N_2, the dissolution of minerals containing K is minimal, and the significant variation observed at the end is possibly associated with the depressurisation of the reactor and consequent disturbance of the chemical balance. The PHREEQC model predicts higher K concentrations in the system with CO_2 and lower with N_2, showing deviations from the experimental values. However, these deviations may be linked to limitations in the representation of processes such as adsorption and precipitation of secondary phases, as well as the difficulty of capturing experimental variations due to possible analytical constraints and heterogeneities in mineral dissolution.

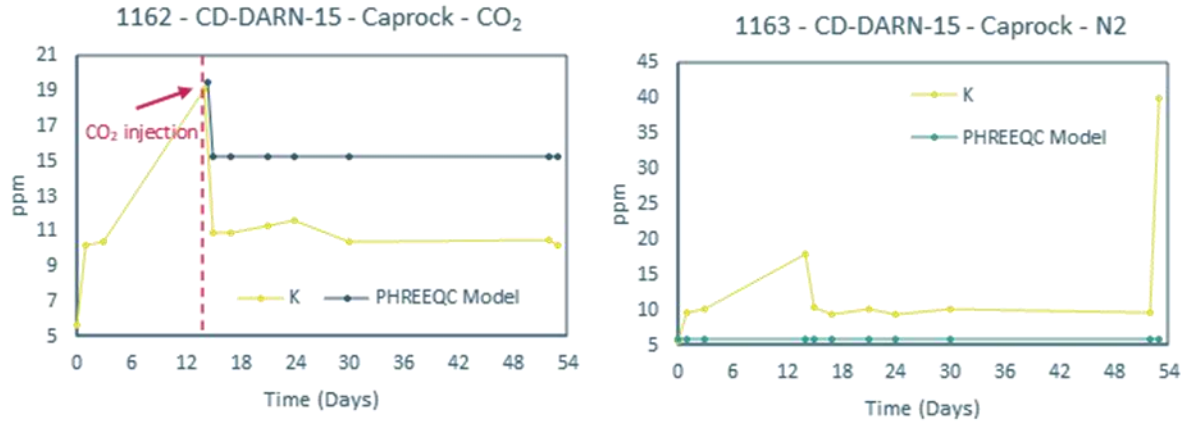

Fig 4.6: Comparison of K measured values with modelled values for the caprock with CO_2 and N_2.

The results presented indicate that the introduction of CO_2 into the experimental system led to significant dissolution of the calcite present in the caprock sample, resulting in a significant increase in the concentration of Ca in the solution. In the experiment, the concentration of Ca reached maximum values of around 1400 ppm, which corresponds to a dissolution of approximately 12% of the total calcite present in the sample (0.5 g of calcite for a 5 g sample), which represents around 11% of the total mass of the rock, as described in deliverable PilotSTRATEGY D2.9. The PHREEQC modelling, on the other hand, predicts a slightly higher dissolution, with the concentration of Ca at approximately 2000 ppm, which is equivalent to 17% of the calcite (0.7g for a 5g sample), which represents approximately 15% of the total mass of the rock.

The dissolution of calcite also plays an important role in buffering the pH. In the experiment, the pH shows a reduction from 6.67 to around 6.3 after the introduction of CO_2, which remained relatively stable throughout the experimental period. This stability suggests the presence of buffering mechanisms, possibly linked to the dissolution of calcite. However, the experimentally measured values were obtained at atmospheric pressure after sampling, which means that part of the dissolved CO_2 escaped from the solution, thus reducing the concentration of carbonic acid and increasing the pH. In the model, despite adding a restriction to the equilibrium with $CO_2(g)$ to reproduce the sampling conditions, the pH shows lower values, reaching around 5, which reflects the interaction of the solution with carbon dioxide and the persistence of the acidifying effect of dissolved CO_2.

The behaviour of silicon indicates that the dissolution of the silicate phases is directly associated with the acidification of the solution. In the system with CO_2, the Si concentration reaches around 2.5 ppm and then stabilises, while in the modelling the values were slightly higher at around 3.2 ppm. This

The PilotSTRATEGY project has received funding from the European Union's Horizon 2020 research and innovation programme under grant agreement No. 101022664

small difference suggests that the modelling is overestimating the dissolution of the minor silicate minerals in the caprock sample. In the system with N_2, the Si concentration remained constant, which indicates very limited dissolution, compatible with the absence of significant acidification.

On the other hand, Al showed the opposite behaviour to silicon, with a reduction in concentration after the introduction of CO_2, which suggests that its concentration is controlled by the precipitation of aluminosilicates or aluminium hydroxides. In the nitrogen control system, Al variations were minimal, indicating a chemically stability. The model reproduces the stability of Al in the N_2 system fairly well.

The Mg concentration increased significantly in the CO_2 experiment, indicating the dissolution of a mineral phase rich in Mg, possibly dolomite, magnesian calcite or magnesian clays. The modelling was able to reproduce the measured values by including dolomite in model, which suggests that it may contribute to the release of Mg into the solution. In the system controlled with N_2, Mg concentrations remained practically constant, which is consistent with a higher pH that limits the dissolution of carbonates.

The behaviour of K indicates that its mobility is strongly influenced by the dissolution and precipitation of silicate and clay minerals. In the CO_2 system, there is an initial increase in K concentration followed by stabilisation, possibly due to the reprecipitation of secondary phases. In the system with N_2, the variation in K was minimal, with an sharp increase at the end of the experiment, possibly due to the depressurisation of the reactor.

The relationship between the dissolution of the caprock sample and its physical properties is fundamental to assessing the integrity of the CO_2 containment. The caprock sample has a measured permeability of 0.6 mD and a porosity of 6%, with an average thickness of approximately 100 metres (information available in PilotSTRATGY deliverable D2.7). The dissolution of up to 15% of the sample's mass in the modelling suggests that there may be a significant change in the rock structure, which could even lead to an increase in porosity and, consequently, its permeability. However, the experiments have very high water-rock ratios, which are unrepresentative of the subsurface. It is important to consider that the chemical balances achieved in the experiment indicate that the dissolution of the caprock sample can stabilise over time, as the porefluids achieve saturation, which limits structural impacts. The buffering of the pH by the dissolution of carbonates can also contribute to limiting the progression of mineral dissolution, thus reducing the risk of CO_2 escaping from the caprock in the long term. However, the differences observed between the measured and simulated values suggest that additional adjustments, especially allowing for kinetic effects and thermodynamic corrections for high pressures, are necessary for a more accurate assessment of the stability of the caprock for long-term CO_2 containment.

4.2.2 Reservoir Rock

The results of the simulations of the reservoir sample (CD-CRR-10) with CO_2 compared to the results of the nitrogen control simulation are presented in terms of the evolution of pH and the concentrations of the main cations.

Figure 4.7 shows the pH evolution over time for the reservoir sample, both the experimental data (1162 - CO_2 and 1163 - N_2) and the results of the simulations with PHREEQC. In the CO_2 system, the pH value drops immediately after the introduction of CO_2, reaching values of around 5 and then stabilising almost immediately afterwards. This stabilisation indicates a possible equilibrium between mineral dissolution and the processes of adsorption and chemical rebalancing with the solution. This reduction in pH is consistent with the dissolution of CO_2 in the brine, promoting acidification of the solution. As

The PilotSTRATEGY project has received funding from the European Union's Horizon 2020 research and innovation programme under grant agreement No. 101022664

previously, the pH measurement was carried out at atmospheric pressure, so it was possible that the real pH values inside the pressurised system were lower. The interaction of the solution with the solid phases cannot be ruled out as a hypothesis for this difference, since iron oxides, silicates and amorphous phases can act as pH buffers.

In the nitrogen control system, where no CO_2 was introduced, the initial pH is higher and gradually increases over time, stabilising at around 7. In contrast, the modelling predicts higher values. This difference can be attributed to the adsorption of species on the mineral surfaces, and to the presence of amorphous particles or small reactive phases which can interact with the solution and influence the pH buffering.

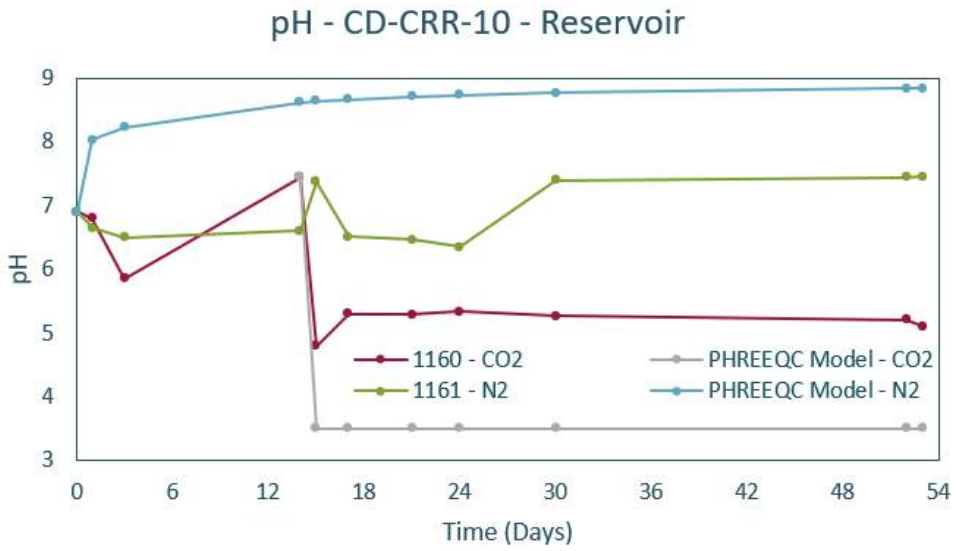

Fig 4.7: Comparison of pH measured values with modelled values for the reservoir sample with CO_2 and N_2.

The mobility of calcium in the brine was evaluated experimentally and compared with the modelling results in PHREEQC for the CO_2 (1160 - CO_2) and N_2 control (1161 - N_2) systems. In figure 4.8, after the introduction of CO_2 on day 14 of the experiment, there is a marked increase in Ca concentration, reaching a maximum of approximately 74 ppm on day 17. This behaviour suggests the dissolution of phases containing calcium carbonate, which may be present in the reservoir sample and which dissolved rapidly in response to the acidification of the solution, although they were not detected by XRD. However, the gradual removal of Ca after the peak cannot be explained by mineral precipitation, since there is no direct evidence of neoformation of carbonate phases, either by thermodynamic modelling or by observation via SEM (Scanning Electron Microscopy). The most plausible explanation is that the Ca was progressively adsorbed onto solid surfaces, such as particles of iron oxides and hydroxides or amorphous layers in contact with water. This behaviour is consistent with a rebalancing of calcium with reactive mineral surfaces, where the initially released Ca is progressively adsorbed or fixed on these surfaces until equilibrium is reached. The PHREEQC modelling, on the other hand, predicts a higher and more constant concentration of Ca over time, thus not reflecting the dynamics observed experimentally. These differences may be related to the fact that the modelling assumes the chemical equilibrium immediately, without considering the kinetic processes of calcium adsorption and re-equilibration with solid surfaces. Furthermore, the modelling does not incorporate the effects of small-scale surface particles, which can play a fundamental role in the progressive removal of Ca from the solution. The dissolution of carbonates and the acidification caused by the dissolution of CO_2 can also promote the dissolution of silicates present in the reservoir sample, thus contributing to the

The PilotSTRATEGY project has received funding from the European Union's Horizon 2020 research and innovation programme under grant agreement No. 101022664

mobilisation of cations in the solution. However, only a small fraction of the calcium can be explained by the dissolution of calcium carbonate, which indicates that there are certainly other sources of Ca available in the system. This could include Ca adsorbed on iron oxides and leached layers of minerals that release calcium into the solution in response to the decrease in pH.

In the control system with N_2, there is no CO_2-induced acidification, so the measured Ca concentration remains low and relatively stable. This indicates that in the absence of significant pH variations, the dissolution of Ca rich phases occurs to a limited extent. The simulation, however, predicts a gradual and continuous increase in Ca concentration, reaching values higher than those observed experimentally. This difference is due to the model being controlled by kinetic dissolution processes.

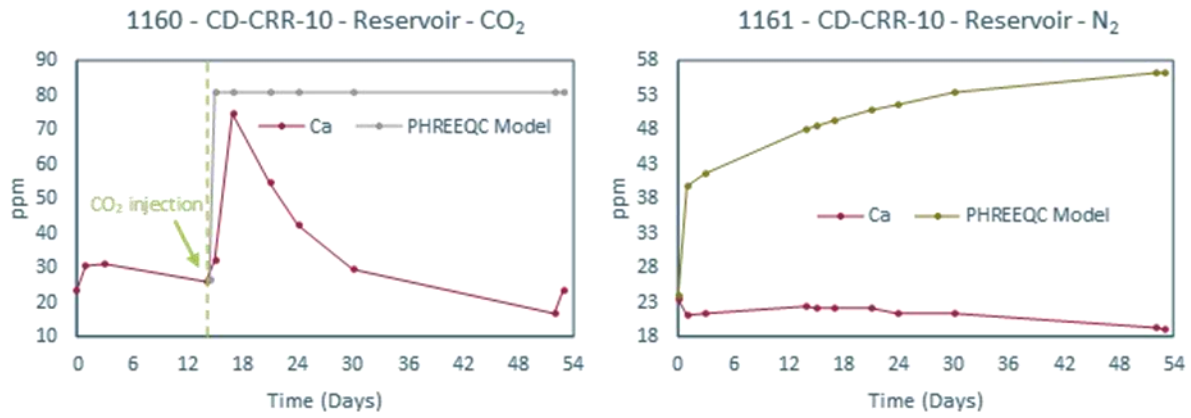

Fig 4.8: Comparison of Ca measured values with modelled values for the reservoir with CO_2 and N_2.

The Si concentration seen in Figure 4.9 increases progressively after the introduction of CO_2. This increase is associated with the incongruent dissolution of aluminosilicates phases, where silicon enters solution more easily than aluminium due to the lower solubility of aluminium. This differential dissolution may occur in K-feldspar but as there is no change in K concentration (see below) then the dissolution of fine-grained or poorly crystalline aluminosilicate material present on grain surfaces is more probable. Such phases may occur below the detection limit of XRD or as surface coatings, even after sample rinsing and pre-equilibration procedures, leading to a preferential release of Si into solution. After the maximum on day 30 (~14 ppm), the Si concentration shows a significant drop, possibly an experimental artefact. The simulated results show that the silicon concentration remains constant throughout the experiment, which indicates that kinetic dissolution processes, the formation of amorphous phases or interactions with iron oxides have not been reproduced in the model. In comparison, the control with N_2 shows a more stable Si concentration over time, with only minor increase, indicating that mineral dissolution occurs much more slowly or even that the system was already close to chemical equilibrium. The PHREEQC model in this case achieves a better approximation to the measured data, since the dissolution and equilibrium processes under neutral conditions are better represented in the thermodynamic databases used.

The PilotSTRATEGY project has received funding from the European Union's Horizon 2020 research and innovation programme under grant agreement No. 101022664

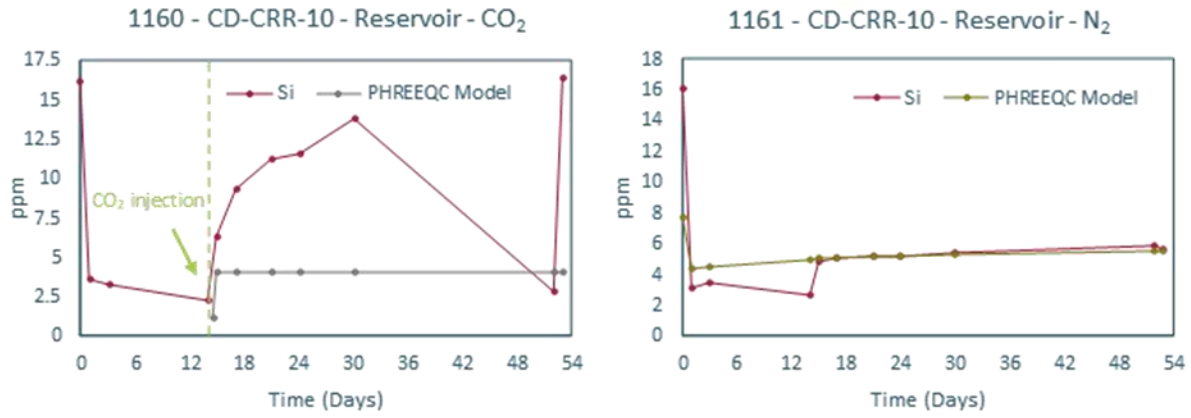

Fig 4.9: Comparison of Si measured values with modelled values for the reservoir with CO_2 and N_2.

The Al concentrations in the system with CO_2 (Figure 4.10), the measured values show an increase after the introduction of CO_2 into the reactor, reaching a maximum with values close to 5 ppm on day 30. This increase is directly related to the acidification of the solution, which enhances the dissolution of aluminosilicate phases present in the rock. K-feldspar is unlikely as there is no increase in concentration of K (see below), suggesting the dissolution of a fine-grained or poorly crystalline Al-bearing material. The measured values follow a trend of continuous release of Al into solution, however, due to its low solubility, this tends to saturate quickly and be removed from the solution, possibly by precipitation processes of secondary phases (possibly during sampling rather than in-situ). The behaviour observed in Si (Figure 4.9) reinforces this interpretation, since silicon has greater solubility, favouring incongruent dissolution, where Si remains dissolved and Al is quickly removed from solution. This effect is expected in systems where silicate dissolution occurs under acidic conditions. The PHREEQC model, on the other hand, shows a stable and relatively low concentration of Al throughout the experiment, which indicates that the processes of rapid dissolution and reprecipitation of Al are not being represented by the model. In the control system with N_2, where the pH remained neutral to slightly alkaline, the concentration of Al in the solution remained close to zero throughout the experiment. This result confirms that the mobilisation of Al in the CO_2 system was induced by the reduction in pH, given that in neutral conditions aluminous minerals remain stable with very low solubility. In this case we can consider that the simulated results were able to adequately reproduce the real behaviour, since the experimental conditions of the control system do not favour significant dissolution of the aluminous silicates.

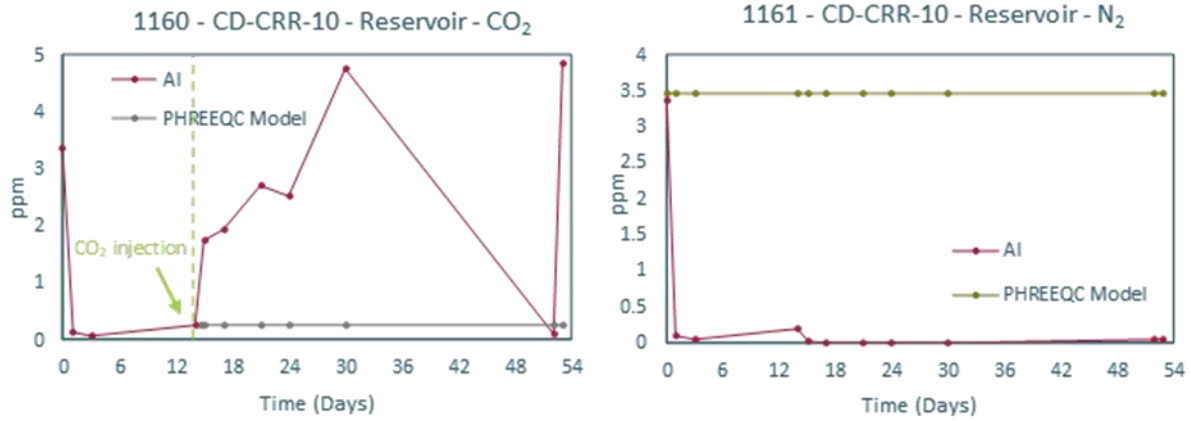

Fig 4.10: Comparison of Al measured values with modelled values for the reservoir with CO_2 and N_2.

The PilotSTRATEGY project has received funding from the European Union's Horizon 2020 research and innovation programme under grant agreement No. 101022664

Figure 4.11 shows the experimental results of the system with CO_2, where a gradual increase in Mg concentration is visible after the introduction of CO_2 on day 14, reaching a maximum of approximately 13 ppm on day 24. This behaviour can be explained by a mechanism of dissolution and reprecipitation of carbonate and silicate minerals. Acidification of the system can lead to accelerated dissolution of calcite, a magnesian calcite phase or dolomite, which explains the increase in Mg concentration. As with the PHREEQC model of the caprock sample, equilibrium was established with dolomite, which suggests that a Ca-Mg carbonate mineral phase may be controlling the concentration of Mg in the system. If dolomite is present in the reservoir sample, its initial dissolution could release both Mg and Ca into the solution. However, as the solution becomes less acidic, calcite reprecipitation mechanism may take place with partial incorporation of Mg, which leads to a decrease in dissolved concentrations over time. The reduction in Mg concentration observed may be associated with a secondary phase precipitation process. On the other hand, the PHREEQC model of the nitrogen control system does not include dolomite in equilibrium, which may indicate that, under neutral conditions, the dissolution of Mg-bearing minerals did not occur significantly, according to the experimental results.

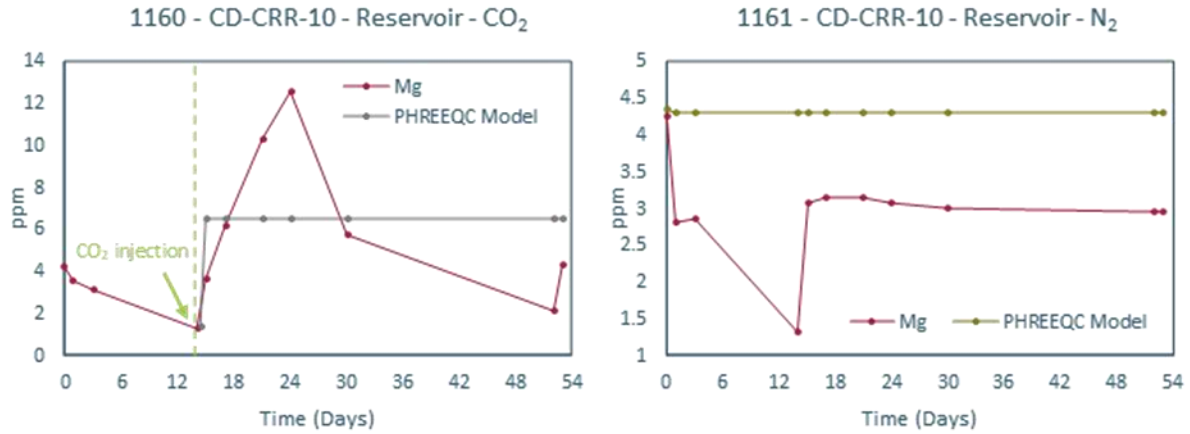

Fig 4.11: Comparison of Mg measured values with modelled values for the reservoir with CO_2 and N_2.

The behaviour of K in the two systems is similar, with no significant pattern over time. In the CO_2 system, there is a slight fluctuation in K concentration throughout the experiment. The measured values vary without a clear trend of sustained increase or decrease. The significant drop at the penultimate sampling point may be an experimental artifact. The PHREEQC model maintains the K concentration throughout the experimental time, suggesting that there was no significant dissolution of K-rich phases, such as the K-feldspars present in the reservoir sample, thus reproducing the experimental results. In the N_2 control system, the measured values show a similar behaviour to that observed in the CO_2 system. The amplitudes of the fluctuations observed may be associated with analytical constraints, as they do not show a clear trend. In the results presented by the simulation, the K concentration remains constant throughout the experimental period, which suggests that once again, under neutral conditions the dissolution and removal of phases with K are balanced and stable over time. We can therefore state that the modelling is representative of the experimental data.

The PilotSTRATEGY project has received funding from the European Union's Horizon 2020 research and innovation programme under grant agreement No. 101022664

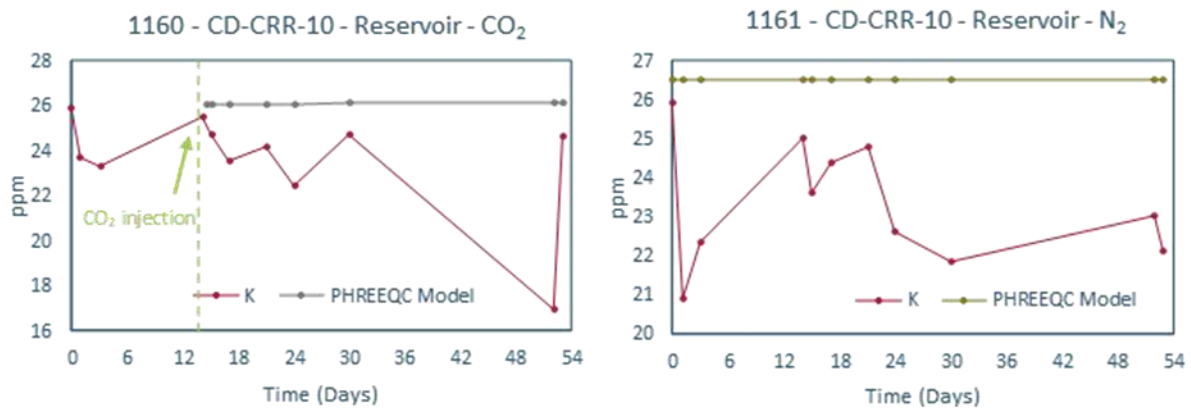

Fig 4.12: Comparison of K measured values with modelled values for the reservoir with CO_2 and N_2

The Fe concentration in the system with CO_2 (Figure 4.13) shows large variations, reaching high peaks followed by abrupt drops. This behaviour suggests that there may have been a dynamic process of dissolution and reprecipitation of phases containing Fe, but possibly not rock-forming minerals. It is possible that the acidification of the solution by the dissolution of CO_2, by reducing the pH, favoured the dissolution of amorphous or microcrystalline phases containing Fe, which cover the surfaces of the samples. These phases can be iron oxyhydroxides with low crystallinity and high reactivity so they enter solution easily. The possible reprecipitation does not necessarily result in the formation of well-crystalised minerals, which can lead to the fixation of Fe by Ca and other elements dissolved in the solution. However, the form of Fe in solution (ferrous - Fe^{2+} or ferric - Fe^{3+}) is uncertain. Fe^{3+} is highly insoluble in most natural conditions, which makes it unlikely to remain in solutions of high concentrations, while Fe^{2+} is more soluble, but depends on the maintenance of reducing conditions to remain dissolved. Comparing to the control system with N_2, as there are no sudden variations in Fe, the hypothesis that the dissolution of iron-containing phases in the CO_2 system is associated with reactive amorphous or microcrystalline phases is strengthened. However, due to variation in solubility with redox state, sampling and analysis of iron from pressurised experiments can be problematic, since samples moving from a reducing environment to a more oxygenating one can be prone to secondary precipitation of iron bearing phases, so some variation in concentration is likely due to sampling and/or analytical error.

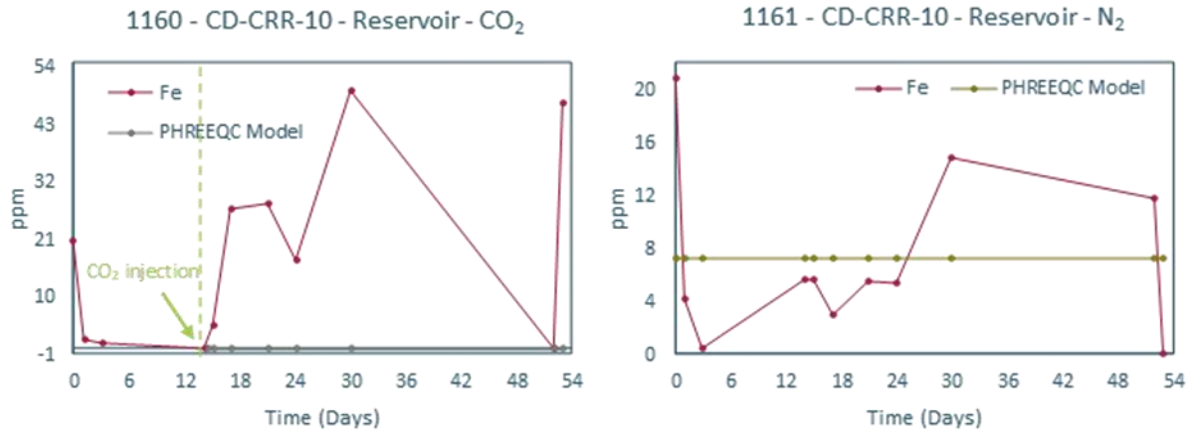

Fig 4.13: Comparison of Fe measured values with modelled values for the reservoir with CO_2 and N_2.

The PilotSTRATEGY project has received funding from the European Union's Horizon 2020 research and innovation programme under grant agreement No. 101022664

4.3 Discussion

The experimental and simulation results indicate that the reservoir sample has a relatively low reactivity in response to CO_2 injection. The addition of CO_2 to the system causes an initial drop in pH due to the dissolution of the gas in the brine and the formation of carbonic acid. This is followed by a rapid stabilisation of the pH, which suggests the presence of buffering mechanisms, possibly associated with the dissolution of small amounts of carbonates and the adsorption of cations on solid surfaces. This buffering effect can be partially attributed to the presence of calcite which, although not detected via XRD, likely contributed to moderating the acidification of the system. The pH values measured were obtained at atmospheric pressure, so the real values within the pressurised system are lower. To correct for this effect, an equilibrium restriction with $CO_2(g)$ was incorporated into the models to better estimate the chemical composition of the brine at the time of sampling.

The introduction of CO_2 led to an initial increase in the concentration of Ca in the solution, reaching a peak of approximately 74 ppm on day 17 of the experiment and beginning to gradually decrease thereafter. This initial input suggests the dissolution of minor carbonate phases or desorption of Ca adsorbed from iron oxy-hydroxides and amorphous phases. The subsequent decrease in Ca after the peak concentration is unlikely to be explained by carbonate mineral precipitation, but rather by re-equilibration processes involving surfaces and small-scale reactive phases. In contrast, the PHREEQC model predicts a sustained increase and stabilisation of Ca concentrations, indicating that adsorption, surface interactions and other small-scale processes affecting Ca are not fully represented within the modelling. A more detailed assessment of the calcium behaviour in the experiment would require the use of surface sensitive analytical techniques such as XPS (X-ray Photoelectron Spectroscopy) as a way to detect the presence of Ca adsorbed on solid surfaces. The drop in pH in the CO_2 system is a key factor in calcium dynamics. As the pH decreases, there is an increase in the availability of aqueous CO_2, which favours the dissolution of minerals and the consequent release of cations into solution. However, it should be emphasised that the system tends to rebalance itself over time.

The concentration of silicon increases progressively after the introduction of CO_2, which indicates the incongruent dissolution of silicates. This process suggests greater mobilisation of Si compared to Al, possibly due to the lower solubility of aluminium. The observed peak in Si concentration, followed by a drop after the reactor was depressurised, may be related to the sudden precipitation of secondary phases. The Si simulations predict a constant concentration, because no kinetic dissolution processes, or formation of amorphous phases, were.

Magnesium shows a similar behaviour to calcium, with a gradual increase after the introduction of CO_2. This pattern can be attributed to the dissolution of dolomite or magnesian calcite. In the control system with N_2, where there was no significant dissolution of carbonates, the Mg concentration remains stable and relatively low. PHREEQC modelling corroborates this behaviour by indicating that a Ca-Mg carbonate may be controlling the Mg concentration in the CO_2 system.

Iron did not show a significant increase in the solution, which suggests that the dissolution of iron oxides was limited, or that the adsorption processes prevented greater mobilisation of this element. This behaviour is in line with what has been observed for other cations, where adsorption in solid phases seems to play an important role in regulating dissolved concentrations.

The mineralogical assemblage of the reservoir sample, characterised by silicates and aluminosilicates with low solubility, does not indicate significant dissolution in the primary matrix or significant precipitation of secondary phases throughout the experimental period. The low mobility of the elements analysed indicates that the reactivity of the system is limited, even under acidic conditions

The PilotSTRATEGY project has received funding from the European Union's Horizon 2020 research and innovation programme under grant agreement No. 101022664

induced by the dissolution of CO_2, as previously mentioned in deliverable D2.9. The permeability of the rock (32.28 mD) and its porosity (13.22%), combined with an average thickness of the reservoir of approximately 350 metres (information available in Deliverable D2.7), suggest a robust geological environment for the storage of CO_2, with little susceptibility to significant dissolution of its constituents.

According to the results, even if there is some localised dissolution of carbonates around the injection site, it is expected that this dissolution will be less than 0.5% of the entire rock mass, which would not compromise the physical stability of the sandstone and could even act as a pH buffering mechanism, reducing the scope for the dissolution of other minerals. In this way, the stability of the reservoir rock for storing CO_2 is not expected to be compromised by the geochemical processes observed, which reinforces the viability of the system for injecting and storing CO_2 in the long term.

It is important to note that the sample of cap rock used in the experiments corresponds only to a specific point of this lithological unit, representing the top of the geological formation, and not its base, which is the portion in contact with the stored CO_2. As such, the results obtained are not necessarily representative of the entire extent and heterogeneity of the cap rock.

The lithological sequence corresponding to the cap rock identified in the Dourada-1C survey (offshore) is represented between the Turonian (770 - 835 m) and Cenomanian (835 - 887 m) intervals, showing a significant vertical transition in its mineralogical and textural characteristics, which play an important role in the effectiveness of the cap rock as a CO_2 containment barrier.

In the upper section, corresponding to the Turonian (770 - 835 m), the rock is predominantly described as a white to cream limestone, with pseudo-oolites and coated grains, and skeletal components, of fine to medium coarse grain size. The matrix is dominated by sparry calcite, although there are areas with a more chalky appearance (limestone with high microporosity and fine texture). This unit has high hardness, with occasional occurrences of dolomitisation, and also exhibits rare vuggy-type porosity, which suggests a rock with low effective permeability, and therefore good sealing characteristics. The presence of veins of sparry calcite may also indicate episodes of fluid circulation throughout the formation's diagenesis.

The PilotSTRATEGY project has received funding from the European Union's Horizon 2020 research and innovation programme under grant agreement No. 101022664

Fig 4.14: The Portuguese caprock at outcrop.

On the other hand, at the base of the stratigraphic sequence of the cap rock (Cenomanian 835 - 887 m), the limestone is described as identical to the previous one, i.e. retaining many of the characteristics described, but showing a progressive evolution towards a more clayey lithology, evidenced by the appearance of light to dark grey marls of medium hardness. This transition to more marly materials with a higher clay content gives the formation greater plasticity and less permeability, which reinforces its potential as a containment barrier. In addition, in this zone there are nacreous lamellar fragments (possibly derived from shells), the presence of siderite (indicative of reducing conditions) and microcrystalline dolomite, which suggests more complex diagenesis. The base of this unit also shows a transition to dolomitic sandstone, as well as the presence of red silty shales, lithologies that influence the heterogeneity of the cap rock.

In short, the stratigraphic sequence of the cap rock indicates that the lower part of the cap rock (Cenomanian) has a more clayey and marly character, typically associated with greater sealing capacity and less geochemical reactivity, while the upper part (Turonian), since it is a purer limestone and occasionally dolomitic, although with less porosity, may be more susceptible to dissolution in contact with CO_2, especially along fractures.

The PilotSTRATEGY project has received funding from the European Union's Horizon 2020 research and innovation programme under grant agreement No. 101022664

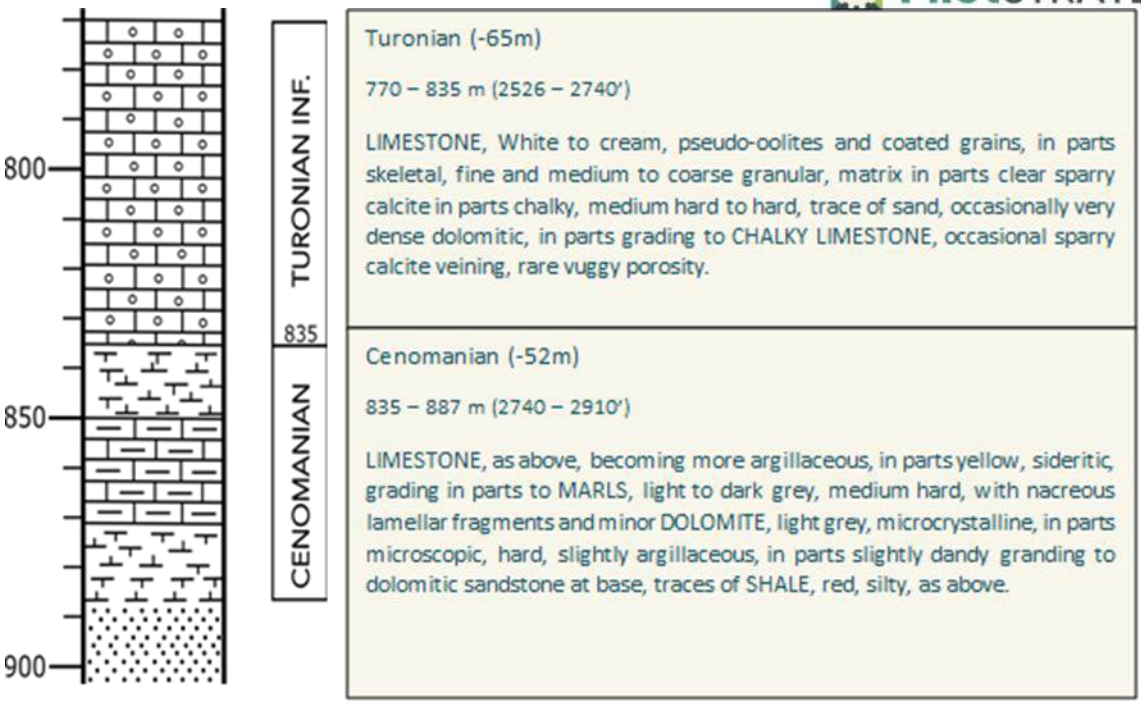

Fig 4.15: The stratigraphy of the Portuguese caprock section.

Results confirm that calcite rich samples are subject to dissolution under acidic conditions associated with CO_2 injection, as confirmed both by tests in the UEDIN and by modelling. The reactivity tests carried out on the cap rock sample with 89% calcite in its composition make this material susceptible to dissolution in contact with CO_2 saturated brine, especially under acidic conduction associated with CO_2 injection.

The through flow tests were carried out on an intact sample, with only an induced fracture, and the results show less pronounced dissolution than in the batch reaction tests in which the sample is pulverised. Still, the experiments indicate that some mobilisation of elements and mineral dissolution occurs, although at a much smaller scale than for the pulverised materials. It should be noted that the throughflow reactivity test is more representative of the real conditions found at depth, since it uses a practically intact sample with an induced fracture, better reflecting the behaviour of the rock in situ. In contrast, the batch experiments with the pulverised sample have a significantly higher relative surface area, leading to higher dissolution rates. Thus, the value of 11% of the original mass of dissolved rock observed in the batch experiment represents an extreme scenario, while in the flow reactivity experiment this percentage will certainly be lower, precisely because of the smaller contact area between the rock and the reactant.

The most serious scenario for the integrity of the cap rock is the existence of natural fractures or faults which, when in contact with CO_2, can increase the surface area available for reactions and encourage the dissolution of carbonate minerals such as calcites. This dissolution could compromise the containment properties of the cap rock and create preferential pathways for CO_2 migration, increasing the potential risk of leakage. However, mineral dissolution processes evolve until they reach a chemical equilibrium with the fluid, which will naturally limit the progression of geochemical reactions. This tendency towards equilibrium was also observed and discussed in the geochemical modelling section of the batch experiments, reinforcing the concept that dissolutions are not unlimited, but are conditioned by the saturation of the fluids in relation to the dissolved minerals.

The PilotSTRATEGY project has received funding from the European Union's Horizon 2020 research and innovation programme under grant agreement No. 101022664

The presence of fractured structures in the cap rock must be assessed in detail, as they are one of the most vulnerable points in terms of the safety of the geological storage of CO_2.

4.4 Interim conclusions

Based on the experimental results and the geochemical modelling carried out, it is possible to establish a comparison between the behaviour of the caprock sample and the reservoir rock samples used, in the presence of CO_2 injection under reservoir conditions, thus allowing important conclusions to be drawn about the stability and efficiency of the storage system.

The caprock sample showed more pronounced reactivity to the presence of CO_2, as evidenced by the dissolution of the calcite present in its matrix. The dissolution of up to 15% of the mass of calcite in the PHREEQC simulation led to a significant increase in the concentration of calcium in the solution, as well as the mobilisation of other cations, such as Mg and K, in response to the initial acidification caused by CO_2. The calcite also played a role in buffering the pH, stabilising the solution around moderately acidic values, which may limit the progression of mineral dissolution over time. This interaction suggests that although the caprock may undergo local structural changes with a possible increase in porosity and permeability, it still preserves part of its function as a geochemical barrier, especially due to buffering by the dissolution of carbonates and its stabilisation in dissolution over time.

Meanwhile, the reservoir rock samples showed very limited geochemical reactivity to CO_2 injection. The initial acidification of the system was quickly stabilised by buffering mechanisms, with minimal carbonate dissolution. The reservoir rock sample, made up predominantly of low-solubility silicates and aluminosilicates, does not suggest any significant structural changes throughout the experiment, which suggests that the system is highly robust even under conditions of CO_2 induced acidity.

When both samples are compared, it can be seen that the caprock sample is more susceptible to mineral dissolution due to acidification by CO_2, while the reservoir rock sample is more resistant, with localised and less significant dissolution. This difference in behaviour is attributed to the presence of more abundant carbonate phases and the lower mineralogical buffering in the caprock sample compared to the reservoir rock sample.

From the point of view of safety for the geological storage of CO_2, the samples fulfil complementary functions. The reservoir rock sample, with its greater permeability and low reactivity, maintains its ability to store CO_2 with long-term geochemical stability. On the other hand, the caprock sample, despite its greater initial reactivity, tends to stabilise after geochemical rebalancing and buffering by dissolved carbonates, thus helping to prevent the upward migration of CO_2.

The PilotSTRATEGY project has received funding from the European Union's Horizon 2020 research and innovation programme under grant agreement No. 101022664

5. Spain

5.1 Model conceptualisation and set-up

As part of the PilotSTRATEGY project two samples from the Ebro Basin, Spain, were tested in geochemical batch reaction experiments. As for Portugal, one caprock sample and one reservoir sample were tested for CO_2-brine-rock reactivity. Details on these experiments can be found in PilotSTRATEGY D2.9. Modelling was undertaken to compare the reactions observed with those predicted by geochemical modelling using available rate equations.

The mineralogy of the two samples used, as determined by XRD analysis, is shown in Table 5.1. For the purposes of modelling the starting amount of each mineral available for reaction within the model were calculated based on this data and the sample weight used in the experiments.

Powdered samples (125-250 µm grain size) were used in the experiments. No direct analysis of the surface area of these was available. For the purposes of modelling the reactive surface area of the samples was assumed to be 1 m^2/g. Based on previous experience this is a reasonable estimate for the surface area of a powdered rock or mineral in this grainsize, which tend to have surface areas in the range 0.1 – 10 m^2/g, depending on composition, but this does represent a large source of uncertainty in the final results. The nominal 1 m^2/g of total surface area for the samples was distributed across the mineral assemblages based on their weight percent as measured by XRD. The values are shown in Table 5.2.

The starting fluid compositions used in the models was as per the experimental samples taken immediately prior to the addition of CO_2, at which point the liquid-solid had undergone some pre-equilibration under nitrogen pressure only. The starting fluid input values are summarised in Table 5.3. Within the model, starting fluids were allowed to react with the mineral assemblages shown under pressure/temperature conditions reflecting those of the original experiments. Mineral assemblages were allowed to dissolve with reaction kinetics defined by the general rate equations presented by Palandri and Kharaka and using the kinetic parameters presented therein (Palandri and Kharaka 2004). Secondary precipitation was suppressed within the model, though model outputs were assessed for likely oversaturation of particular minerals which may have precipitated. The models were run for 850 hours of simulated time.

The PilotSTRATEGY project has received funding from the European Union's Horizon 2020 research and innovation programme under grant agreement No. 101022664

Lab ID	*AGH0016*	*AGH0017*
ID as supplied	*TA-03*	*PR-11*
Description	*Sample of sandstone reservoir rock from the Ebro onshore reservoir, supplied as disagregated sample by Repsol*	*Sample of caprock from the Ebro onshore reservoir, supplied as disag. Sample by Repsol*
	% Mineral Phase	
Quartz	***86.2***	***33.2***
K feldspar	***5.7***	***9.7***
Chlorite	*N.D.*	***10.4***
Mica	***6.1***	***18.4***
calcite	*N.D.*	***13.2***
Hematite	***0.2***	*N.D.*
Montmorillonite	*N.D.*	***15***
Clinochlore	***1.8***	*N.D.*

Table 5.1: Spanish Reservoir and Caprock sample mineralogy.

Sample		Quartz	K-Feldspar	Chlorite(14A)	Biotite	Calcite	Hematite	Montmorillonite	Clinochlore
PR11	Moles in Model	2.76E-02	1.74E-03	9.36E-04	1.80E-03	6.59E-03	0.00E+00	3.44E-03	0.00E+00
	Surface area in model, m2	1.66	0.49	0.52	0.92	0.66	0.00	0.75	0.00
TA03	Moles in Model	7.17E-02	1.02E-03	1.62E-04	5.96E-04	0.00E+00	6.26E-05	0.00E+00	0.00E+00
	Surface area in model	4.31	0.29	0.09	0.31	0.00	0.01	0.00	0.00

Table 5.2: Model mineralogy.

	Sample/Experiment			
	PR_11/CO2	PR_11/N2	TA_03/CO2	TA_03/N2
pH	7.11	6.93	6.94	7.57
pe	2.00	0.05	0.39	1.62
Element	Concentration (ppm)			
Al	BD	1.00E-20	2.01E-01	7.96E-01
As	1.70E-01	BD	BD	BD
Ba	BD	BD	BD	BD
Ba	9.33E-01	9.71E-01	2.78E-01	2.75E-01
Ca	8.92E+01	8.49E+01	3.20E+01	2.62E+01
Cd	BD	BD	BD	BD
Ce	1.73E-02	2.35E-02	BD	BD
Co	1.60E-02	BD	1.68E-02	BD
Cr	1.40E-02	BD	BD	BD
Cu	1.01E-01	8.19E-02	2.06E-01	6.51E-02
Fe	1.50E-01	1.23E+00	7.74E-01	2.08E-01
Hg	BD	BD	BD	BD
K	6.74E+01	6.92E+01	8.38E+01	9.12E+01
Li	BD	BD	BD	BD
Mg	3.02E+01	3.05E+01	1.02E+00	8.51E-01
Mn	5.18E-02	3.67E-02	5.54E-02	5.16E-02
Mo	BD	BD	BD	BD
Na	6.33E+04	6.34E+04	7.22E+04	7.70E+04
Ni	7.50E-02	1.33E-01	2.75E-01	1.50E-01
P	7.54E-02	9.85E-02	BD	1.12E-01
Pb	6.38E-02	BD	7.37E-02	BD
Rb	6.44E-01	6.39E-01	3.62E-01	3.32E-01
S	2.37E+01	2.19E+01	2.16E+01	2.02E+01
Se	BD	BD	BD	BD
Si	5.06E+00	5.10E+00	3.28E+00	3.12E+00
Sr	6.15E-01	6.76E-01	5.59E-01	5.58E-01
Ti	BD	BD	BD	BD
Tl	8.60E-02	8.69E-02	BD	BD
V	1.20E-02	1.03E-02	BD	BD
Zn	BD	BD	BD	BD

Table 5.3: Model starting fluid compositions, as determined from experimental samples.

The PilotSTRATEGY project has received funding from the European Union's Horizon 2020 research and innovation programme under grant agreement No. 101022664

5.2 Results

5.2.1 TA-03 (reservoir sample)

TA-03 is a sample of a potential Spanish reservoir rock, an arkosic sandstone. In hand specimen the rock is well-sorted, with grain sizes ranging from 100–120 microns in diameter. The porosity is around 10%, predominantly intergranular in type. Petrographically, framework grains consist of mono- and polycrystalline quartz, K-feldspar (25-30 %), metamorphic rock fragments (<5 %), together with Ti and Fe oxides-hydroxides, muscovite and zircon as accessories components. The cementing phase is an iron-rich matrix, likely composed of phyllosilicates (mica and kaolinite) and finely dispersed iron compounds (iron oxides/hydroxides). A small amount of siliceous cement (<5%) is also present. The XRD analysis (see Table 5.1) on the specific sample used in the experimental work indicates a composition dominated by quartz (86%) with significant k-feldspar (6%) and micas (6%) and minor clinochlore (<1%) and hematite (2%). These were represented within the model as quartz (SiO_2), K-feldspar ($KAlSi_3O_8$), biotite (for mica, $KFe_3(AlSi_3)O_{10}(OH)_2$), chlorite(14A) (for clinochlore, $Mg_5Al_2Si_3O_{10}(OH)_8$) and hematite (Fe_2O_3).

Figures 5.1–5.4 presents selected results from the models of the CO_2 and N_2 pressurised batch experiments carried out using this sample: both mineral amounts and elemental concentrations over time are presented, together with the measured results from the experiments in the case of the elemental concentrations. In both the CO_2 and N_2 cases the results reflect systems which are out of equilibrium but with low rates of reactivity and low overall levels of reaction over the time period employed.

In the CO_2 case quartz remains stable while K-feldspar, biotite, chlorite and hematite show very minor dissolution (in each case <0.5% of the material initially present was dissolved over the 850 hour model run time). Biotite and K-feldspar show the most dissolution ($4x10^{-6}$ and $3x10^{-6}$ M, respectively). Al and K are released into solution and overall concentrations track those measured from the batch experiment reasonably closely, indicating that the reaction rates (and, by extension, surface areas) used for these minerals within the model match the reality of the batch experiment reasonably closely. Measured Fe and Si concentrations, however, rise much more rapidly within the batch experiments than in the model outputs (in the case of Si these rise to near silica saturation within 300 hours), suggesting that dissolution of other minerals bearing these elements is underrepresented within the model. Significant Ca release also occurs within the experiments which is not reflected within the model (none of the modelled phases contain Ca). Within the experiment this rise presents as a very rapid increase in concentration in the initial hours of the experiment, plateauing at a level well below carbonate saturation. In this case the mismatch may be due to a small amount of Ca bearing carbonate or feldspar or, more likely, Ca held within or on the surface of the micas present released through cation exchange with the brine as CO_2 dissolved and pH drops. Modelled pH is lower, by around 2 pH units, than measured values, though both data sets remain largely constant following addition of CO_2. The discrepancy in pH values is due, primarily, to the fact that model values assume a constant dissolved CO_2 content, calculated based on solution species activity, temperature and CO_2 gas pressure. The relationships between these factors and CO_2 solubility and speciation (and hence solution pH) are well established. Experimental samples were removed from the vessel prior to measurement of pH. Although measurements were made swiftly, the drop in pressure inevitably leads to some degassing of dissolved CO_2 and, hence, rise in pH, as sampled solutions move to a new equilibrium with atmospheric CO_2 partial pressure.

The PilotSTRATEGY project has received funding from the European Union's Horizon 2020 research and innovation programme under grant agreement No. 101022664

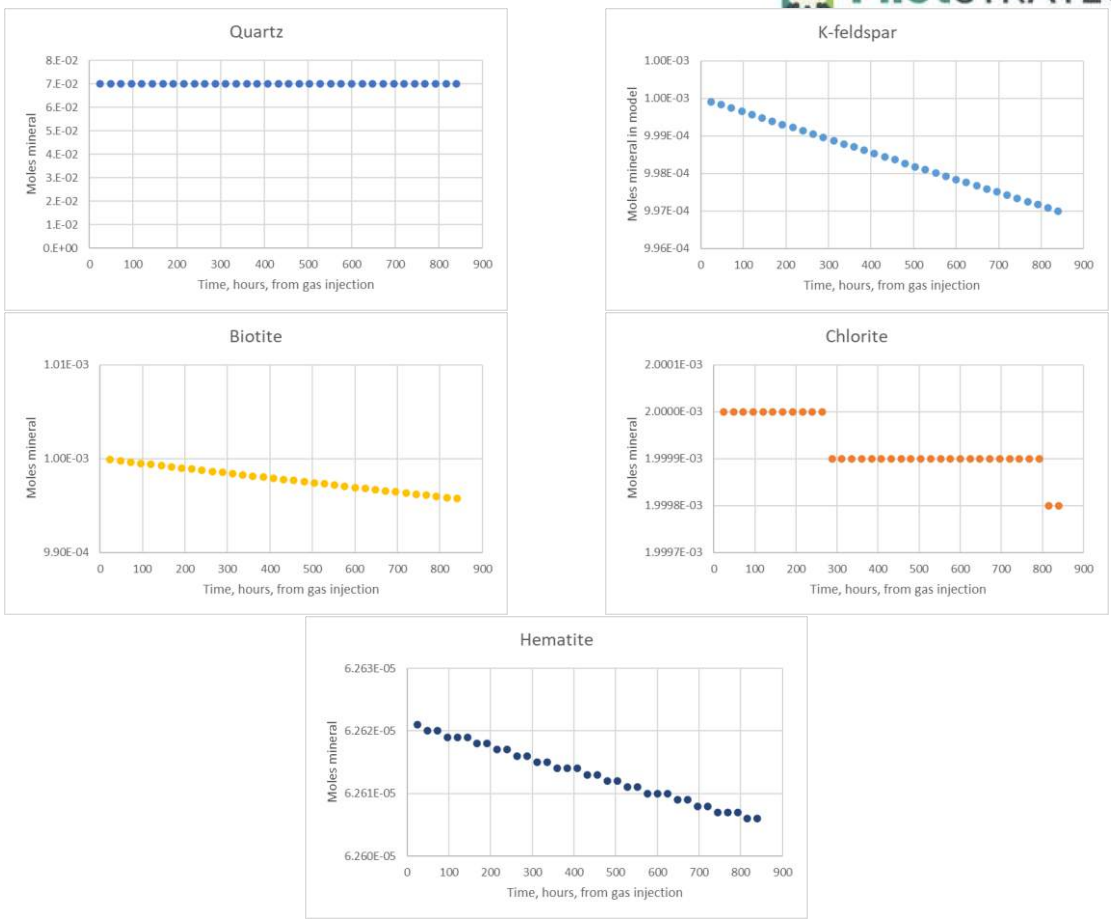

Figure 5.1: Amount of mineral in reservoir sample model run with CO_2.

Figure 5.2: Modelled and measured fluid chemistry for reservoir sample experiment with CO_2.

The modelled results for the nitrogen only run, as for the measured results, indicate less reaction in the CO_2 free system. K-feldspar and chlorite are undersaturated and dissolve during the model run but to a much lesser extent than noted in the CO_2 model (around an order of magnitude less for K-feldspar and around half for chlorite). Other phases present remain stable, other than quartz which does show some, slight, dissolution (while it remained stable in the CO_2 model). This likely reflects

The PilotSTRATEGY project has received funding from the European Union's Horizon 2020 research and innovation programme under grant agreement No. 101022664

the higher pH in the nitrogen model/experiment, at which quartz is slightly more soluble than at the relatively low pH induced by CO_2 acidification.

Aluminium concentrations within the model drop across the run, reflecting fluid oversaturation with respect to bioitite and montmorillonite which precipitate within the model equilibrium assemblage in small amounts (total precipitate of $7x10^{-9}$ mol and $1.5x10^{-6}$ mol, respectively) during the model runs. Aluminium concentrations do appear to drop in the experimental samples which may, likewise, suggest some precipitation of secondary clay or other Al bearing phase within the experiments. K and Mg concentrations show distinct drops in concentration during the experimental run, not reflected by the model results, indicating some, minor, secondary precipitation of a phase or phases not included in the model equilibrium assemblage: again, some minor precipitation of secondary clay phases is likely. The rise in silicon concentrations, due in the model to dissolution of k-feldspar, is more pronounced in the experimental results, suggesting more rapid dissolution of this phase than is predicted by the model, or contribution of Si from minor dissolution of other phases in the primary assemblage. pH values remain relatively stable throughout the run, both in the model and in the experiment and experimental values closely match those predicted by the model run.

The PilotSTRATEGY project has received funding from the European Union's Horizon 2020 research and innovation programme under grant agreement No. 101022664

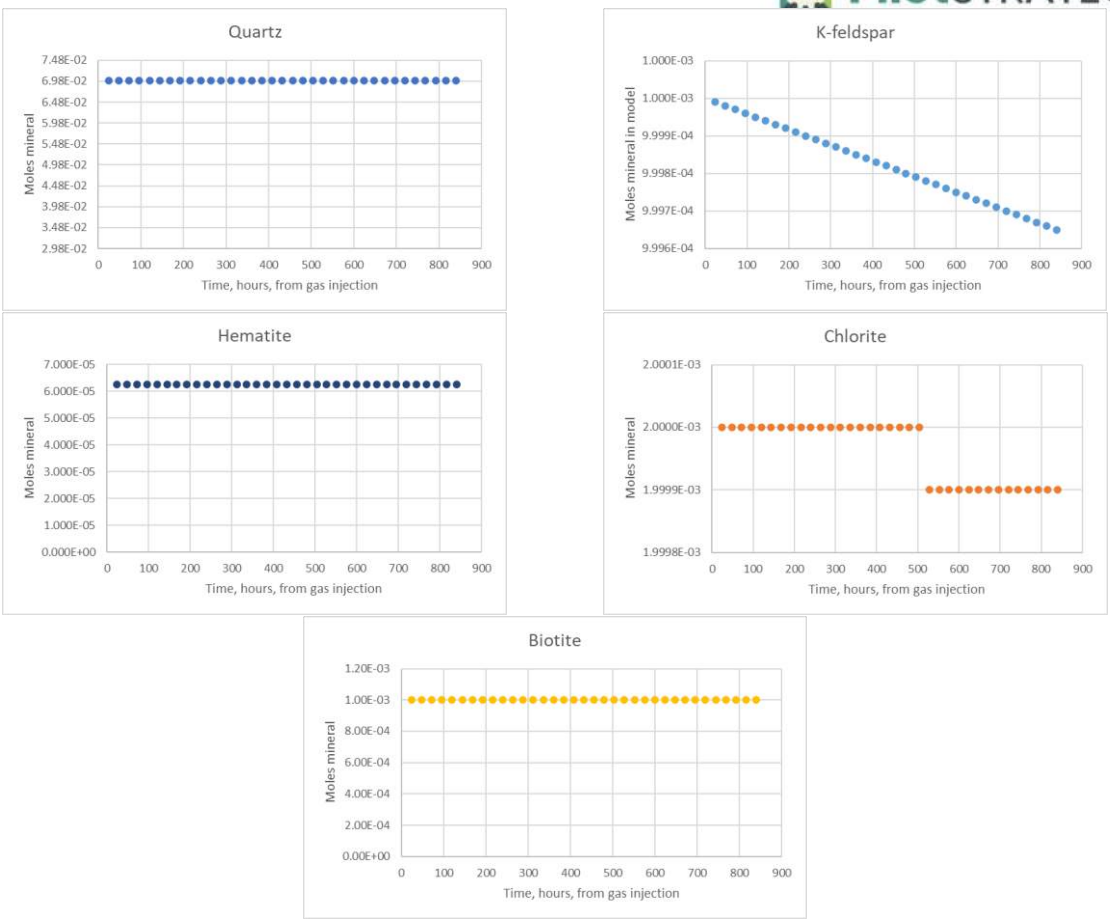

Figure 5.3: Amount mineral in reservoir sample model run with N_2.

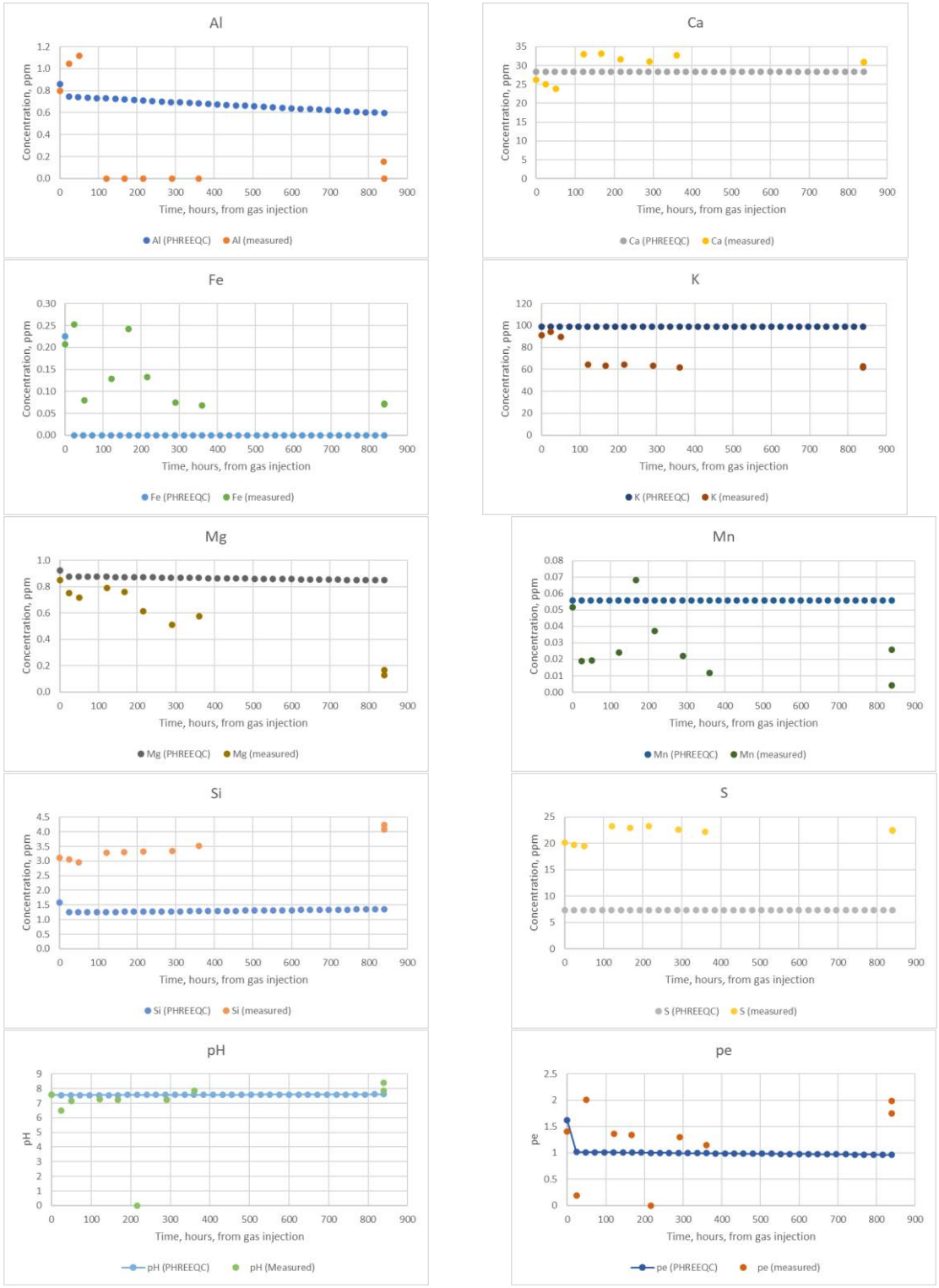

Figure 5.4: Modelled and measured fluid chemistry for reservoir sample experiment with N_2.

5.2.2 PR-11 (caprock sample)

The PR-11 sample is an anisotropic and heterogeneous marl from the Röt facies. Two varieties are distinguished according to the clay or carbonate predominance. Mineralogically, the marl has significant carbonate and clay content, with minor feldspar in a clay matrix with minor calcite cement. Both the grains and the matrix contain occasional Fe-oxides and/or hydroxides. The mineralogical composition includes calcite, dolomite, phyllosilicates (mica, kaolinite, smectite), quartz, K-feldspar and chlorite. XRD analysis of the specific sample used in the experimental work (see Table 5.1) indicates a primary assemblage of quartz (33%) K-feldspar (10%) chlorite (10%), micas (18%), calcite (13%) and montmorillonite (15%).

Figures 5.5–5.8 presents select results from the models of the CO_2 and N_2 pressurised batch experiments carried out using this sample: both mineral amounts and elemental concentrations over time are presented, together with the measured results from the experiments in the case of the elemental concentrations. In both the CO_2 and N_2 cases the model results reflect systems which are out of equilibrium but with low rates of reactivity and low overall levels of reaction over the time period employed, with the notable exception of calcite dissolution. Within the CO_2 model all available calcite is dissolved within the first timestep (one day), while other minerals within the primary assemblage remain stable, with the exception of K-feldspar which shows some minor dissolution over the course of the run.

Modelled Al, K and Si concentrations rise steadily for the duration of the run, reflecting dissolution of primary K-feldspar. Si and K concentrations in the experiment rise much more rapidly than predicted by the model results, exceeding modelled concentrations within the first few tens of hours of the runs and thereafter remaining largely stable. This may reflect a larger reactive surface area available within the experiment relative to the assumed model value, allowing for faster dissolution of the available K-feldspar. Aluminium remained below detection in the experimental samples, possibly reflecting precipitation of secondary aluminium oxide either in the experiments or during sampling.

Ca concentrations rise relatively sharply within the experiment, reflecting calcite dissolution, as per the model predictions. The dissolution is not as rapid as predicted and concentrations level off at around 900 ppm, well below the predicted concentration of 1900 ppm and show a slight drop in concentration towards the end of the run. The discrepancy may be explained by a lower than assumed available reactive surface area within the experiment, possibly through armouring of the calcite surface by secondary precipitate or by transport limitations (although experiments were agitated regularly). Magnesium concentrations also show a sharp, early, increase in the experiments, likely reflecting some magnesic/dolomitic component to the primary carbonate present, which is not reproduced within the model and which may also have contributed to the discrepancies between the modelled and experimental results.

The PilotSTRATEGY project has received funding from the European Union's Horizon 2020 research and innovation programme under grant agreement No. 101022664

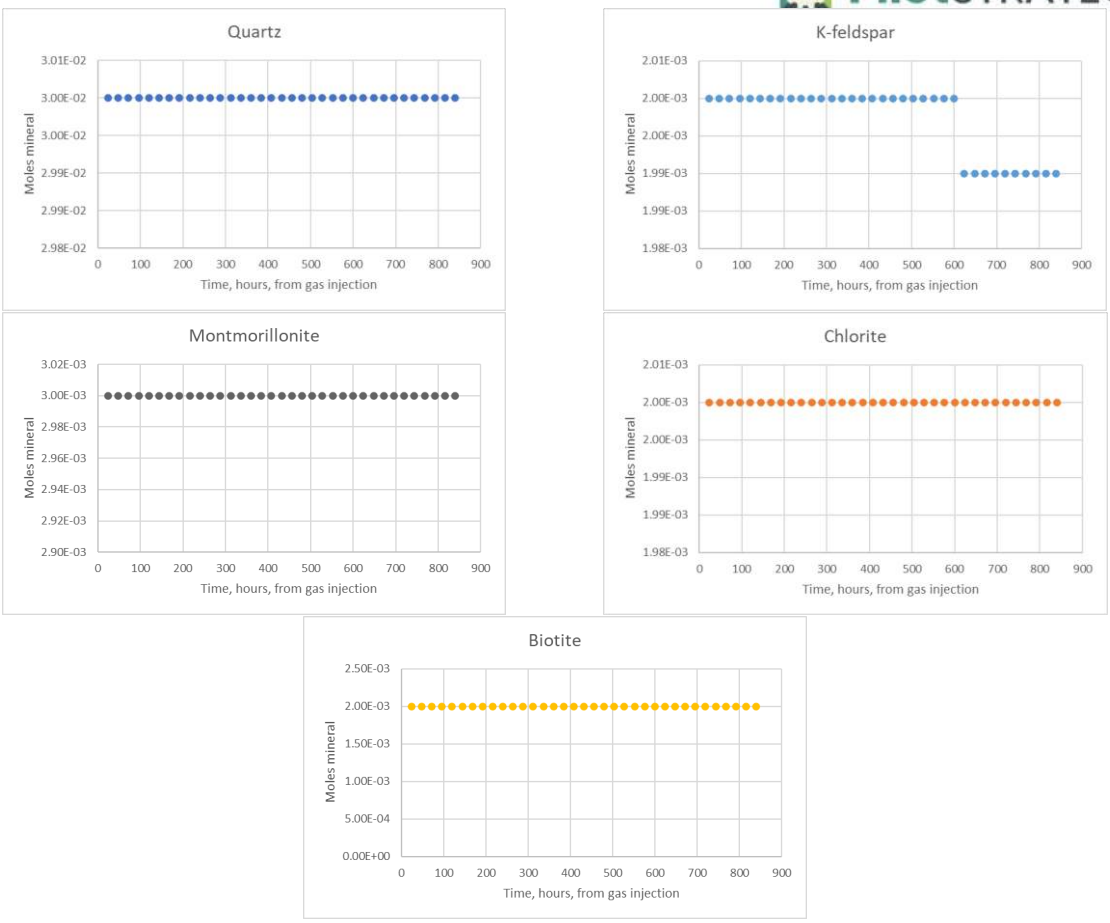

Figure 5.5: Amount mineral in reservoir sample model run with CO_2.

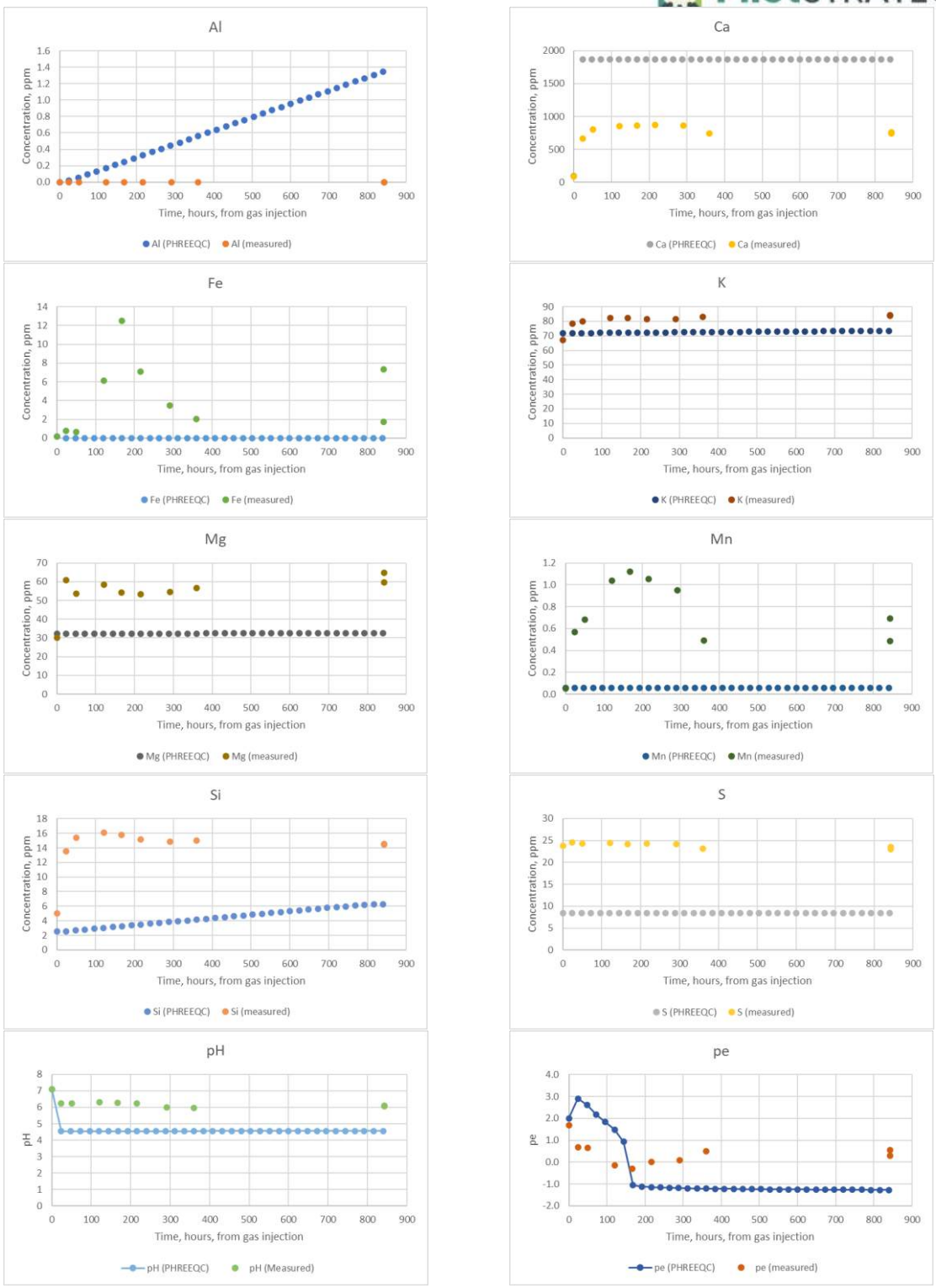

Figure 5.6: Modelled and measured fluid chemistry for reservoir sample experiment with CO_2.

The model results for the nitrogen case show very minor levels of reaction. Quartz and K-feldspar are dissolved throughout, though at very low rates. A minor amount of calcite is initially dissolved to bring the model fluid to equilibrium with calcite after which the calcite in the primary assemblage appears stable. However, between timesteps at 216 and 240 hours the equilibrium within the model appears

The PilotSTRATEGY project has received funding from the European Union's Horizon 2020 research and innovation programme under grant agreement No. 101022664

to shift, such that very low levels of calcite dissolution begins to occur. Other minerals within the primary assemblage remain stable throughout.

Modelled changes in fluid composition are likewise relatively small and largely reflect the stable concentrations observed in the experimental samples. A slight jump in Al concentrations is seen in the model between 216 and 240 hours, again reflecting a change in equilibrium and mineral saturation state within the model, while concentrations remain below detection in the experimental samples. Si shows a slight increase during the experimental run, while concentrations in the model are relatively suppressed, though approaching those observed in the samples by the end of the run. Potassium concentrations, through K-feldspar dissolution, increase during both the experimental and modelled runs, approaching similar values. Magnesium concentrations decrease slightly across both modelled and experimental runs. In the model run this reflects some minor precipitation of secondary montmorillonite and biotite. The drop in Mg is stronger in the experimental run but likely also reflects precipitation of a secondary Mg bearing phase.

The PilotSTRATEGY project has received funding from the European Union's Horizon 2020 research and innovation programme under grant agreement No. 101022664

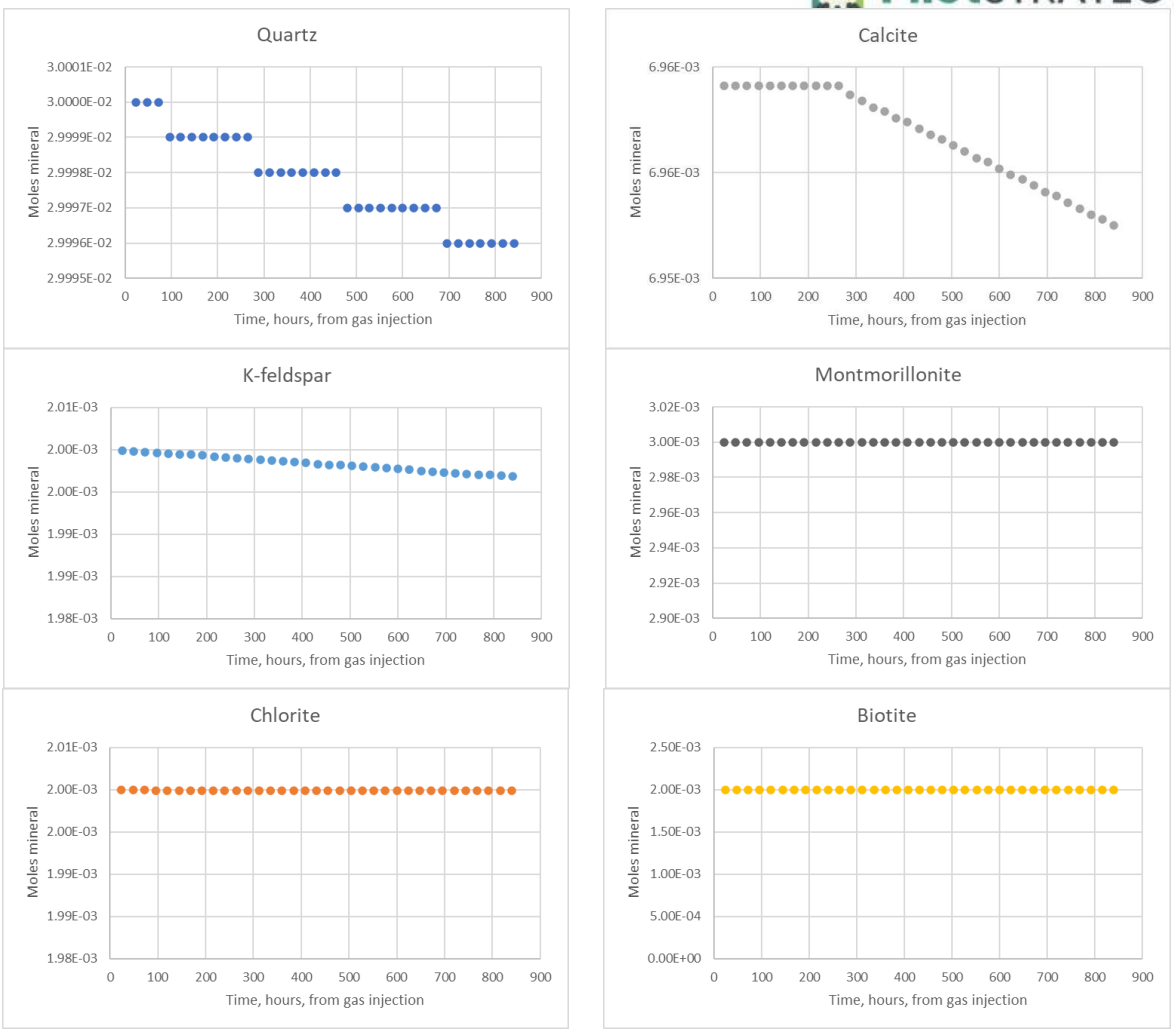

Figure 5.7: Amount mineral in reservoir sample model run with N_2.

The PilotSTRATEGY project has received funding from the European Union's Horizon 2020 research and innovation programme under grant agreement No. 101022664

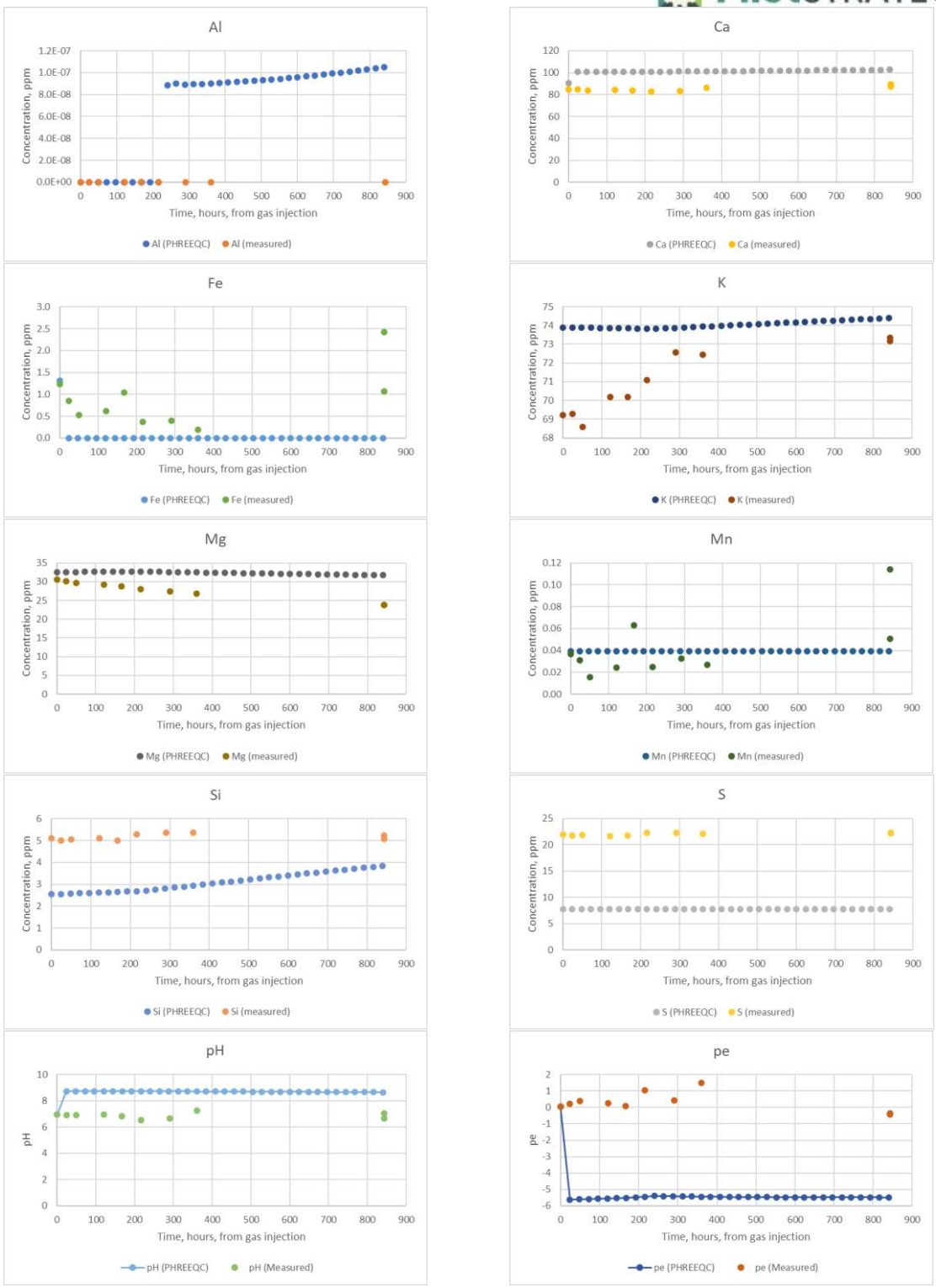

Figure 5.8: Modelled and measured fluid chemistry for reservoir sample experiment with N_2.

5.3 Discussion

The results from the modelling of the experiments utilising samples TA03 and PR11 show agreement, in a broad sense, to the results taken directly from the experiments. In the case of the CO_2 runs the models predict that reaction is largely limited to rapid dissolution of calcite (where present) with some, rate limited, dissolution of K-feldspar, with dissolution of other phases being minor, if occurring at all. This broadly agrees with results observed for the experiments themselves, where comparable increases in Ca, Al, Si and K were all noted. The accuracy of model predictions on the rate and absolute magnitude of dissolution varied somewhat between analytes and samples. In the case of the TA03 sample, the PHREEQC model very accurately predicts the rate of Al and K release as well as their absolute concentrations at most points during the run, while Si release is significantly under-reported by the model results. In the case of PR11 Ca and Al are released at rates and magnitudes considerably higher than those observed in the experiments, while Si release was, again, underreported.

These findings highlight some of the strengths of applying geochemical modelling to these kind of systems: a strong sense of the of the overall direction and magnitude of any major reaction can be easily established (e.g. carbonate dissolution, feldspar leaching, acidification of the brine, etc.). However, in detail, the results also highlight some of the shortcomings and issues with applying such models to complex mixed mineral systems.

As already pointed out the model results appear to vary considerably in their accuracy of prediction on dissolution magnitude and rate. A major shortcoming of the modelling here is the lack of any quantitative data on mineral reactive surface areas and how they change during the experimental runs. Even if a measurement of the total reactive surface area of the samples were available, the apportioning of that surface area between the different minerals in the system would still be problematic without considerable further effort. An attempt here was made to estimate reactive surface area based on grainsize and apportioned according to the weight percent of each mineral in the system. In some cases this appears to be a reasonable approach to reality (the results suggest that the K-feldspar in sample TA03 is reasonably accurately modelled, for example) while in other cases the surface area assumptions fall short (the excess Ca in solution predicted by the modelling for sample PR11, for example) and/or fail to take into account more complex processes such as armouring or significant secondary precipitation.

The other major issue likely to have caused discrepancy between the modelled and experimental results is mineral composition and purity. The XRD data used here to characterise sample mineralogy does not easily provide detail on mineral impurities, precise composition, or surface held cations all of which can have impacts on solution chemistry during dissolution, leaching, and solution-mineral ion exchange. Similarly, geochemical modelling relies on thermodynamic and kinetic data generally derived for “pure” mineral phases. Overcoming these limitations would require mineral specific compositional data (derived from micro-probe analysis, for example) and further tailoring of thermodynamic data choices to more closely match the phases in question. Such an approach clearly involves considerable effort and arguably, in many cases, negates the point of modelling in the first place: to provide a simplified conceptualisation of a system with broad-brush outputs.

Thus the modelling work provided here, when compared with the “real-life” experimental results indicates that simple geochemical modelling, using the likes of PHREEQC, can recreate major reaction where it occurs in these systems (i.e. calcite dissolution) and may be usefully employed at a larger scale (e.g. in reservoir modelling) to predict major impacts on system geochemistry. Where caution

The PilotSTRATEGY project has received funding from the European Union’s Horizon 2020 research and innovation programme under grant agreement No. 101022664

should be used is in over-extrapolation of detailed results from models for which major underlying assumptions (on, for example, surface area or mineral composition) have been made. In these cases such assumptions should be borne in mind and reliance on the absolute magnitude and rate of predicted reactions should be treated with due caution.

The PilotSTRATEGY project has received funding from the European Union's Horizon 2020 research and innovation programme under grant agreement No. 101022664

6. France

The geochemical reactivity of the lithostratigraphic units at the proposed pilot storage site in France was evaluated by the BRGM through a site-specific experimental program (PilotSTRATEGY Deliverable D2.9; Kilpatrick et al., 2025). The storage complex comprises a vertically stratified carbonate platform consisting of three principal formations (Figure 6-1): the Oolithe Blanche (Late Bathonian), the Comblanchian limestones (Late Bathonian), and the Dalle Nacrée (Early Callovian). The Oolithe Blanche serves as the primary reservoir for CO_2 injection due to its favorable petrophysical properties, while the overlying Comblanchian limestones and the Dalle Nacrée contribute additional intervals to the effective reservoir sequence. The reservoir sequence is overlain by Callovian marls, which form the basal unit of the regional caprock.

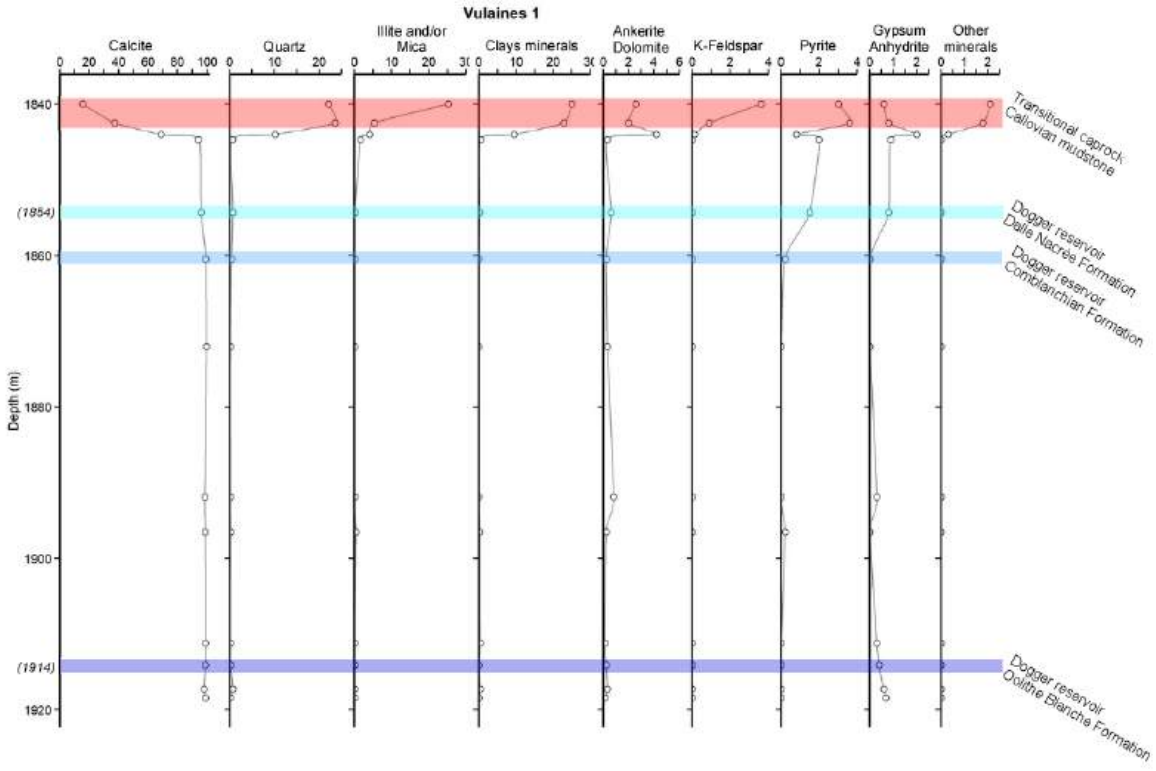

Figure 6-1. Semi-quantitative mineral composition of the formations with depth along the Vulaines 1 core, covering the three main formations composing the Dogger reservoir and the Callovian mudstone. Colored horizontal bars highlight the selected samples for the batch experiments.

The reservoir formations are characterized by a markedly carbonate-dominated mineralogy, with calcite constituting more than 95 wt.% of the bulk rock (Figure 6-1). The remaining mineral phases occur at very low abundances, generally near or below the quantification and detection limits (1–6 wt.%). Despite their minor proportions, these minerals are consistently present across the reservoir interval and include quartz, ankerite, dolomite, and gypsum. Pyrite and kaolinite are nearly ubiquitous, while illite is additionally detected in the uppermost reservoir unit (Dalle Nacrée), directly underlying the caprock. The overall homogeneity and strong dominance of calcite highlight the highly reactive carbonate nature of the reservoir formations, a key parameter for predicting mineral–fluid interactions during CO_2 storage.

The PilotSTRATEGY project has received funding from the European Union's Horizon 2020 research and innovation programme under grant agreement No. 101022664

The transitional caprock interval, represented by two distinct mudstone samples included in the batch experiments (pink line, Figure 6-1), exhibits a contrasting mineralogical composition. It is dominated by quartz and smectite, with variable quantities of calcite in the lower transitional unit (overlying the Dalle Nacrée) and illite in the intermediate caprock section. Minor constituents are a diverse assemblage comprising (i) clay minerals such as chlorite and kaolinite, (ii) detrital silicates including K-feldspar and plagioclase, (iii) carbonate phases such as dolomite, (iv) sulfate-bearing minerals including gypsum and redox-sensitive minerals such as pyrite and ankerite. Compared with the underlying carbonate -rich reservoir rocks, this mineralogical heterogeneity and reduced carbonate content impart distinct geochemical reactivity (and sealing properties) to the caprock.

Based on the availability of the representative core material, batch reaction experiments were conducted by BRGM on each major formation within the storage complex (PilotSTRATEGY Deliverable D2.9; Kilpatrick et al., 2025), including the transitional mudstone representative of the caprock interval. Batch reaction tests were conducted under in-situ reservoir pressure and temperature conditions (P_{tot} = 180 bar; T = 70 °C). Three CO_2 partial pressures (pCO_2) were imposed to reproduce natural reservoir conditions and to quantify the influence of CO_2 injection on fluid–rock interactions: (i) a pre-injection reference state (pCO_2 = 1 bar), (ii) a supercritical CO_2 condition (pCO_2 = 180 bar), and (iii) a dissolved CO_2 condition (pCO_2 = 50 bar).

Across all four tested formations, no unequivocal evidence for the formation of new secondary mineral phases – i.e., minerals absent from the initial mineralogical assemblage – was detected by either X-ray diffraction (XRD)–Rietveld refinement or SEM–EDS examination of post-experiment samples. Quantifying changes in the abundance of pre-existing minerals remains challenging due to the detection limits and analytical precision of X-ray diffraction. Temporal variations in synthetic brine composition over reaction durations of up to 35 days suggest that most mineralogical transformations occur over a very short time scale, likely preceding the earliest experimental sampling steps. Quantifying changes in the abundance of pre-existing minerals remains challenging due to the detection limits and analytical precision of X-ray diffraction

Although certain reactions could be inferred from the evolution of the fluid composition – such as the dominant role of calcite and, to a lesser extent, gypsum/anhydrite – a robust conceptual model could not be established consistently across the entire set of imposed pCO_2 conditions. This was particularly the case for the caprock, whose geochemical behaviour is difficult to generalize with confidence due to the complex mineralogical assemblage of the Callovian mudstone (containing up to 13 distinct mineral phases).

The modelling of the experimental results provides key constraints on the geochemical system, enabling improved calibration of the geochemical model and evaluation of the ability of numerical simulations to reproduce the observed evolution of brine composition over the course of the batch experiments. Overall, the extent to which numerical models can replicate the geochemical behaviour observed at laboratory scale contributes to building confidence in predictions of CO_2–brine–mineral interactions – specifically their nature, magnitude, and timescales – expected to occur in the reservoir and caprock when exposed to CO_2 under various physical states.

The PilotSTRATEGY project has received funding from the European Union's Horizon 2020 research and innovation programme under grant agreement No. 101022664

6.1 Model conceptualisation and set-up

The numerical simulations were carried out using a comprehensive geochemical modelling based on (i) a numerical code and a thermodynamic database to simulate geochemical equilibrium and reaction, and (ii) a conceptual model of CO_2–brine–mineral reactions and mineral-specific kinetic rate laws to constraint the geochemical system to the simulated reservoir sedimentary sequence and transitional caprock.

All simulations were performed with the PHREEQC v3 code (Parkhurst and Appelo, 2013), which enables the simulation of complex interactions between dissolved gases, aqueous solutions, and mineral assemblages in a batch configuration. Aqueous speciation and thermodynamic properties of most mineral phases were taken from the Thermoddem.dat database developed by BRGM (Blanc et al., 2012). To accurately represent the behaviour of CO_2 under reservoir pressure and temperature conditions, the modelling framework employed the Peng–Robinson equation of state (Peng & Robinson, 1976), implemented through PHREEQC. The Peng–Robinson equation of state is essential for describing the thermodynamic properties of CO_2 in both its gaseous and supercritical states, particularly near the critical point where non-ideal behaviour becomes significant. Its inclusion enables reliable calculation of fugacity coefficients, gas densities, and the solubility of CO_2 in brine, all of which directly affect the amount of dissolved CO_2 and is critical for constraining mineral-fluid reaction pathways. The models incorporated detailed aqueous speciation, mineral assemblages (Figure 6-1), and kinetic rate laws derived from Transition State Theory following Palandri and Kharaka (2004), with kinetic parameters accounting for pH-dependent effects on dissolution rates sourced from Palandri and Kharaka (2004) and Marty et al. (2015).

Geochemical models were developed for each of the three reservoir formations of the Dogger (one representative sample per formation) and for the two transitional caprock samples (Figure 6-1), to reflect the natural mineralogical variability within the storage complex. For each of these five samples, simulations were performed for the three pCO_2 conditions applied experimentally (1 bar, 50 bar, and 180 bar; Figure 6-2). To preserve reservoir pressure conditions, experiments at pCO_2 = 1 bar and 50 bar were conducted at a total pressure of 180 bar by adding nitrogen gas, at partial pressures of 179 bar and 130 bar, respectively. The same partial pressures (pN_2) were applied in the numerical models, after redefining N_2 as an inert species in the Phreeqc code to prevent spurious formation of NO_3^- or NH_4^+.

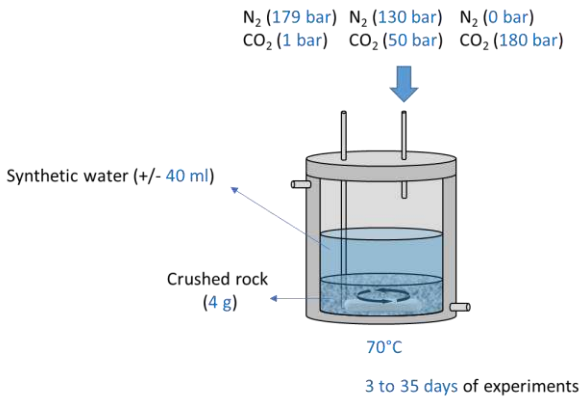

Figure 6-2. Batch experiments performed in reactors (total volume: 500 ml) of the BioREP platform.

The PilotSTRATEGY project has received funding from the European Union's Horizon 2020 research and innovation programme under grant agreement No. 101022664

All batch experiments were conducted using a synthetic brine of identical chemical composition for both for the reservoir and the caprock samples. The composition of the initial solution (t = 0) was formulated to match the experimental conditions (*Table 6.1.1*). Because the solution initially contained no dissolved carbonate species, the charge balance – imposed by fixing the initial pH – resulted in a numerically slightly more saline and strongly alkaline synthetic brine prior to addition of CO_2(g).

Table 6.1.1. Initial brine composition used in the batch experiment and resulting composition of the solution in PhreeqC with charge balance set on pH.

	Synthetic brine (Laboratory)	Synthetic brine (PhreeqC)
pH		11.34
Na (mg/l)	5600	5702
K (mg/l)	172	175
Ca (mg/l)	901	917
Mg (mg/l)	188	191
Cl (mg/l)	10167	10352
SO4 (mg/l)	762	776
HCO3 (mg/l)	(-)	(-)
SiO2 (mg/l)	39	40
Fe (mg/l)	(-)	(-)
Al (mg/l)	(-)	(-)

The reservoir formations exhibit broadly similar mineralogical compositions across the upper Dogger sequence, particularly in terms of mineral types. However, XRD–Rietveld analyses could not unambiguously differentiate the magnesium-rich carbonate phases – ankerite and dolomite – which are in any case a solid-solution series. There were uncertainties regarding both the phase identities and relative proportions. SEM analysis using the powdered samples is equally imprecise. However, the presence of pyrite within the mineralogical assemblage indicates reducing conditions within the reservoir, which supports the occurrence of ankerite. Together, pyrite and ankerite play a key role in controlling the redox state of the porous medium. Accordingly, both dolomite and ankerite were included within the batch simulation. Their relative proportions were arbitrarily set to 0.75 and 0.25 of the quantified mass of the combined total, respectively.

Pure Fe ankerite $CaFe(CO_3)_2$ has neither been observed in nature nor successfully synthetised in laboratory settings. Instead, natural ankerite occurs as part of the dolomite-ankerite solid-solution series, in which Fe^{2+} partially substitutes for Mg^{2+} within dolomite structure to form $Ca(Fe_xMg_{x-1})(CO_3)_2$, where x can vary from 26 to 71 mol% (Pham et al. 2011). For the present study, an ankerite composition of $CaFe_{0.7}Mg_{0.3}(CO_3)_2$ was selected, corresponding to a solid solution 70% ankerite and 30% dolomite. The thermodynamic parameters for ankerite were taken from Xu et al. (2006) and incorporated into the geochemical model as an additional mineral phase.

Dissolution kinetics were applied to all minerals except calcite, while precipitation rate constants were generally assumed equal to dissolution constants. At the onset of nucleation – i.e., when the mineral amount is zero, but the saturation index is positive – a nucleation surface area of 10^{-5} m² was imposed, since a mineral with no surface area will not grow in the simulations. Challenges remain in applying kinetic laws in numerical models, notably the uncertain representation of evolving surface roughness and reactive surface area during reaction progress. Initial specific surface areas were estimated between 20 to 60 m²/g for clay minerals and 2 m²/g for non-clay minerals (powder < 80 µm), following subsequent adjustments made during model calibration. This modelling framework provided a

The PilotSTRATEGY project has received funding from the European Union's Horizon 2020 research and innovation programme under grant agreement No. 101022664

consistent basis for evaluating mineral reactivity across the range of pCO_2 conditions investigated experimentally and for integrating laboratory findings into a coherent conceptual geochemical model.

Because most of the water-rock reactivity occurred over a very short time scale in the experiments, the initial conditions of the batch simulation (initialisation period, hereafter), were conceptually reformulated to reproduce the rapid early evolution of the system. The initialisation period includes an equilibration phase at atmospheric pressure and a temperature of 20°C, during which the crushed rock and synthetic brine are first brought into contact, followed by a sequence of simulations that replicate the experimental procedure (*Figure 6-3*). These operations comprise: (i) the removal of atmospheric air through injection of CO_2(g) at just above atmospheric pressure, (ii) an increase in total pressure achieved by adding CO_2 and N_2 partial pressures depending on the scenario, and (iii) a progressive increase of the temperature to reach reservoir conditions. This sequence imposes substantial variations in temperature, total pressure, and CO_2 partial pressure within a short period (< 90 minutes), representing a phase during which the system undergoes rapid geochemical adjustment. Incorporating this initialisation period into the numerical simulations allows these fast, pressure and temperature driven reactions to be captured, thereby enabling the model to subsequently track the evolution of slower driven reactions to be captured over the 1 to 35- to 35-day period reproduced experimentally.

Throughout both the initialisation and the subsequent 40 day period at reservoir pressure and temperature, the model allowed reversible dissolution and precipitation of primary and secondary minerals. Candidate secondary phases were selected based on literature data and on the evolution of mineral saturation indices during the simulations.The mineral assemblages of the rock samples, potential secondary minerals and their associated specific surface area considered within batch models are summarized for the Oolithe Blanche Formation (*Table 6.1.2*; *Table 6.1.3*), the Comblanchian Formation (

The PilotSTRATEGY project has received funding from the European Union's Horizon 2020 research and innovation programme under grant agreement No. 101022664

Table 6.1.4; *Table 6.1.5*), the Dalle Nacrée Formation (

The PilotSTRATEGY project has received funding from the European Union's Horizon 2020 research and innovation programme under grant agreement No. 101022664

Table 6.1.6; *Table 6.1.7*), the lower transitional caprock formation (

The PilotSTRATEGY project has received funding from the European Union's Horizon 2020 research and innovation programme under grant agreement No. 101022664

Table 6.1.8; *Table 6.1.9*) and the upper transitional caprock formation (

The PilotSTRATEGY project has received funding from the European Union's Horizon 2020 research and innovation programme under grant agreement No. 101022664

Table 6.1.10; *Table 6.1.11*).

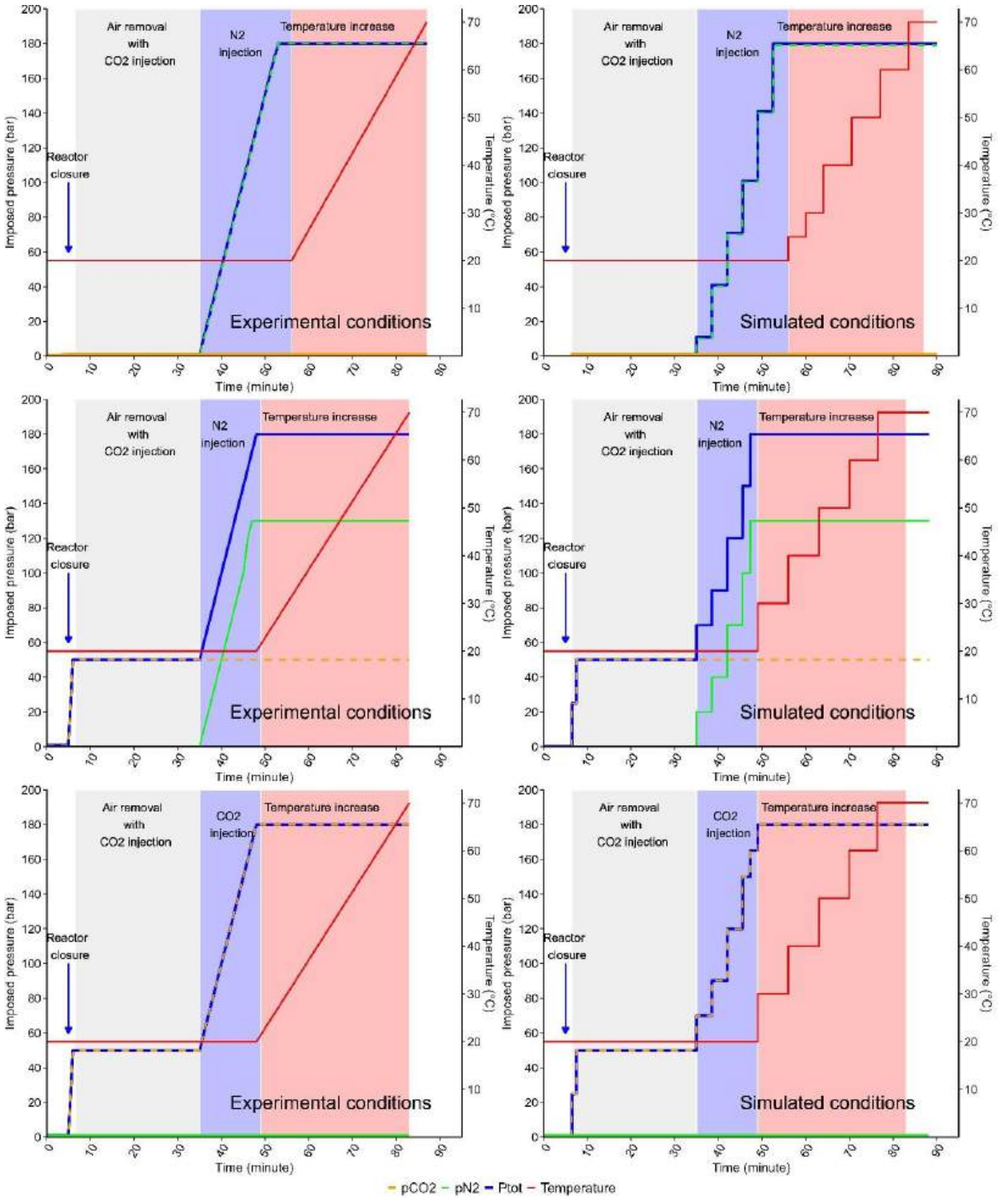

Figure 6-3. Evolution of the pressure and temperature conditions during the initialisation period of the experiments (left) and associated steps considered in the numerical simulations (right), for the experiment pCO_2 = 1 bar (top), pCO_2 = 50 bar (middle) and pCO_2 = 180 bars (bottom). The 40 days simulation following the initialisation period, not illustrated, starts after reaching a 70°C temperature in the reactor.

The PilotSTRATEGY project has received funding from the European Union's Horizon 2020 research and innovation programme under grant agreement No. 101022664

Table 6.1.2. Mineral assemblage identified by XRD-Rietveld and potential secondary minerals considered for the numerical simulation of the laboratory experiments dedicated to the Oolithe Blanche Formation.

Identified mineral by XRD Oolithe Blanche: VUS 1-1914 m	Weight percent (%)	Modelled mineral	Weight percent (%)	Composition
Calcite	99	Calcite	99	$CaCO_3$
Quartz	0.2	Quartz	0.2	SiO_2
Ankerite and/or Dolomite	0.2	Ankerite	0.05	$Ca(Mg_{0.3},Fe^{2+}_{0.7})(CO_3)_2$
		Dolomite	0.15	$Ca_{0.5}Mg_{0.5}CO_3$
Gypsum	0.4	Gypsum	0.4	$CaSO_4{:}2H_2O$
Kaolinite	0.1	Kaolinite	0.1	$Al_2SiO_2O_5(OH)_4$
Potential secondary minerals		Anhydrite	0	
		Chalcedony	0	
		Siderite	0	
		Magnesite	0	
		Gibbsite	0	
		Dawsonite	0	
		Montmorillonite	0	
		Illite	0	

Table 6.1.3. Mineral phase considered and associated specific surface area (SSA), kinetical parameter used for the numerical simulation of the laboratory experiments dedicated to the Oolithe Blanche Formation.

Modelled mineral	Moles in contact with 1l pore water	SSA (m^2/g)	Kinetic parameters
Calcite	0.0794197013	(-)	Equilibrium
Quartz	0.0002672649	2	Marty et al. 2015 *(dissolution/precipitation)*
Ankerite	0.0000194430	2	Palandri and Kharaka 2004 *(= dolomite; reversible dissolution)*
Dolomite	0.0000653129	2	Marty et al. 2015 *(dissolution/precipitation)*
Gypsum	0.0001865384	2	Palandri and Kharaka 2004 *(dissolution)*
Kaolinite	0.0000311015	20	Marty et al. 2015 *(dissolution/precipitation)*
Anhydrite	0.0	0.00001 / 0.01	Palandri and Kharaka 2004
Chalcedony	0.0	0.00001 / 0.01	Palandri and Kharaka 2004
Siderite	0.0	0.00001 / 0.01	Marty et al. 2015
Magnesite	0.0	0.00001 / 0.01	Palandri and Kharaka 2004
Gibbsite	0.0	0.00001 / 0.01	Marty et al. 2015
Dawsonite	0.0	0.00001 / 0.01	Palandri and Kharaka 2004
Montmorillonite	0.0	0.00001 / 0.01	Marty et al. 2015
Illite	0.0	0.00001 / 0.01	Smith et al, 2017

The PilotSTRATEGY project has received funding from the European Union's Horizon 2020 research and innovation programme under grant agreement No. 101022664

Table 6.1.4. Mineral assemblage identified by XRD-Rietveld and potential secondary minerals considered for the numerical simulation of the laboratory experiments dedicated to the Comblanchian Formation.

Identified mineral by XRD Comblanchian : VUS 1-1860 m	Weight percent (%)	Modelled mineral	Mass percent (%)	Composition
Calcite	99.2	Calcite	99.2	$CaCO_3$
Quartz	0.4	Quartz	0.4	SiO_2
Ankerite and/or Dolomite	0.2	Ankerite	0.05	$Ca(Mg,Fe^{2+})(CO3)_2$
		Dolomite	0.15	$Ca_{0.5}Mg_{0.5}CO_3$
Pyrite	0.2	Pyrite	0.2	FeS_2
Pressumed secondary minerals		Anhydrite	0	
		Chalcedony	0	
		Siderite	0	
		Magnesite	0	
		Gibbsite	0	
		Dawsonite	0	
		Kaolinite	0	
		Montmorillonite	0	
		Illite	0	

Table 6.1.5. Mineral phase considered and associated specific surface area (SSA), kinetical parameter used for the numerical simulation of the laboratory experiments dedicated to the Comblanchian Formation.

Modelled mineral	Moles in contact with 1l pore water	SSA (m^2/g)	Kinetic parameters
Calcite	0.0794620787	(-)	Equilibrium
Quartz	0.0005337367	2	Marty et al. 2015 *(dissolution/precipitation)*
Ankerite	0.0000194141	2	Palandri et al. 2004 *(= dolomite; reversible dissolution)*
Dolomite	0.0000652160	2	Marty et al. 2015 *(dissolution/precipitation)*
Pyrite	0.0001336444	0.001	Marty et al. 2015 *(dissolution only)*
Anhydrite	0.0	0.00001 / 0.01	Palandri and Kharaka 2004
Chalcedony	0.0	0.00001 / 0.01	Palandri and Kharaka 2004
Siderite	0.0	0.00001 / 0.01	Marty et al. 2015
Magnesite	0.0	0.00001 / 0.01	Palandri and Kharaka 2004
Gibbsite	0.0	0.00001 / 0.01	Marty et al. 2015
Dawsonite	0.0	0.00001 / 0.01	Palandri and Kharaka 2004
Kaolinite	0.0	0.00001 / 0.01	Marty et al. 2015
Montmorillonite	0.0	0.00001 / 0.01	Marty et al. 2015
Illite	0.0	0.00001 / 0.01	Smith et al, 2017

The PilotSTRATEGY project has received funding from the European Union's Horizon 2020 research and innovation programme under grant agreement No. 101022664

Table 6.1.6. Mineral assemblage identified by XRD-Rietveld and potential secondary minerals considered for the numerical simulation of the laboratory experiments dedicated to the Dalle Nacrée Formation.

Identified mineral by XRD Dalle Nacrée : VUS 1-1854 m	Weight percent (%)	Modelled mineral	Mass percent (%)	Composition
Calcite	96	Calcite	96	$CaCO_3$
Quartz	0.7	Quartz(alpha)	0.7	SiO_2
Ankerite and/or Dolomite	0.6	Ankerite	0.15	$CaMg_{0.3}Fe_{0.7}(CO_3)_2$
		Dolomite	0.45	$CaMg(CO_3)_2$
Illite and/or mica	0.1	Illite	0.1	$K_{0.85}Al_{2.85}Si_{3.15}O_{10}(OH)_2$
Pyrite	1.5	Pyrite	1.5	FeS_2
Gypsum	0.8	Gypsum	0.8	$CaSO_4$:2H2O
Kaolinite	0.3	Kaolinite	0.3	$Al_2Si_2O_5(OH)_4$
Pressumed secondary minerals		Anhydrite	0	
		Chalcedony	0	
		Siderite	0	
		Magnesite	0	
		Gibbsite	0	
		Dawsonite	0	
		Montmorillonite	0	

Table 6.1.7. Mineral phase considered and associated specific surface area (SSA), kinetical parameter used for the numerical simulation of the laboratory experiments dedicated to the Dalle Nacrée Formation.

Modelled mineral	Moles in contact with 1l pore water	SSA (m^2/g)	Kinetic parameters
Calcite	0.0764947777	(-)	Equilibrium
Quartz(alpha)	0.0009291320	2	Marty et al. 2015 *(dissolution/precipitation)*
Ankerite	0.0000579364	2	Palandri et al. 2004 *(= dolomite; reversible dissolution)*
Dolomite	0.0001946200	2	Marty et al. 2015 *(dissolution/precipitation)*
Illite(Al)	0.0000203132	40	Smith et al, 2017
Pyrite	0.0009970668	0.001	Marty et al. 2015 *(dissolution only)*
Gypsum	0.0003705661	2	Palandri et al. 2004 *(dissolution)*
Kaolinite	0.0000926767	5	Marty et al. 2015 *(dissolution/precipitation)*
Anhydrite	0.0	0.00001 / 0.01	Palandri and Kharaka 2004
Chalcedony	0.0	0.00001 / 0.01	Palandri and Kharaka 2004
Siderite	0.0	0.00001 / 0.01	Marty et al. 2015
Magnesite(Natur)	0.0	0.00001 / 0.01	Palandri and Kharaka 2004
Gibbsite	0.0	0.00001 / 0.01	Marty et al. 2015
Dawsonite	0.0	0.00001 / 0.01	Palandri and Kharaka 2004
Montmorillonite	0.0	0.00001 / 0.01	Marty et al. 2015

The PilotSTRATEGY project has received funding from the European Union's Horizon 2020 research and innovation programme under grant agreement No. 101022664

Table 6.1.8. Mineral assemblage identified by XRD-Rietveld and potential secondary minerals considered for the numerical simulation of the laboratory experiments dedicated to the lower transitional caprock Formation.

Identified mineral by XRD Transitional caprock: VUS 1-1842.5 m	Weight percent (%)	Modelled mineral	Mass percent (%)	Composition
Calcite	37.2	Calcite	37.2	$CaCO_3$
Quartz	23.6	Quartz	23.6	SiO_2
Ankerite	2	Ankerite	2	$CaMg_{0.3}Fe_{0.7}(CO_3)_2$
Illite and/or mica	5.3	Illite	5.3	$K_{0.85}Mg_{0.25}Al_{2.35}Si_{3.4}O_{10}(OH)_2$
Pyrite	3.6	Pyrite	3.6	FeS_2
Gypsum	0.8	Gypsum	0.8	$CaSO_4{:}2H_2O$
Kaolinite	1.5	Kaolinite	1.5	$Al_2Si_2O_5(OH)_4$
Dolomite	1.3	Dolomite	1.3	$CaMg(CO_3)_2$
Smectite and/or interstratified illite/smectite	19.2	Montmorillonite	19.2	$Na_{0.34}Mg_{0.34}Al_{1.66}Si_4O_{10}(OH)_2{:}3.003H_2O$
Chlorite	2.2	Clinochlore	2.3	$Mg_5Al(AlSi_3)O_{10}(OH)_8$
K Feldspar	0.9	Microcline	1.4	$K(AlSi_3)O_8$
Anatase	0.5		(-)	
Pressumed secondary minerals		Anhydrite	0	
		Chalcedony	0	
		Siderite	0	
		Magnesite(Natur)	0	
		Gibbsite	0	
		Dawsonite	0	

Table 6.1.9. Mineral phase considered and associated specific surface area (SSA), kinetical parameter used for the numerical simulation of the laboratory experiments dedicated to the lower transitional caprock Formation.

Modelled mineral	Moles in contact with 1l pore water	SSA (m2/g)	Kinetic parameters
Calcite	0.0306213213	(-)	Equilibrium
Quartz	0.0323602467	2	Marty et al. 2015 *(dissolution/precipitation)*
Ankerite	0.0007980143	2	Palandri et al. 2004 *(= dolomite; reversible dissolution)*
Illite	0.0011121779	40	Smith et al, 2017
Pyrite	0.0024720424	0.001	Marty et al. 2015 *(dissolution only)*
Gypsum	0.0003828125	2	Palandri et al. 2004 *(dissolution)*
Kaolinite	0.0004786973	20	Marty et al. 2015 *(dissolution/precipitation)*
Dolomite	0.0005808162	72	Marty et al. 2015 *(dissolution/precipitation)*
Montmorillonite	0.0037544628	60	Marty et al. 2015
Clinochlore	0.0003261108	5	Marty et al. 2015
Microcline	0.0002664023	2	Palandri and Kharaka 2004
Anhydrite	0.0	0.00001 / 0.01	Palandri and Kharaka 2004
Chalcedony	0.0	0.00001 / 0.01	Palandri and Kharaka 2004
Siderite	0.0	0.00001 / 0.01	Marty et al. 2015
Magnesite	0.0	0.00001 / 0.01	Palandri and Kharaka 2004
Gibbsite	0.0	0.00001 / 0.01	Marty et al. 2015
Dawsonite	0.0	0.00001 / 0.01	Palandri and Kharaka 2004

The PilotSTRATEGY project has received funding from the European Union's Horizon 2020 research and innovation programme under grant agreement No. 101022664

Table 6.1.10. Mineral assemblage identified by XRD-Rietveld and potential secondary minerals considered for the numerical simulation of the laboratory experiments dedicated to the upper transitional caprock Formation.

Identified mineral by XRD Transitional caprock: VUS 1-1840 m	Weight percent (%)	Modelled mineral	Mass percent (%)	*Composition*
Calcite	15.8	Calcite	15.8	$CaCO_3$
Quartz	22.1	Quartz	22.1	SiO_2
Ankerite	2.6	Ankerite	2.6	$CaMg_{0.3}Fe_{0.7}(CO_3)_2$
Illite and/or mica	25.2	Illite	25.2	$K_{0.85}Mg_{0.25}Al_{2.35}Si_{3.4}O_{10}(OH)_2$
Pyrite	3	Pyrite	3	FeS_2
Gypsum	0.6	Gypsum	0.6	$CaSO_4{:}2H_2O$
Kaolinite	3.2	Kaolinite	3.2	$Al_2Si_2O_5(OH)_4$
Dolomite	1.3	Dolomite	1.3	$CaMg(CO_3)_2$
Smectite and/or interstratified illite/smectite	19.5	Montmorillonite	19.5	$Na_{0.34}Mg_{0.34}Al_{1.66}Si_4O_{10}(OH)_2{:}3.003H_2O$
Chlorite	2.3	Clinochlore	2.3	$Mg_5Al(AlSi_3)O_{10}(OH)_8$
Plagioclase	2.2	Albite	2.2	$NaAlSi_3O_8$
K Feldspar	1.4	Microcline	1.4	$K(AlSi_3)O_8$
Anatase	0.8		(-)	
Pressumed secondary minerals		Anhydrite	0	
		Chalcedony	0	
		Siderite	0	
		Magnesite	0	
		Gibbsite	0	
		Dawsonite	0	

Table 6.1.11. Mineral phase considered and associated specific surface area (SSA), kinetical parameter used for the numerical simulation of the laboratory experiments dedicated to the upper transitional caprock Formation.

Modelled mineral	Moles in contact with 1l pore water	SSA (m2/g)	Kinetic parameters
Calcite	0.0126139886	(-)	Equilibrium
Quartz	0.0293904648	2	Marty et al. 2015 *(dissolution/precipitation)*
Ankerite	0.0010061631	2	Palandri et al. 2004 *(= dolomite; reversible dissolution)*
Illite	0.0051287710	40	Smith et al, 2017
Pyrite	0.0019979703	0.001	Marty et al. 2015 *(dissolution only)*
Gypsum	0.0002784593	2	Palandri et al. 2004 *(dissolution)*
Kaolinite	0.0009904534	20	Marty et al. 2015 *(dissolution/precipitation)*
Dolomite	0.0005633173	2	Marty et al. 2015 *(dissolution/precipitation)*
Montmorillonite	0.0036982439	60	Marty et al. 2015
Clinochlore	0.0003306623	5	Marty et al. 2015
Albite	0.0006703860	2	Palandri and Kharaka 2004
Microcline	0.0004019184	2	Palandri and Kharaka 2004
Anhydrite	0.0	0.00001 / 0.01	Palandri and Kharaka 2004
Chalcedony	0.0	0.00001 / 0.01	Palandri and Kharaka 2004
Siderite	0.0	0.00001 / 0.01	Marty et al. 2015
Magnesite	0.0	0.00001 / 0.01	Palandri and Kharaka 2004
Gibbsite	0.0	0.00001 / 0.01	Marty et al. 2015
Dawsonite	0.0	0.00001 / 0.01	Palandri and Kharaka 2004

The PilotSTRATEGY project has received funding from the European Union's Horizon 2020 research and innovation programme under grant agreement No. 101022664

6.2 Modelling results for the reservoir formation

The mineral composition of the three reservoir formations exhibits limited qualitative variability. All units contain carbonate minerals—primarily calcite, dolomite, and ankerite—together with quartz, with calcite representing the dominant phase (96 – 99%).

The Oolithe Blanche Formation is further distinguished by the presence of accessory minerals such as gypsum and kaolinite (*Table 6.1.2*). In contrast, the Comblanchien Formation is characterized by the occurrence of pyrite and by the absence of clay minerals or gypsum (

The PilotSTRATEGY project has received funding from the European Union's Horizon 2020 research and innovation programme under grant agreement No. 101022664

Table 6.1.4). The Dalle Nacrée Formation displays the greatest mineralogical diversity, incorporating sulfur-bearing phases (gypsum and pyrite) as well as clay minerals (kaolinite and illite), thus encompassing the full suite of mineral phases identified separately in the Oolithe Blanche and Comblanchien Formations (

Table 6.1.6).

The evolution of these mineral phases under varying pCO_2 conditions, as predicted by geochemical modeling, is presented for each reservoir formation. The corresponding impacts on aqueous phase composition are then evaluated and compared with the water chemistry measured during laboratory experiments.

6.2.1 Oolithe blanche Formation

During the initialisation period, the first interaction between the crushed rock material and the synthetic brine results in rapid and extensive gypsum dissolution, leading to a near-total dissolution: –99.9 % of the initial mineral concentration in 1L of brine (hereafter mol%). This dissolution is slightly offset by minor calcite precipitation (+0.13 mol%) (Figure 6-4). Limited dissolution of dolomite (–0.1 mol%) and ankerite (–1.25 mol%) is also observed during this stage.

The subsequent air-removal sub-step, achieved through CO_2(g) injection, induces rapid calcite dissolution (–0.35 mol% to –1.95 mol%) within the first minutes of exposure (Figure 6-4). The magnitude of dissolution correlates directly with the imposed pCO_2. Under conditions representative of natural systems (pCO_2 = 1 bar), calcite dissolution remains moderate (3.01×10^{-4} mol·L^{-1}). In contrast, in experimental scenarios where pCO_2 increases to 50 bar during air removal, calcite dissolution is markedly higher (1.94×10^{-3} mol·L^{-1}). Although present in lower modal proportions, ankerite and dolomite also undergo partial dissolution during this sub-step, reaching up to -36.6% for ankerite and -9.1 mol% for dolomite.

During the subsequent pressurisation sub-step, in which the system pressure is increased to 180 bar, calcite dissolution remains limited under the scenario targeting a final pCO_2 of 1 bar (–0.25 mol%) (Figure 6-4). In this case, most of the pressure increase is achieved via the addition of pN_2, an inert gas with negligible solubility in the aqueous phase. Conversely, in scenarios targeting final pCO_2 of 50 and 180 bar, the models predict pronounced dissolution of calcite (–2.0 mol% and –2.8 mol%, respectively), as well as extensive dissolution of ankerite (–40% and –43%) and dolomite (–12.6 mol% and –13.32 mol%). This enhanced dissolution is driven by the rise in total pressure primarily through an increase in pCO_2 during this sub-step.

The PilotSTRATEGY project has received funding from the European Union's Horizon 2020 research and innovation programme under grant agreement No. 101022664

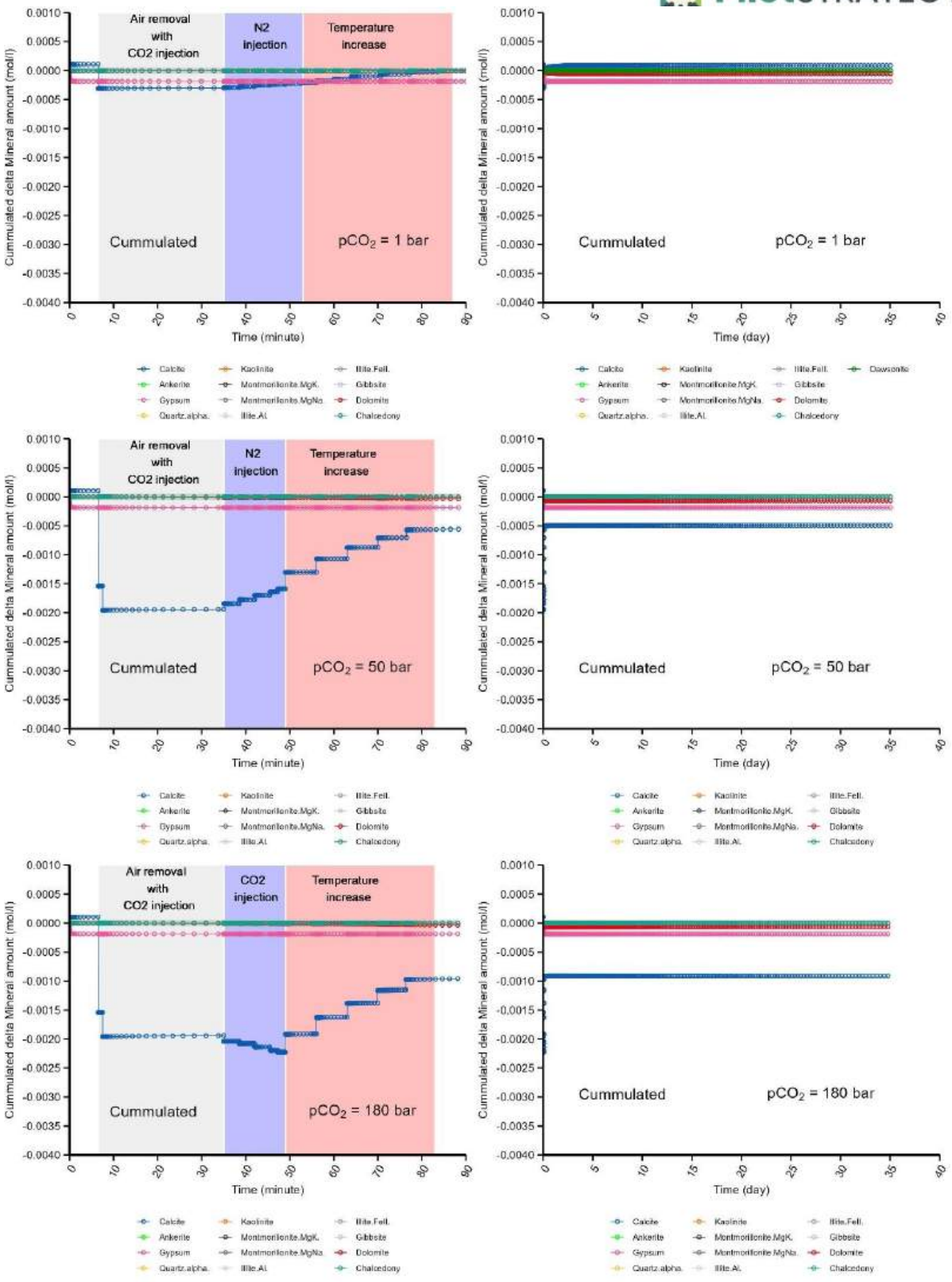

Figure 6-4: Amount of dissolved (< 0) or precipitated (> 0) mineral – compared to the initial concentration –composing the mineral assemblage of the Oolithe Blanche Formation over the initialisation period (left; time in minute) and the experimental part (left, time in day) for the three study scenarios: pCO_2 1 bar (top), pCO_2 50 bar (middle), pCO_2 180 bar (bottom).

The PilotSTRATEGY project has received funding from the European Union's Horizon 2020 research and innovation programme under grant agreement No. 101022664

During the temperature -increase sub-step, from 20 to 70 °C, calcite (re)precipitation is promoted (Figure 6-4). Following the rise to 70 °C – corresponding to the end of the initialization phase – the calcite content in the scenario with pCO_2 = 1 bar returns to a value essentially equal to its initial abundance (99.9%$_{t0}$). Although calcite (re)precipitation also occurs in the scenarios with elevated pCO_2, the modeled calcite proportions remain below their initial values (98.9%$_{t0}$ at pCO_2 = 50 bar; 98.5%$_{t0}$ at pCO_2 = 180 bar). This temperature -increase sub-step additionally induces systematic ankerite precipitation and enhances dolomite dissolution, the latter being substantially more pronounced under high pCO-pCO_2 conditions (−27 mol% at 50 bar; −33 mol% at 180 bar). Furthermore, the model predicts anhydrite precipitation once the system reaches 40 °C, occurring exclusively in the pCO_2 = 180 bar scenario.

Beyond the initialization period, carbonate mineral concentrations remain relatively stable, with only minor calcite precipitation driven by ongoing dolomite dissolution (Figure 6-4). Dolomite continues to dissolve progressively under all scenarios, reaching 22% t_0 of its initial mass fraction in the 1 bar scenario, and undergoing near -complete dissolution (−99.9%) in both the 50 and 180 bar scenarios (Figure 6-5). Over the 40 day period, the minerals exhibiting the greatest relative changes in abundance are, in decreasing order: calcite, gypsum/anhydrite, dolomite, and ankerite – all of which display fast reaction kinetics. Within the Oolithe Blanche mineralogical assemblage, kaolinite is the only primary mineral with slow dissolution kinetics, and models indicate a gradual dissolution throughout the initialisation and experimental periods (Figure 6-5).

A mass balance assessment of the modeled reaction processes – based on the conceptual framework underlying the numerical simulations – shows that the greatest calcite dissolution occurs at the end of the pressure increase sub-step. At this stage, dissolved calcite quantity relative to the initial content reach 1.75×10^{-4} mol·L^{-1} (−0.22 mol%) at pCO_2 = 1 bar, 1.30×10^{-3} mol·L^{-1} (−1.64 mol%) at pCO_2 = 50 bar, and 1.91×10^{-3} mol·L^{-1} (−2.41 mol%) at pCO_2 = 180 bar. After 40 days, calcite dissolution amounts to 4.95×10^{-4} mol·L^{-1} (−0.62 mol%) and 9.12×10^{-4} mol·L^{-1} (−1.15 mol%) in the 50 bar and 180 bar scenarios, respectively, while slight calcite precipitation occurs in the 1 bar scenario (8.81×10^{-5} mol·L^{-1}; +0.11 mol%). In mass fraction terms within the solid phase, the rapid dissolution of gypsum and the progressive dissolution of dolomite and kaolinite across the simulation period lead to slightly increase the proportion of calcite (> 99.35%) within the mineral assemblage compared to its initial content determined by XRD-Rietveld (99%).

Among the accessory minerals, quartz remains inert, while ankerite (−8 to −24 mol%), dolomite (−77 to −100 mol%), and gypsum (−100 mol%) exhibit substantial dissolution over the 40 day interval, with lower dissolution extents observed in the 1 bar scenario. Despite continuous kaolinite dissolution, the total amount dissolved remains negligible (< 0.36 mol%).

The PilotSTRATEGY project has received funding from the European Union's Horizon 2020 research and innovation programme under grant agreement No. 101022664

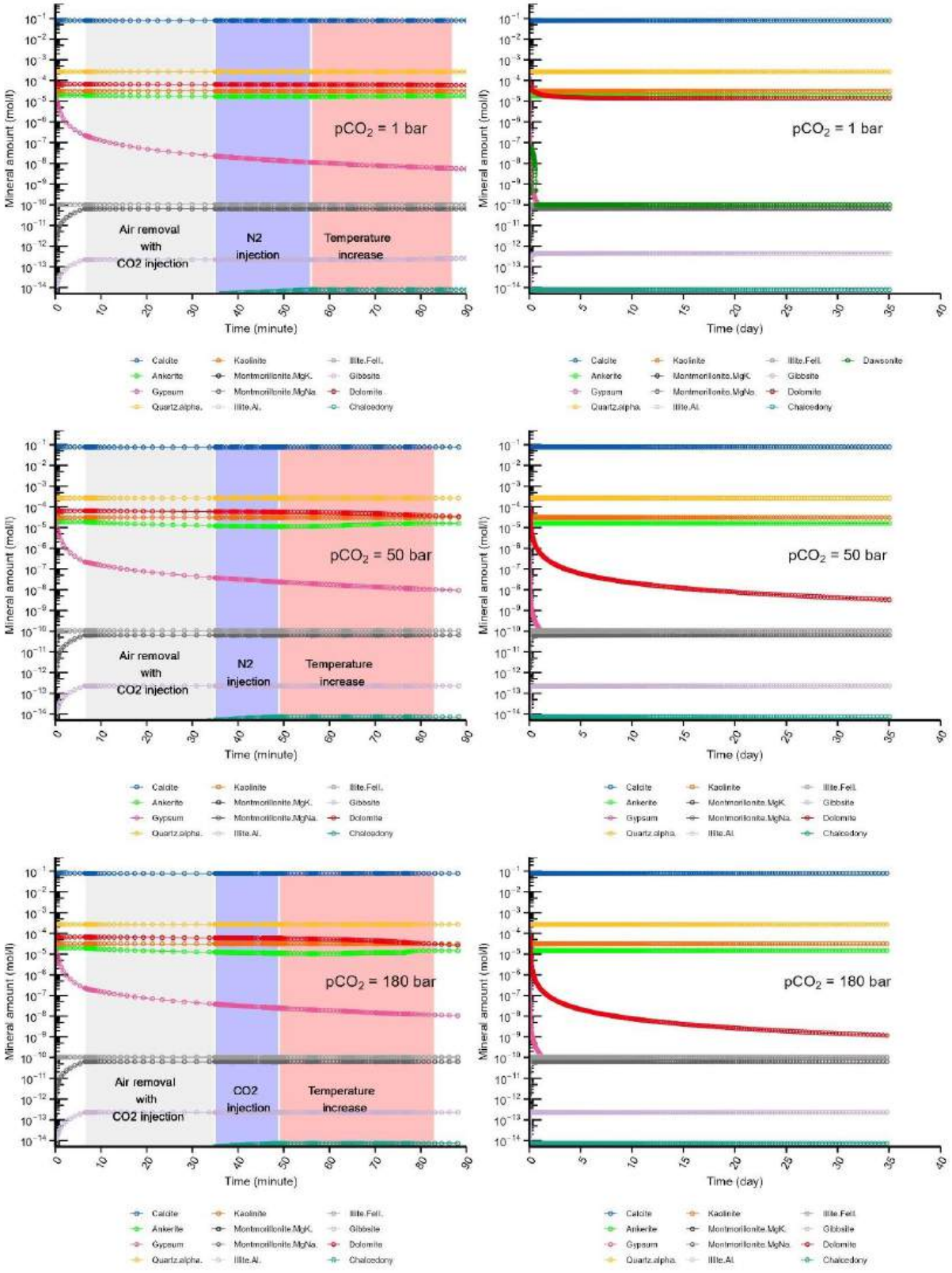

Figure 6-5: Evolution of the mineral total amount (in mol for 1L of brine) within the mineral assemblage of the Oolithe Blanche Formation over the initialisation period (left; time in minute) and the experimental part (left, time in day) for the three study scenarios: pCO_2 1 bar (top), pCO_2 50 bar (middle), pCO_2 180 bar (bottom).

The PilotSTRATEGY project has received funding from the European Union's Horizon 2020 research and innovation programme under grant agreement No. 101022664

No newly formed secondary mineral phases were detected by XRD–Rietveld analysis at the end of the laboratory experiments, although this could be due to high water-rock ratios. Nevertheless, numerical simulations incorporating available reaction kinetic data suggest the potential precipitation of secondary minerals such as gibbsite (<3.2 x 10^{-15} mol·L^{-1}), chalcedony (<3.2 x 10^{-16} mol·L^{-1}), and clay phases (illite and mixed smectite–illite assemblages). These phases are predicted to form predominantly at the onset of the initialisation period, during the first interaction between the synthetic brine and the crushed mineral material. The pressure increase associated with elevated pCO_2 exerts only a limited influence on the stability or evolution of these secondary minerals throughout the experimental period.

Despite substantial uncertainties in predicted concentrations – arising from factors such as reactive surface area, nucleation thresholds, and precipitation kinetics – the simulations indicate that the formation of illite and/or smectite–illite (montmorillonite) phases within the Oolithe Blanche Formation is plausible. The extremely low concentrations of these predicted phases (< 10^{-11} mol·L^{-1}) are consistent with the slow kinetics of clay precipitation and their absence in XRD–Rietveld measurements at the end of the experiment, given the detection limits of this analytical method. Moreover, their negligible mass fractions imply that these secondary phases exert no meaningful influence on the overall reactivity of the mineral assemblage under conditions involving either supercritical CO_2 (pCO_2 = 180 bar) or dissolved CO_2 (pCO_2 = 50 bar).

6.2.2 Comblanchian Formation

The reactions occurring in the Comblanchian Formation are broadly comparable to those identified in the Oolithe Blanche Formation, reflecting the close similarity in their mineralogical composition.

During the initial interaction between the rock powder and the synthetic brine, calcite precipitation is observed (+0.13%) (Figure 6-6). Minor dissolution of dolomite (−0.09 mol%) and ankerite (−1.1 mol%) also occurs (Figure 6-6), accompanied by negligible pyrite dissolution (−0.0005 mol%).

During the air removal and subsequent pressurization steps – achieved through CO_2(g) and N_2(g) injection – progressive calcite dissolution takes place, together with limited dolomite dissolution (Figure 6-6). The magnitude of carbonate mineral dissolution is directly controlled by the imposed pCO_2. Under the pCO_2 = 1 bar scenario, calcite and dolomite dissolution remain minor (−0.14 mol% and −3.9 mol%, respectively). Dissolution intensifies under elevated pCO_2, with moderate to substantial dissolution observed at 50 bar (calcite: −2.0 mol%; dolomite: −12 mol%) and pronounced dissolution at 180 bar (calcite: −2.9 mol%; dolomite: −13 mol%).

The PilotSTRATEGY project has received funding from the European Union's Horizon 2020 research and innovation programme under grant agreement No. 101022664

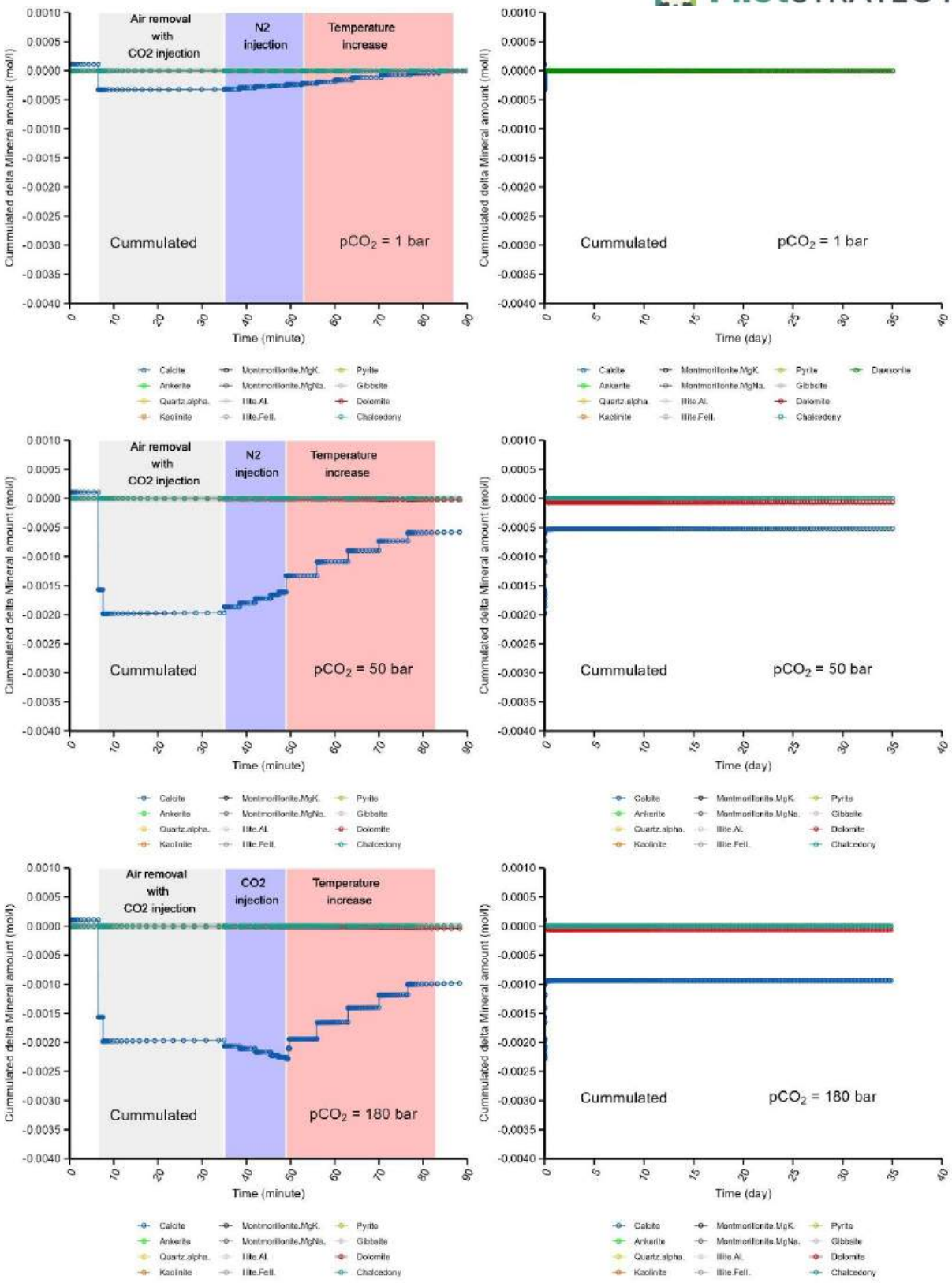

Figure 6-6: Amount of dissolved (< 0) or precipitated (> 0) mineral – compared to the initial concentration – composing the mineral assemblage of the Comblanchian Formation over the initialisation period (left; time in minute) and the experimental part (left, time in day) for the three study scenarios: pCO_2 1 bar (top), pCO_2 50 bar (middle), pCO_2 180 bar (bottom).

The PilotSTRATEGY project has received funding from the European Union's Horizon 2020 research and innovation programme under grant agreement No. 101022664

Ankerite behavior exhibits scenario-dependent variability, but dissolution predominates during intervals of CO_2 injection and pressure increase. At pCO_2 = 1 bar, ankerite dissolution occurs mainly during the brief CO_2 injection period (−12 mol%), followed by a re-equilibration. In the 50 bar scenario, ankerite undergoes substantial dissolution during CO_2(g) injection (−38 mol%), with additional dissolution during N_2 driven pressurization (−42 mol%). Under the 180 bar condition, ankerite dissolution persists throughout the entire pressure increase phase (−42 mol%), as pCO_2 continues to rise within the batch system. In contrast, pyrite dissolution remains minimal in all scenarios, indicating a very low sensitivity to pCO_2 variations.

The temperature increase sub-increase sub-step promotes substantial calcite (re)precipitation, resulting in calcite abundances equivalent to 100.12%$_{t0}$ of the initial concentration under the pCO_2 = 1 bar scenario, 99.1%$_{t0}$ under the pCO_2 = 50 bar scenario, and 98.5%$_{t0}$ under the pCO_2 = 180 bar scenario (Figure 6-6). This temperature rise also enhances dolomite dissolution – although to a much lesser extent than calcite – and induces ankerite (re)precipitation across all scenarios. Dolomite dissolution becomes particularly significant under elevated pCO_2 conditions, reaching −33 mol% and −32 mol% in the 50 bar and 180 bar scenarios, respectively. Ankerite (re)precipitation proceeds continuously in the pCO_2 = 1 bar (93%$_{to}$) and pCO_2 = 50 bar (81%$_{to}$) scenarios, whereas in the pCO_2 = 180 bar scenario, (re)precipitation initiates only once temperatures exceed 30 °C (73%$_{to}$). Pyrite dissolution remains minor and continuous throughout the temperature increase phase (<−0.004 mol%).

Beyond the initialization period, carbonate minerals evolve along stable trajectories, with only very limited calcite (re)precipitation and modest ankerite (re)precipitation (pCO_2 = 1 bar: 93%$_{to}$; pCO_2 = 50 bar: 86%$_{to}$; pCO_2 = 180 bar: 79%$_{to}$), primarily driven by continued dolomite dissolution (Figure 6-7). Dolomite persists only under the pCO_2 = 1 bar scenario (90%$_{to}$), whereas nearly complete dissolution is predicted in the 50 bar and 180 bar scenarios (Figure 6-7). Pyrite dissolution remains slow throughout reservoir condition simulations; although the brine approaches equilibrium in the pCO_2 = 1 bar (−0.002 mol%) and pCO_2 = 50 bar (−0.003 mol%) scenarios, it reaches nearequilibrium conditions in the pCO_2 = 180 bar scenario (−0.004 mol%). After 40 days, the primary minerals showing the most marked deviations from their initial abundances are, in decreasing order of magnitude, calcite, dolomite, and ankerite (Figure 6-7). From a mass balance-balance perspective, calcite dissolution reaches 5.19×10^{-4} mol·L^{-1} (−0.65%) and 9.39×10^{-4} mol·L^{-1} (−1.2 mol%) in the 50 bar and 180 bar scenarios, respectively, whereas slight calcite precipitation occurs under the 1 bar scenario (9.97×10^{-5} mol·L^{-1}; +0.12 mol%). Pyrite dissolution remains negligible over the experimental timeframe.

The PilotSTRATEGY project has received funding from the European Union's Horizon 2020 research and innovation programme under grant agreement No. 101022664

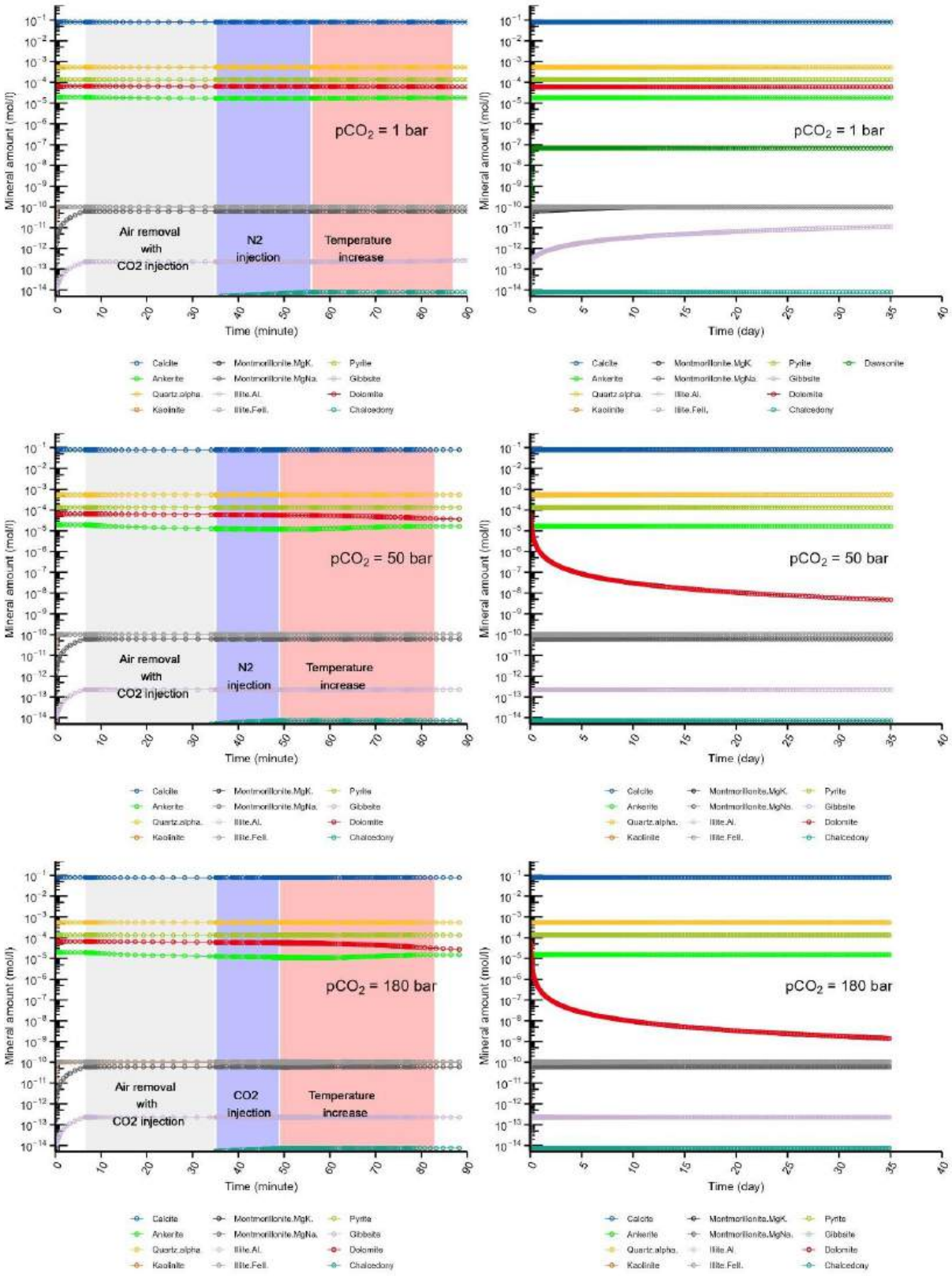

Figure 6-7: Evolution of the mineral total amount (in mol for 1L of brine) within the mineral assemblage of the Comblanchian Formation over the initialisation period (left; time in minute) and the experimental part (left, time in day) for the three study scenarios: pCO_2 1 bar (top), pCO_2 50 bar (middle), pCO_2 180 bar (bottom).

The PilotSTRATEGY project has received funding from the European Union's Horizon 2020 research and innovation programme under grant agreement No. 101022664

With respect to secondary mineral precipitation (Figure 6-7), numerical simulations incorporating available reaction kinetic parameters predict the formation of clay minerals such as illite (up to 1.05×10^{-10} mol·L^{-1}), kaolinite (up to 1.01×10^{-10} mol·L^{-1}), and montmorillonite (up to 1.00×10^{-10} mol·L^{-1}). Additional phases, including gibbsite (up to 1.28×10^{-11} mol·L^{-1}) and chalcedony (up to 1.16×10^{-15} mol·L^{-1}), are predicted to form primarily at the onset of the initialization step, during the first interaction between the synthetic brine and the mineral powder. The very low concentrations of these phases – far below those of accessory primary minerals such as pyrite (1.34×10^{-4} mol·L^{-1}) – explain their absence in XRD–Rietveld analyses following the laboratory experiments.

6.2.3 Dalle Nacrée Formation

The Dalle Nacrée Formation displays the most mineralogically diverse assemblage of primary accessory minerals among the investigated reservoir units. Although its bulk composition broadly resembles that of the Oolithe Blanche Formation (calcite rich), the Dalle Nacrée Formation is distinguished by the consistent presence of pyrite and illite, in addition to dolomite, ankerite, gypsum and kaolinite. This assemblage contributes to a higher degree of chemical heterogeneity, which governs the formation's response to CO_2-rich brine exposure.

The initial interaction between rock powder and synthetic brine induced a near -complete dissolution of gypsum (–99.8 mol%; Figure 6-8). This process was accompanied by minor dissolution of dolomite (–0.10 mol%) and ankerite (–1.1 mol%). Limited compensatory precipitation of calcite (+0.14 mol%) and illite (+0.13 mol%) was recorded. Dissolution of pyrite and precipitation of kaolinite were negligible during this stage, indicating minimal reactivity of these kinetically slow minerals under initial conditions.

The injection of CO_2(g) during air removal, accompanied by minor N_2(g), and subsequent pressurization up to 180 bar resulted in complete dissolution of gypsum across all simulated conditions. Carbonate minerals underwent systematic dissolution, the magnitude of which increased with pCO_2 (Figure 6-8). Dissolution intensities for calcite, dolomite, and ankerite raised with increasing pCO_2, with loss of –0.23 mol% at pCO_2 = 1 bar, –2 mol% at pCO_2 = 50 bar and –2.81 mol% at pCO_2 = 180 bar for calcite; loss of –4.5 mol% at pCO_2 = 1 bar, –13 mol% at pCO_2 = 50 bar and –13.8 mol% at pCO_2 = 180 bar for dolomite; and loss of –6 mol% at pCO_2 = 1 bar, –18 mol% at pCO_2 = 50 bar and –21 mol% at pCO_2 = 180 bar for ankerite. Dissolution of pyrite, kaolinite, and illite remained minimal regardless of pCO_2, consistent with their slow dissolution kinetics.

The progressive increase in temperature produced notable changes in carbonate stability. Calcite underwent significant (re)precipitation, reaching between 98.5 mol% (pCO_2 = 180 bar) and 100 mol% (pCO_2 = 1 bar) of its initial concentration depending on pCO_2 (Figure 6-8; Figure 6-9) Dolomite dissolution increased markedly, with losses of –10.5 mol% at pCO_2 = 1 bar, –34 mol% at pCO_2 = 50 bar and –42 mol% at pCO_2 = 180 bar (Figure 6-8). Ankerite displayed continuous (re)precipitation in all scenarios, stabilizing between 90% (pCO_2 = 180 bar) and 96 mol% (pCO_2 = 1 bar) of its initial concentration. Anhydrite precipitation initiated once temperatures reach or exceeded 60°C in the pCO_2 50 and 180 bar scenarios (Figure 6-9). Dissolution of pyrite, illite, and kaolinite remained negligible throughout this stage. Kaolinite exhibited slight precipitation for pCO_2 = 1, when temperatures reached 70°C.

The PilotSTRATEGY project has received funding from the European Union's Horizon 2020 research and innovation programme under grant agreement No. 101022664

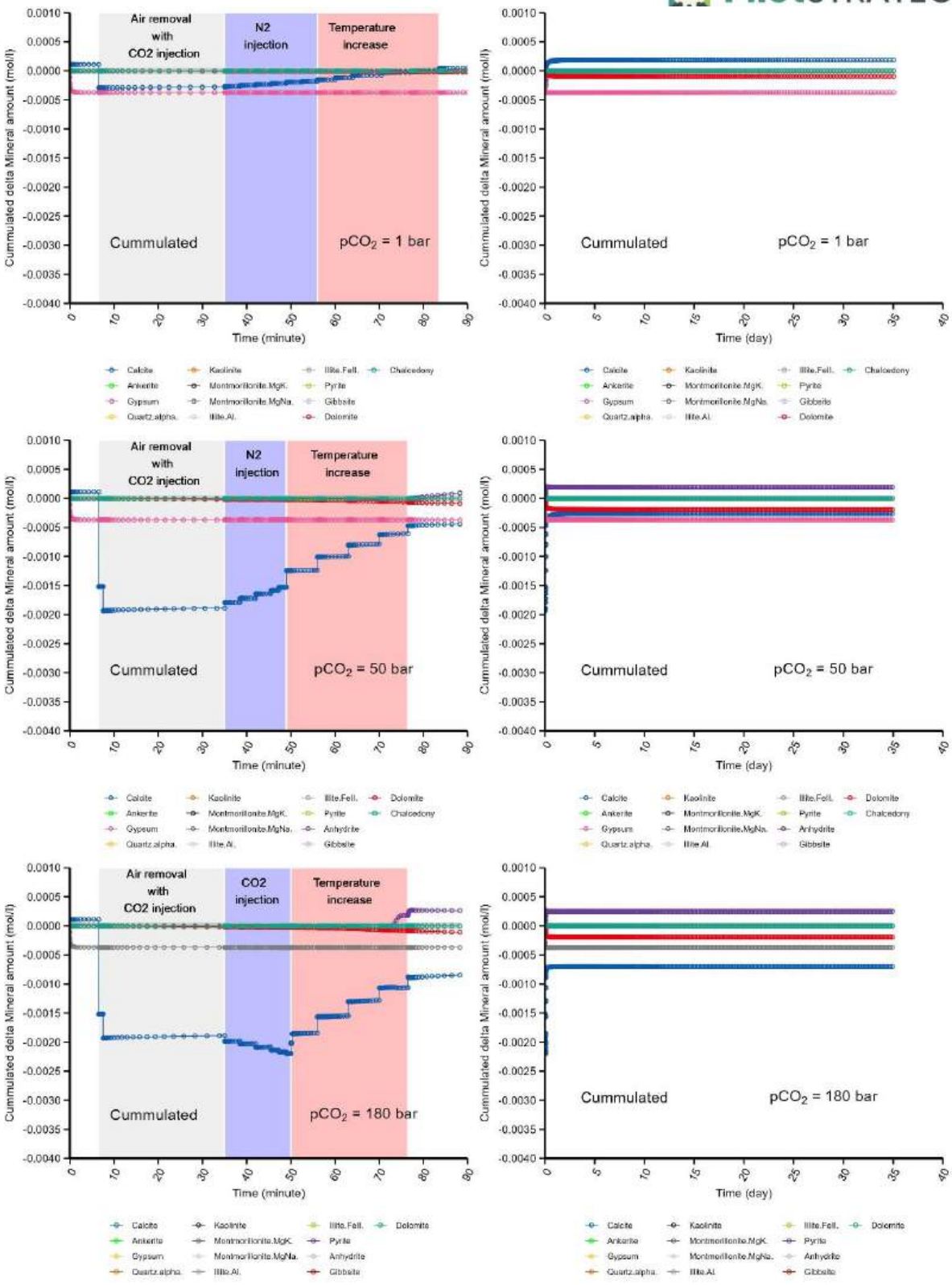

Figure 6-8: Amount of dissolved (< 0) or precipitated (> 0) mineral – compared to the initial concentration – composing the mineral assemblage of the Dalle Nacrée Formation over the initialisation period (left; time in minute) and the experimental period (left, time in day) for the three study scenarios: pCO_2 1 bar (top), pCO_2 50 bar (middle), pCO_2 180 bar (bottom), with a total pressure of 180 bar and a temperature of 70 °C over the experimental period.

The PilotSTRATEGY project has received funding from the European Union's Horizon 2020 research and innovation programme under grant agreement No. 101022664

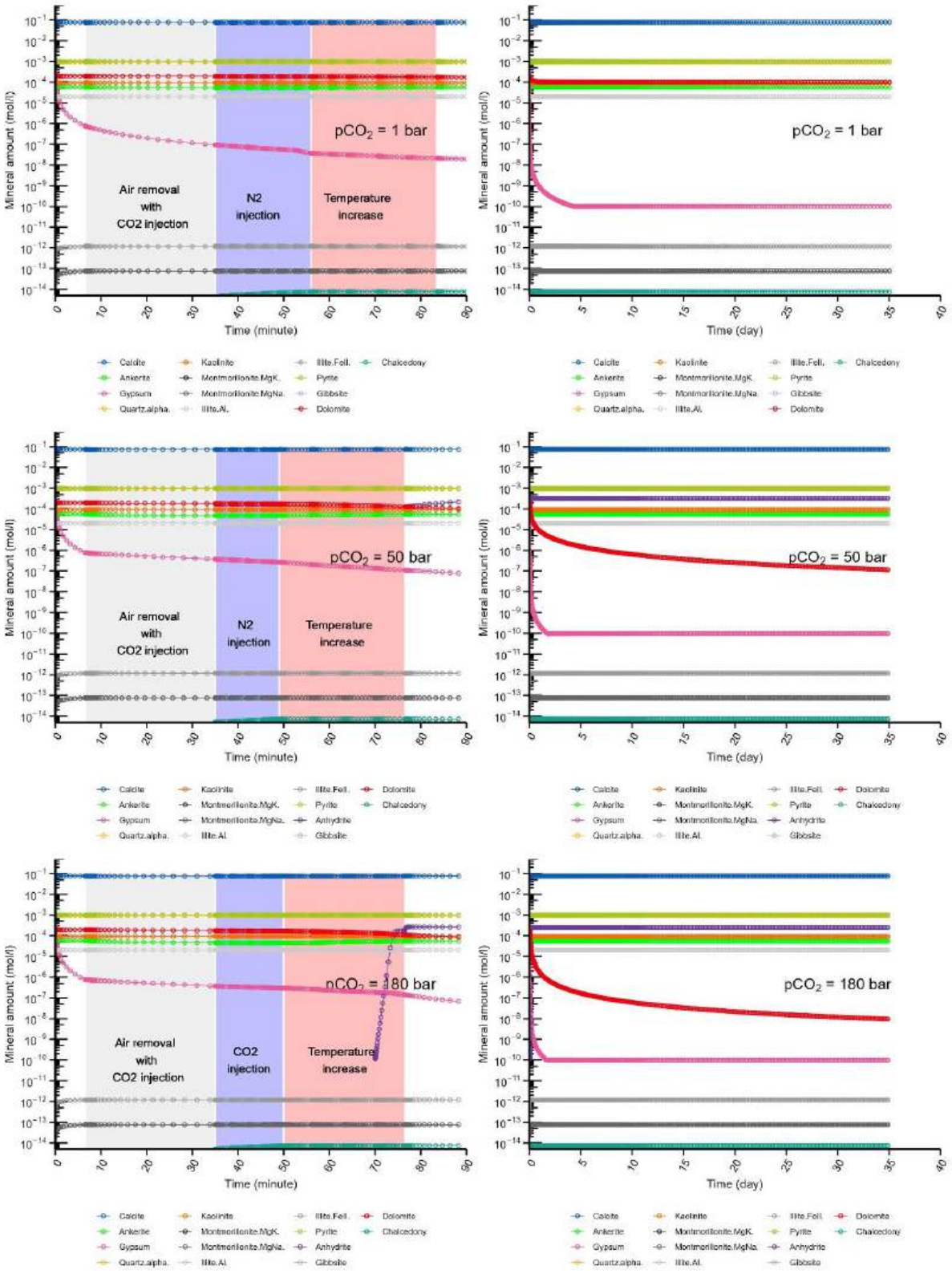

Figure 6-9: Evolution of the mineral total amount (in mol for 1L of brine) within the mineral assemblage of the Dalle Nacrée Formation over the initialisation period (left; time in minute) and the experimental period (left, time in day) for the three study scenarios: pCO_2 1 bar (top), pCO_2 50 bar (middle), pCO_2 180 bar (bottom), , with a total pressure of 180 bar and a temperature of 70°C over the experimental period.

The PilotSTRATEGY project has received funding from the European Union's Horizon 2020 research and innovation programme under grant agreement No. 101022664

Following the initialization period, carbonate mineral concentrations remained relatively stable during the 40-day reaction period (Figure 6-8; Figure 6-9). Calcite experienced only minor (re)precipitation. Ankerite exhibited minor but measurable (re)precipitation, resulting in final concentrations of 97%$_{to}$ (1 bar), 95.6%$_{to}$ (50 bar) and 94%$_{to}$ (180 bar). Dolomite dissolution acted as a principal driver controlling carbonate re-equilibration, with a complete dissolution at pCO_2 = 50 and 180 bar, and advanced dissolution (–51 mol%) at pCO_2 = 1 bar. Pyrite and illite dissolved slowly but continuously, although the total amount dissolved remained very small – Illite: > 99.3%$_{to}$; Pyrite > 99.9%$_{to}$. Anhydrite precipitation continued steadily until reaching equilibrium and was partly sourced from the dissolution (oxidation) of pyrite. Kaolinite showed contrasting tendencies, with minor precipitation under pCO_2 = 1 bar (+0.19 mol%), 50 bar (+0.07 mol%) and under pCO_2 = 180 bar (+0.05 mol%).

The minerals exhibiting the greatest relative changes at the end of the simulation period were, in decreasing order, for kinetically fast minerals Gypsum/anhydrite ≈ Dolomite > Ankerite > Calcite and for slow kinetic minerals Kaolinite (precipitation) ≈ Illite (dissolution) > Pyrite > Quartz. Collectively, these results highlight the strong dependence of carbonate mineral stability on both pCO_2 and temperature, as well as the contrasting behavior of fastand slow-kinetic minerals within the Dalle Nacrée Formation.

Numerical simulations incorporating available reaction kinetics indicate that the precipitation of secondary clay minerals – primarily illite (up to 3.56×10^{-12} mol·L^{-1}) and montmorillonite (up to 1.32×10^{-13} mol·L^{-1}) – may occur at the onset of the initialization period, coinciding with the first contact between the synthetic brine and the mineral powder. However, the concentrations of these phases remain extremely low (Figure 6-9), several orders of magnitude below the levels required to exert any geochemical influence. Consequently, their contribution to the overall mineralogical evolution is considered negligible, and their explicit representation within the geochemical model does not affect either reaction pathways or mass balance outcomes.

6.2.4 Impact of chemical reactivity on aqueous phase composition

Geochemical models developed from mineralogical characterization (XRD–Rietveld) and literature-derived reaction rates provide a framework to predict the reaction pathways likely to occur under the specific physicochemical conditions imposed during the experimental tests. In addition to numerical predictions, it is essential to evaluate the consistency of the modelling results against the experimental dataset to validate the main reaction trends. By confronting the model outputs with empirical observations, potential discrepancies can be identified, leading either to an adjustment of kinetic parameters, reactive surface areas, or to a refinement of the conceptual model itself. Verification of the modelling results primarily relies on comparing the simulated outputs with the temporal evolution of the aqueous phase composition (Figure 6-10). Such comparison is necessary to ensure that the simulated mineralogical and geochemical evolutions accurately reflect the processes occurring under controlled laboratory conditions.

The PilotSTRATEGY project has received funding from the European Union's Horizon 2020 research and innovation programme under grant agreement No. 101022664

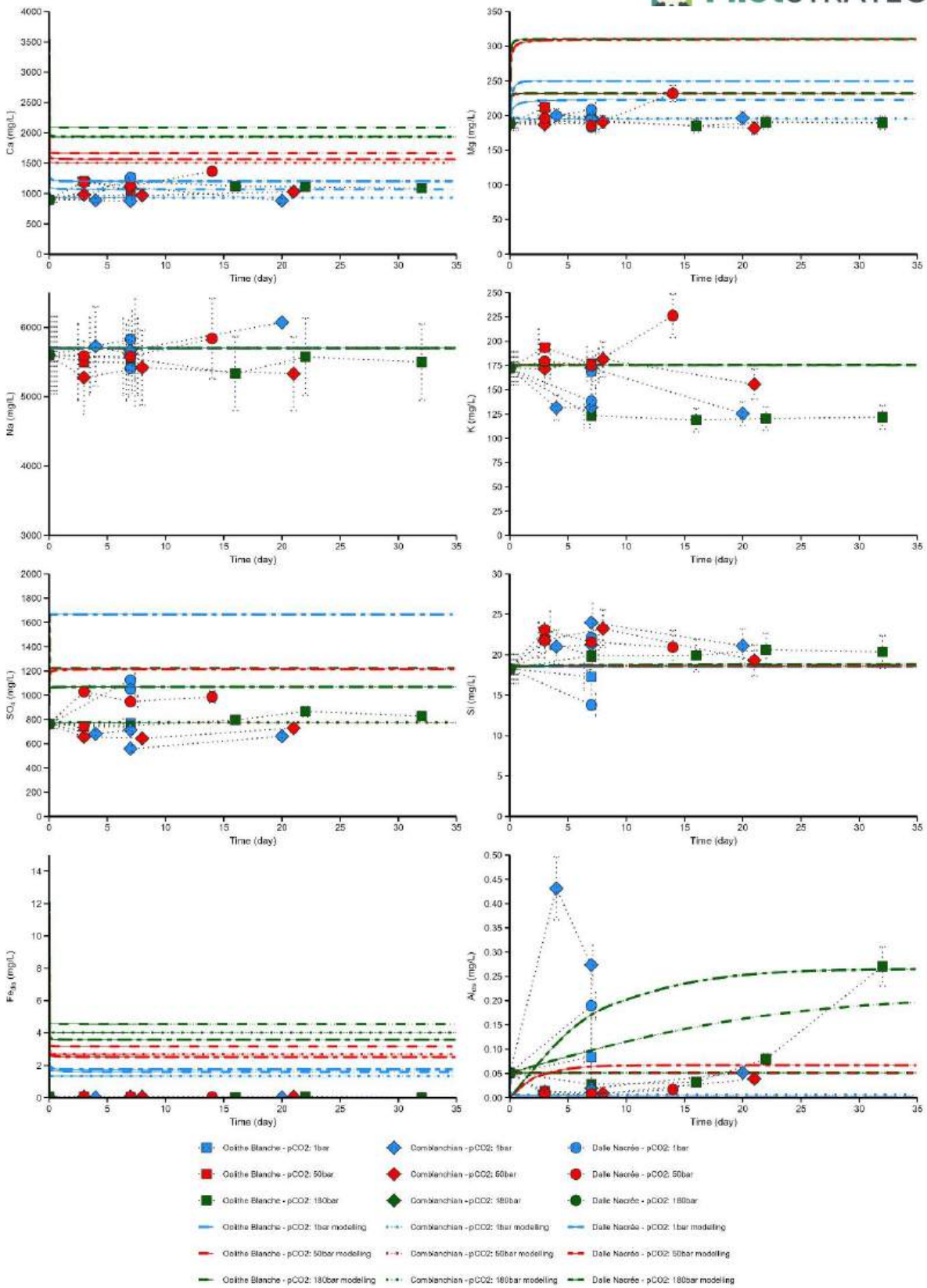

Figure 6-10: Modelled and measured fluid chemistry for reservoir sample experiments(Oolithe Blanche, Camblanchian and Dalle Nacrée) with different set of the pCO_2 (1 bar, 50 bar and 180 bar).

The PilotSTRATEGY project has received funding from the European Union's Horizon 2020 research and innovation programme under grant agreement No. 101022664

The inherent role of carbonate minerals – predominantly calcite and, to a lesser extent, dolomite and ankerite – in controlling the dominant reaction pathways within the reservoir formations arises from their strong sensitivity to pCO_2 and, more specifically, from their capacity to buffer the acidity generated by CO_2 dissolution. Upon CO_2 injection, the resulting decrease in pH promotes the rapid dissolution of calcite, which acts as the primary neutralizing phase due to its high reactivity and fast dissolution kinetics. Dolomite and ankerite participate more gradually in this buffering process, contributing additional Ca^{2+}, Mg^{2+}, and Fe^{2+} to the aqueous system as reaction conditions evolve.

While the modelling results are consistent with the underlying conceptual understanding, the experimental data do not show the expected increase in Ca, Mg, and Fe concentrations with rising imposed pCO_2 (Figure 6-10), and the simulations systematically overestimate the measured concentrations. Only the experiments conducted at $pCO_2 \approx 1$ bar are satisfactorily reproduced by the model for Ca, and partially for Mg (notably for the Comblanchien Formation). The narrow range of Ca concentrations observed experimentally, together with the measured pH values remaining between 6 and 6.5 (Figure 6-11), suggests that calcite and/or dolomite reprecipitation was more extensive than simulated. The most plausible explanation is that partial CO_2 degassing occurred prior to filtration despite the precautions taken, triggering mineral precipitation outside the reactor and causing the samples to reflect conditions close to $pCO_2 \approx 1$ bar rather than the higher pCO_2 imposed during the experiments.

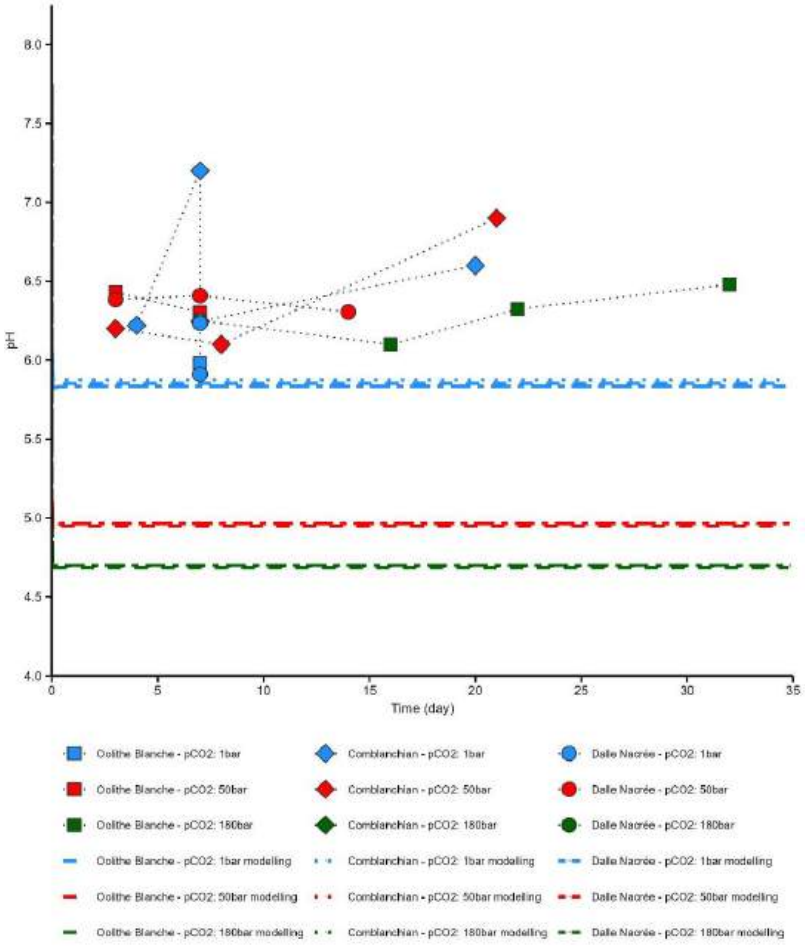

Figure 6-11: Modelled and measured pH of the fluid for reservoir sample experiments at pCO_2 1 bar, 50 bar and 180 bar.

The PilotSTRATEGY project has received funding from the European Union's Horizon 2020 research and innovation programme under grant agreement No. 101022664

With respect to Ca-bearing phases such as anhydrite, the modelling results suggest that only scenarios involving precipitation of anhydrite (pCO_2: 50 and 180 bars) reproduced the measured SO_4 concentration (Figure 6-10). This supports the sulphate in the brine being controlled by equilibrium with respect to anhydrite – involving precipitation processes – that become thermodynamical more effective at elevated pCO_2, even though precipitation of anhydrite might have experimentally occurred within the reactor for 1 bar pCO_2 scenario.

In contrast to Ca, Mg, and Fe concentrations, the silica concentrations predicted by the models remain stable compared with the range covered by the experimental results (Figure 6-11). The silica-bearing phases within the mineral assemblage are limited to quartz and kaolinite. Because the fluid is supersaturated with respect to quartz, it is thermodynamically impossible for the increase in dissolved Si observed experimentally to originate from quartz dissolution. Only kaolinite dissolution can account for the observed increase, although the slow dissolution kinetics of this mineral do not allow the initial rise to be reproduced.

The minerals identified by XRD–Rietveld analysis and used in the simulations do not contain potassium, which prevents the model simulating dissolved K concentrations. Even if muscovite – another mica mineral – had been included in the mineral assemblage instead of illite, its dissolution would not have produced an increase in dissolved K. In contrast, the experimental results show a decreasing trend in K concentrations. This suggests that the precipitation of a K-bearing secondary mineral cannot be ruled out, although no such phase was detected in the XRD–Rietveld analyses.

The modeled evolution of sodium and aluminum concentrations is generally consistent with experimental observations (Figure 6-11). For Na, this agreement reflects its high initial concentration in the fluid and the absence of any Na--bearing mineral phase in the system. Kaolinite dissolution – identified in the Oolithe Blanche and Dalle Nacrée – partly explains the increase in Al concentrations over the 35 day experimental period. However, its slow dissolution kinetics cannot reproduce the variability observed during the first 10 days under the 1 bar pCO_2 scenario.

Taken together, these results highlight that the models provide a coherent theoretical framework. However, further refinement of both the experimental design and the geochemical parameterization is required to achieve a more robust interpretation of fluid–rock interactions under elevated pCO_2 conditions in carbonate reservoir.

The PilotSTRATEGY project has received funding from the European Union's Horizon 2020 research and innovation programme under grant agreement No. 101022664

6.3 Results for transitional caprock

The restricted length of the cored interval, limited to the Callovian transgressive deposits overlying the reservoir, means that the available samples predominantly represent the lowermost section of the Massengis Marl Formation, i.e. the transitional Callovian caprock. Due to a limited amount of rock (only rock fragments are available), specimens from both intervals 1840 m and 1842 m were selected and used to encompass the range of conditions investigated in the experimental program. Despite the short interval difference, the mineralogical assemblage displays measurable variations with decreasing depth within the transitional caprock, reflecting depositional heterogeneities (Figure 6-1).

XRD–Rietveld quantification reveals a complex mineral assemblage comprising up to thirteen distinct mineral phases in the initial samples (Table 6.1.*11*). The dominant constituents include illite (≈25 wt.%); a series of clay minerals (≈25 wt.%) – notably smectite and/or interstratified illite–smectite (≈20 wt.%) together with kaolinite and chlorite; quartz (≈22 wt.%) and calcite (≈16 wt.%), with a decrease in clay minerals towards the base of the interval counterbalanced by an increase in calcite minerals (Figure 6-1). These depth-elated variations, though moderate due to the limited thickness of the cored interval, indicate a trend toward a mineralogical assemblage more representative of a mudstone in the sample collected along the 1840 m section. To account for the mineralogical variability observed between the two samples, two geochemical models were developed: one for the intermediate – section (VUS 1 - 1840 m) of the – transitional caprock and one for the lower – section (sample VUS 1 - 1842 m) of the – transitional caprock.

6.3.1 Intermediate transitional caprock

Although richer in clay minerals, the mineral phases constituting the transitional caprock differ only moderately from those of the Dalle Nacrée Formation. The intermediate section of the transitional caprock is characterized by the additional presence of smectite and/or illite–smectite interstratifications (in high proportions), along with minor amounts of plagioclase, K-feldspar and chlorite (Table 6.1.*11*). The principal mineral phases are still calcite, together with smectite, quartz, and illite (Figure 6-1). The mineralogical composition of the transitional caprock is largely dominated by phases exhibiting slow dissolution kinetics, which might result in a more pronounced evolution over the course of the experimental period than that observed in the reservoir rock samples.

The initial interaction between the rock powder and the synthetic brine induces an almost complete dissolution of gypsum (-99 mol%), accompanied by a minor precipitation of calcite (+0.03 mol%) (Figure 6-12; Figure 6-13). Slight dissolution of dolomite (-0.33 mol%) and ankerite (-3.4 mol%) is also observed (Figure 6-12), together with negligible dissolution of kaolinite, illite, interstratified I/S, albite, K-feldspar, and pyrite (< −0.006 mol%), as well as negligible precipitation of chlorite.

The PilotSTRATEGY project has received funding from the European Union's Horizon 2020 research and innovation programme under grant agreement No. 101022664

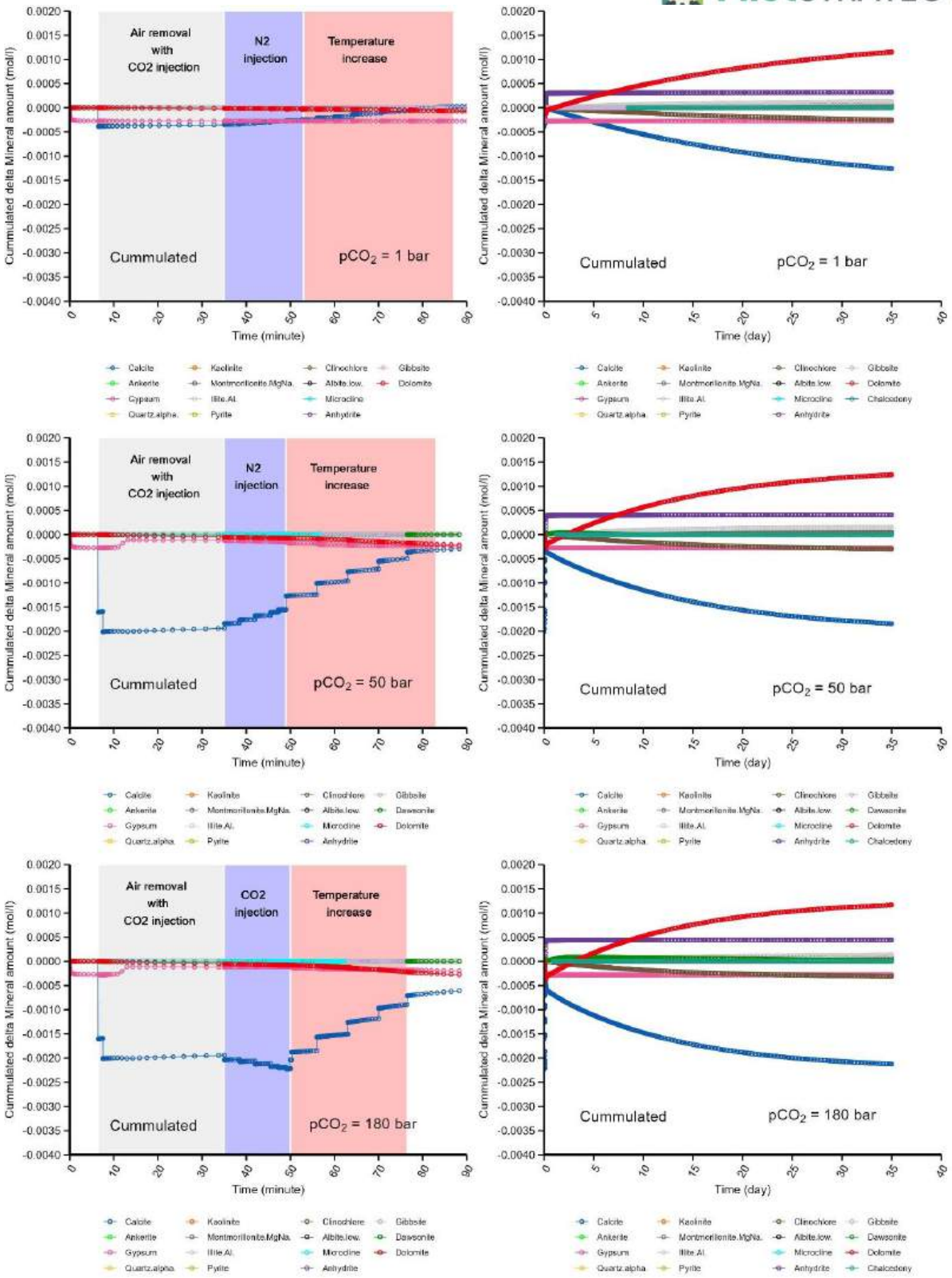

Figure 6-12: Amount of dissolved (< 0) or precipitated (> 0) mineral – compared to the initial concentration – composing the mineral assemblage of the intermediate interval of the transitional caprock over the initialisation period (left; time in minute) and the experimental part (left, time in day) for the three study scenarios: pCO_2 1 bar (top), pCO_2 50 bar (middle), pCO_2 180 bar (bottom).

The PilotSTRATEGY project has received funding from the European Union's Horizon 2020 research and innovation programme under grant agreement No. 101022664

Injection of CO_2(g) (and N_2(g)) during the air-removal and pressurization steps up to 180 bar promotes rapid dissolution of carbonate minerals. This process results in significant dissolution of calcite, minor dissolution of dolomite, and very minor dissolution of ankerite (Figure 6-12). The magnitude of carbonate dissolution is directly controlled by the imposed pCO_2:

- pCO_2 = 1 bar: very minor to moderate dissolution of calcite (-1.9 mol%) and dolomite (-4.6 mol%);
- pCO_2 = 50 bar: moderate to high dissolution of calcite (-12 mol%) and dolomite (-12.7 mol%);
- pCO_2 = 180 bar: high dissolution of calcite (-17.5 mol%) and dolomite (-13.6 mol%).

During air removal, carbonate dissolution leads to partial reprecipitation of gypsum in the 50 and 180 bar scenarios. The introduction of N_2(g) during pressurization in the 1 and 50 bar pCO_2 scenarios promotes partial reprecipitation of calcite and for the 50 bar pCO_2 scenario moderate partial dissolution of the previously reprecipitated gypsum (Figure 6-12). Among silicate and aluminosilicate minerals, kaolinite, albite, microcline, interstratified illite–smectite, and illite undergo negligible dissolution due to their slow dissolution kinetics. Chlorite (clinochlore) displays the most significant, though still limited, reactivity, with dissolution up to -0.2 mol% at pCO_2 = 180 bar.

The subsequent temperature -increase step triggers substantial (re)precipitation of calcite, restoring the mineral to 99.9 $\%_{t0}$ of its initial concentration in the 1 bar scenario, 96 $\%_{t0}$ at 50 bar, and 93 $\%_{t0}$ at 180 bar (Figure 6-12). This thermal step further enhances dolomite and gypsum dissolution and induces very minor precipitation of ankerite across all scenarios. Dolomite dissolution is more pronounced in the 50 and 180 bar scenarios. Additionally, anhydrite starts to slowly precipitate from temperatures ≥ 50°C (Figure 6-13). During this stage, kaolinite and illite precipitate slowly and continuously but to negligible extents. Albite and microcline undergo limited dissolution, while chlorite dissolution continues, reaching -0.3 mol% (1 bar), -0.45 mol% (50 bar), and -0.4 mol% (180 bar). Quartz, pyrite, and interstratified illite/smectite remain essentially unaffected.

Beyond the brief initialization phase, the 35 day experimental period highlights the dominant reaction pathways under reservoir pressure–temperature conditions. These reactions are characterized by rapid precipitation of anhydrite, progressive dissolution of calcite and chlorite (clinochlore), and concomitant precipitation of dolomite (Figure 6-13). The extent of calcite and chlorite dissolution, as well as dolomite and ankerite precipitation, increases with pCO_2:

- Calcite dissolution: -10.5 mol% (1 bar), -15 mol% (50 bar), -17 mol% (180 bar);
- Chlorite dissolution: -80 mol% (1 bar), -93 mol% (50 bar), -95 mol% (180 bar);
- Dolomite precipitation: +317 mol% (1 bar), +327 mol% (50 bar), +313 mol% (180 bar) relative to the initial concentration;
- Ankerite precipitation very limited over the experimental period: +0.05 mol% (1 bar), +0.13 mol% (50 bar), +0.19 mol% (180 bar).

The PilotSTRATEGY project has received funding from the European Union's Horizon 2020 research and innovation programme under grant agreement No. 101022664

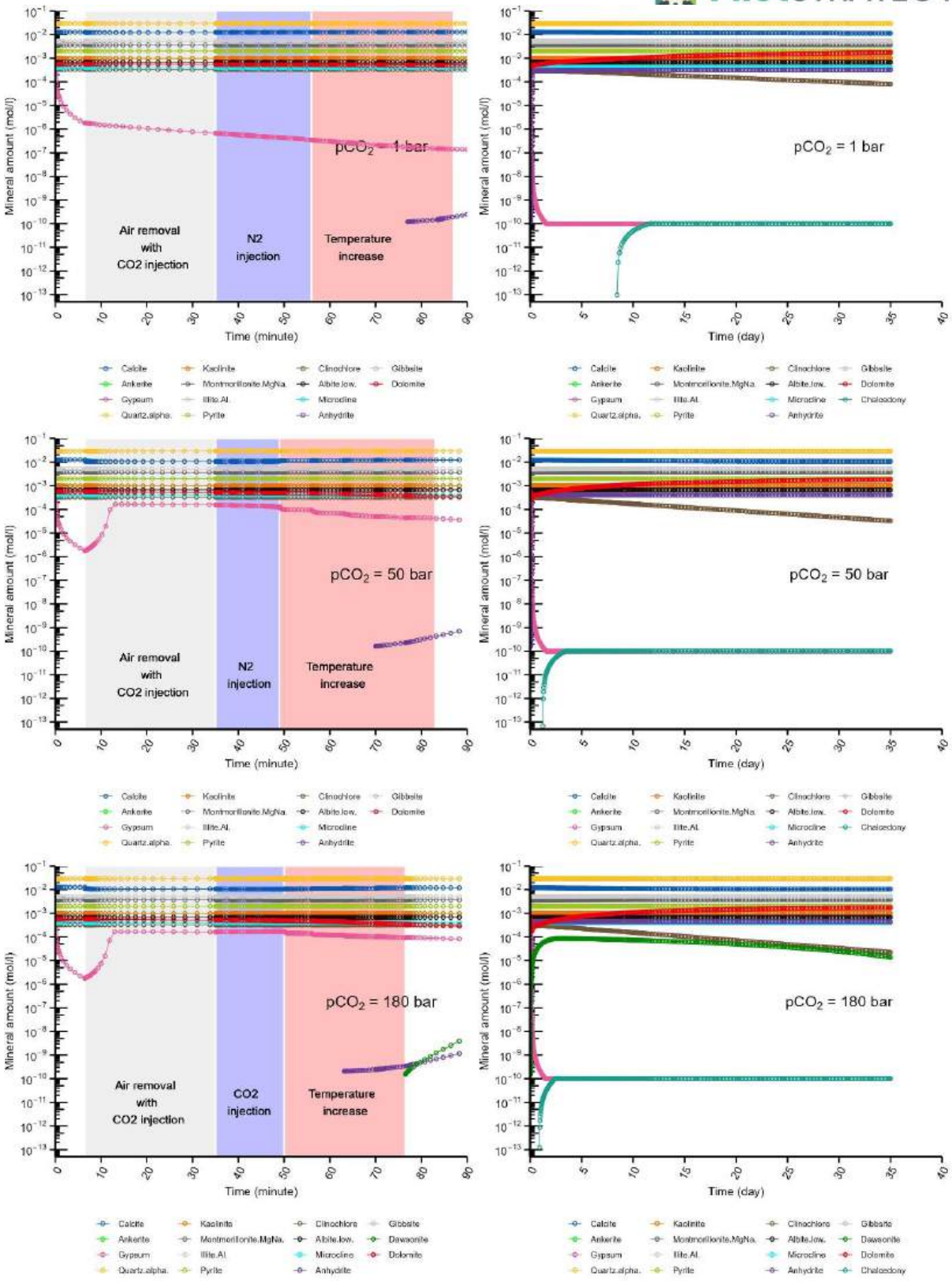

Figure 6-13: Evolution of the mineral total amount (in mol for 1L of brine) within the mineral assemblage of the intermediate interval of the transitional caprock over the initialisation period (left; time in minute) and the experimental part (left, time in day) for the three study scenarios: pCO_2 1 bar (top), pCO_2 50 bar (middle), pCO_2 180 bar (bottom).

The PilotSTRATEGY project has received funding from the European Union's Horizon 2020 research and innovation programme under grant agreement No. 101022664

Dawsonite ($NaAlCO_3(OH)_2$) precipitation is expected at higher pCO_2 (50 and 180 bar; Figure 6-13), providing a sink for dissolved Al and explaining the comparatively lower increase in dolomite concentration at high pCO_2. The system also evolves toward the formation of secondary clay minerals—illite (~+2.75 mol%), interstratified illite/smectite (~+2 mol%) independently of the pCO_2 condition, whereas precipitation of kaolinite occurred mainly under high pCO_2 conditions. These secondary clays derive from the dissolution of chlorite and feldspars (albite, K-feldspar) and contribute to the progressive geochemical stabilization of the system. Additional phases, including gibbsite (up to 5.7×10^{-15} mol·L^{-1}) and chalcedony (up to 1.0×10^{-10} mol·L^{-1}), are predicted to form primarily at the onset of the initialization period and during the experimental period, respectively (Figure 6-13). The very low concentrations of these phases over the experimental timeframe suggest that they have no real-world significance.

The overall geochemical evolution remains broadly consistent across the different pCO_2 scenarios. This convergence largely reflects the inherently slow reaction kinetics of clay minerals and, more importantly, the dominant control exerted by the initial water–rock disequilibrium, as the synthetic brine used in the experiment was representative of the porewater from the reservoir – i.e. not from the caprock.

6.3.2 Lower transitional caprock

The mineralogical composition of the lower section of the transitional caprock remains broadly comparable to that of the intermediate transitional caprock, displaying the same primary mineral phases, apart from the lack of plagioclase (albite). However, the lower transitional caprock exhibits a higher calcite content, which is counterbalanced by a significantly lower proportion of illite (Figure 6-1). This interval also shows a lower proportion of K-feldspar and kaolinite, reflecting subtle mineralogical evolution within the transitional domain.

In the intermediate transitional caprock, the dissolution of plagioclase plays only a minor role in the overall reaction network, as the aqueous solution rapidly reaches thermodynamic equilibrium with this mineral. The absence of plagioclase in the lower transitional caprock exerts a negligible influence on the modeled geochemical evolution. Consequently, given the strong mineralogical similarity between the two units, the reaction pathways identified for the intermediate transitional caprock are generally applicable to the lower transitional caprock as well (Figure 6-14; Figure 6-15).

During the initial interaction between the rock powder and the synthetic brine, the reactions reproduce those previously identified for the intermediate transitional caprock. However, the injection of CO_2(g) (and N_2(g)) during the air-removal and pressurization steps (up to 180 bar) results in complete gypsum dissolution, with no evidence of partial reprecipitation. This step also promotes pronounced dissolution of calcite, minor dissolution of dolomite, and only very limited dissolution of ankerite, consistent with trends observed for the intermediate transitional caprock. Chlorite (clinochlore) exhibits the highest reactivity among the accessory minerals, though still modest overall, with dissolution reaching up to −0.2% at pCO_2 = 180 bar.

The PilotSTRATEGY project has received funding from the European Union's Horizon 2020 research and innovation programme under grant agreement No. 101022664

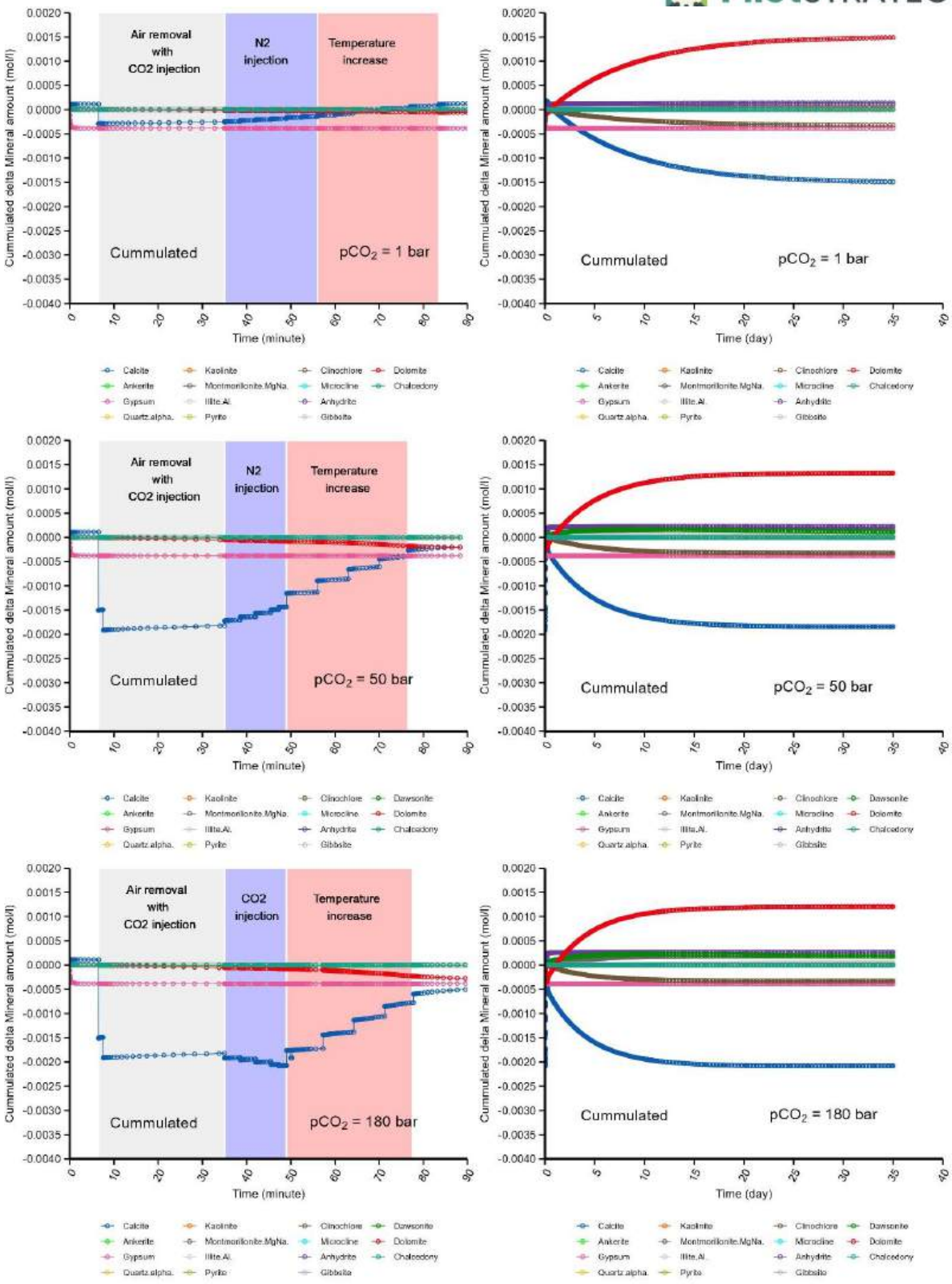

Figure 6-14: Amount of dissolved (< 0) or precipitated (> 0) mineral – compared to the initial concentration – composing the mineral assemblage of the lower interval of the transitional caprock over the initialisation period (left; time in minute) and the experimental part (left, time in day) for the three study scenarios: pCO_2 1 bar (top), pCO_2 50 bar (middle), pCO_2 180 bar (bottom).

The PilotSTRATEGY project has received funding from the European Union's Horizon 2020 research and innovation programme under grant agreement No. 101022664

The subsequent temperature increase step induces substantial calcite (re)precipitation, restoring calcite to 100.3 mol% of its initial concentration in the 1 bar scenario, to 98.7 mol% at 50 bar, and to 97.5 mol% at 180 bar (Figure 6.12). This thermal step further enhances dolomite dissolution and triggers very minor ankerite precipitation across all scenarios, while the other mineral phases follow reaction pathways similar to those observed for the intermediate transitional caprock.

Reaction pathways that are specific to the lower transitional caprock emerge mainly during the experimental period (Figure 6-14; Figure 6-15). These are characterized by rapid anhydrite precipitation, progressive dissolution of calcite and chlorite (clinochlore), and concomitant dolomite precipitation (Figure 6-15). In contrast with the intermediate transitional caprock, chlorite undergoes nearly complete dissolution within 35 days, regardless of the imposed pCO_2, suggesting a continuous disequilibrium of the evolving brine chemistry with respect to this mineral phase over the entire period. Furthermore, calcite dissolution and associated dolomite precipitation evolve toward comparable concentrations by the end of the experimental period between the different pCO2 scenarios for the lower transition caprock (Figure 6-14). This behaviour reflects the progressive establishment of thermodynamic equilibrium between the brine and the carbonate minerals. Both dolomite saturation (with slower precipitation kinetics than calcite) and complete chlorite dissolution are attained earlier for the lower transitional caprock at higher pCO_2 values (Figure 6-14).

The extent of calcite dissolution and dolomite precipitation is partly influenced by dawsonite precipitation, which is mainly predicted to occur at pCO_2 = 50 and 180 bar (Figure 6.13). The predicted changes relative to the initial concentrations are as follows:

- Calcite dissolution: −4.9 mol% (1 bar), −6 mol% (50 bar), −6.8 mol% (180 bar)
- Dolomite precipitation: +357 mol% (1 bar), +329 mol% (50 bar), +307 mol% (180 bar)

The system has limited precipitation of ankerite (~ +0.2 mol%) and the precipitation of secondary clay minerals – namely illite (~ +2.75 mol%), interstratified illite–smectite (~ +2 mol%), and kaolinite (~ +4 mol%). The precipitation of interstratified illite–smectite and, to a lesser extent, kaolinite shows limited sensitivity to the imposed pCO_2, whereas illite precipitation decreases progressively with increasing pCO_2. Additional secondary phases, including gibbsite (up to 7.52×10^{-15} mol·L^{-1}) and chalcedony (up to 1.02×10^{-10} mol·L^{-1}), are predicted in very small amounts, forming primarily during the temperature increase step and throughout the experimental period, respectively (Figure 6-15).

The PilotSTRATEGY project has received funding from the European Union's Horizon 2020 research and innovation programme under grant agreement No. 101022664

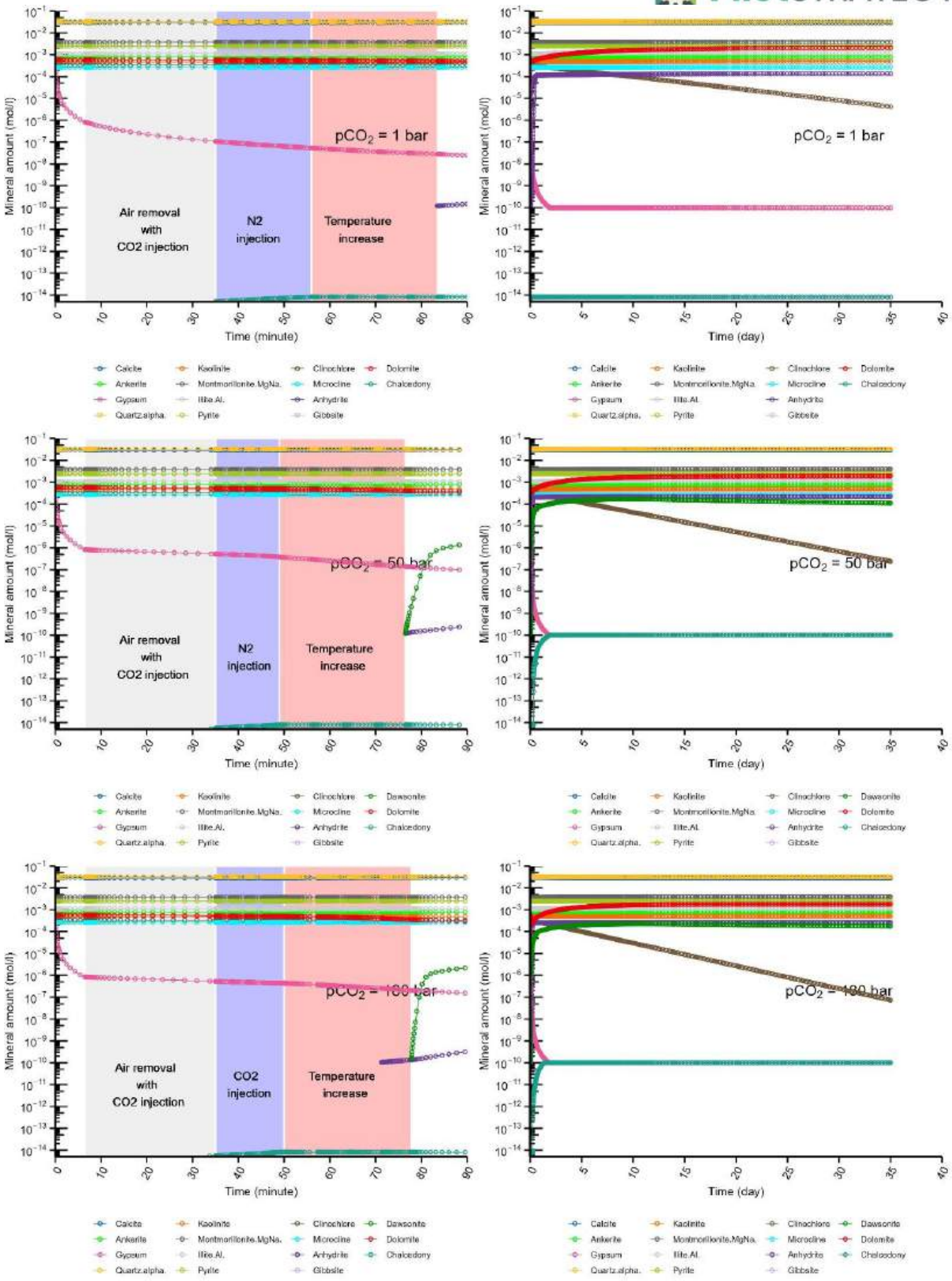

Figure 6-15: Evolution of the mineral total amount (in mol for 1L of brine) of the lower interval of the transitional caprock over the initialisation period (left; time in minute) and the experimental part (left, time in day) for the three study scenarios: pCO_2 1 bar (top), pCO_2 50 bar (middle), pCO_2 180 bar (bottom).

The PilotSTRATEGY project has received funding from the European Union's Horizon 2020 research and innovation programme under grant agreement No. 101022664

6.3.3 Impact of chemical reactivity on aqueous phase composition

XRD-Rietveld analysis identified a complex mineral assemblage comprising up to thirteen minerals in the initial rock samples from the transitional caprock. A major challenge in interpreting the experimental results arises from the fact that each dissolved ion is typically associated with several distinct mineral phases. Consequently, changes in aqueous concentrations cannot be directly attributed to a single reaction pathway. The proposed geochemical models for the transitional caprock result therefore from the interpretation of experimental observations – both from the evolution of the fluid composition and the XRD-Rietveld analysis over the experimental time – for the selection of the reactive mineralogical assemblage. Certain modelling choices are discussed in more detail where required by the interpretation of the results.

In a carbonate-rich transitional caprock, the role of carbonate minerals – dominated by calcite and, to a lesser extent, dolomite and ankerite – remains central in governing the early geochemical responses to CO_2 ingress. Their strong sensitivity to variations in pCO_2 and their intrinsic capacity to buffer acidity generated by dissolved CO_2 make them key phases controlling chemical perturbations at the reservoir–caprock interface. When CO_2-charged fluids migrate upward into the caprock, the associated drop in pH initiates rapid calcite dissolution, which acts as the primary neutralizing mechanism due to calcite's high reactivity and fast dissolution kinetics. Dolomite and ankerite, although generally less reactive under these conditions, contribute progressively to this buffering capacity by uptake of Ca^{2+}, Mg^{2+}, and Fe^{2+} as fluid–rock interactions advance.

Modelled Ca, Mg, and Fe concentrations match the experiments only at 1 bar pCO_2, while simulations overestimate dissolved concentrations at 50 and 180 bar (Figure 6-16). As previously noted, measured pH values remain between 6.2 and 7 (Figure 6-17), far from the acidity expected under high -pCO_2 conditions. This persistent mismatch – likely caused by calcite precipitation induced by CO_2 degassing during sampling – prevents the experiments from reproducing true high CO_2 chemical conditions and limits validation of the geochemical models for carbonate-controlled species.

Within the carbonate-rich transitional caprock, aqueous Mg concentrations are controlled not only by dolomite but also by reactions involving illite, smectite, and chlorite. Dolomite precipitation regulates the Mg released through chlorite dissolution, whose kinetics are strongly pH dependent; however, the lack of reliable in-situ pH measurements prevents the extent of chlorite dissolution being accurately quantified. Modelling results show that the brine is oversaturated with respect to magnesite, and its precipitation would theoretically reduce the mismatch between measured and simulated Mg concentrations. However, such precipitation would involve significant magnesite precipitation by the end of the experiment, yet no magnesite was detected in XRD–Rietveld analyses. Its formation was therefore considered unrealistic and excluded from the conceptual model. In contrast, the >300% increase in dolomite precipitation predicted by the model aligns with XRD–Rietveld observations showing a marked rise in dolomite weight percent over time (PilotSTRATEGY Deliverable D2.9; Kilpatrick et al., 2025), supporting overall the validity of the conceptual model for magnesium-bearing phases in the transitional caprock.

The PilotSTRATEGY project has received funding from the European Union's Horizon 2020 research and innovation programme under grant agreement No. 101022664

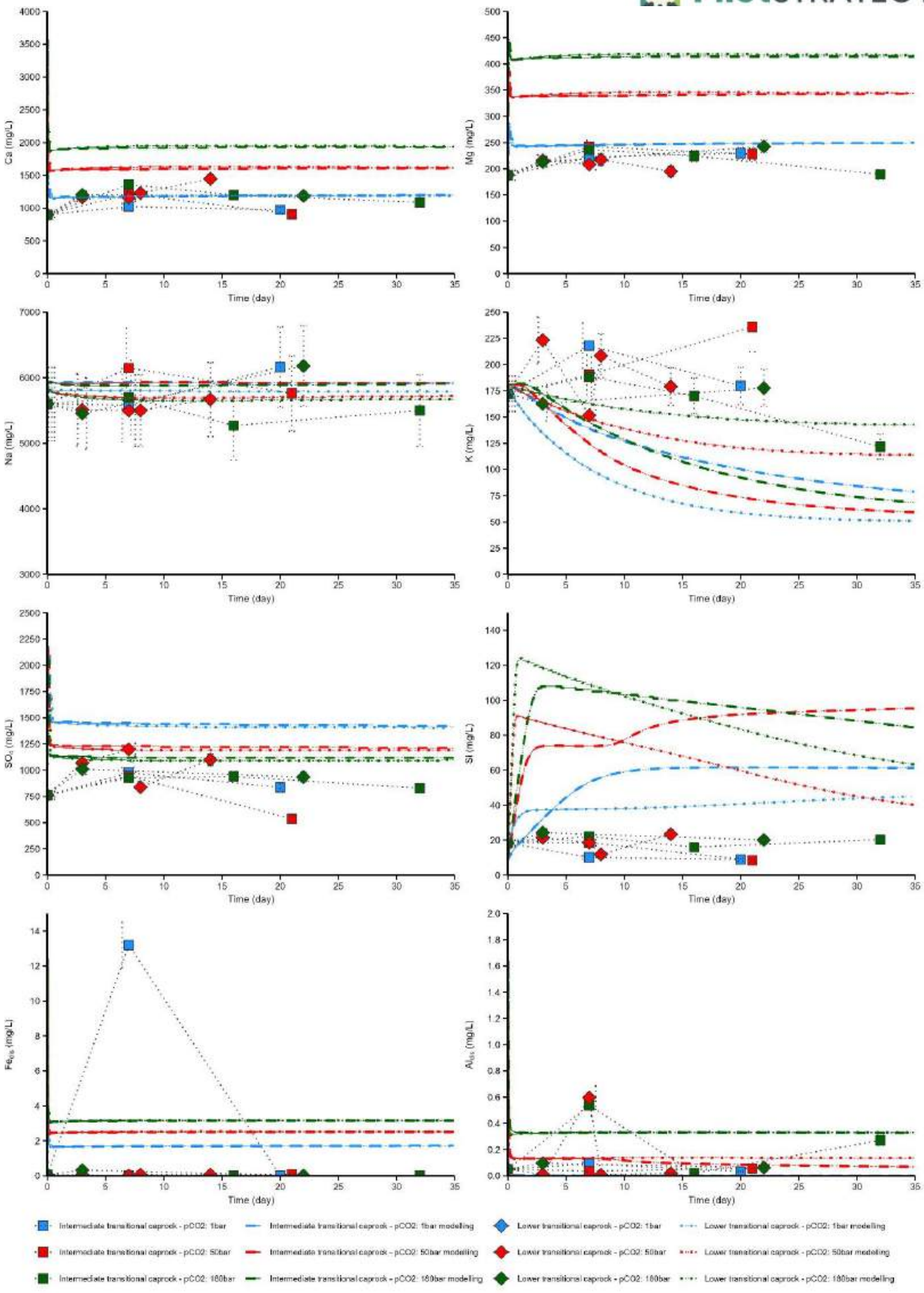

Figure 6-16: Modelled and measured fluid chemistry for the lower interval of the transitional caprock

The PilotSTRATEGY project has received funding from the European Union's Horizon 2020 research and innovation programme under grant agreement No. 101022664

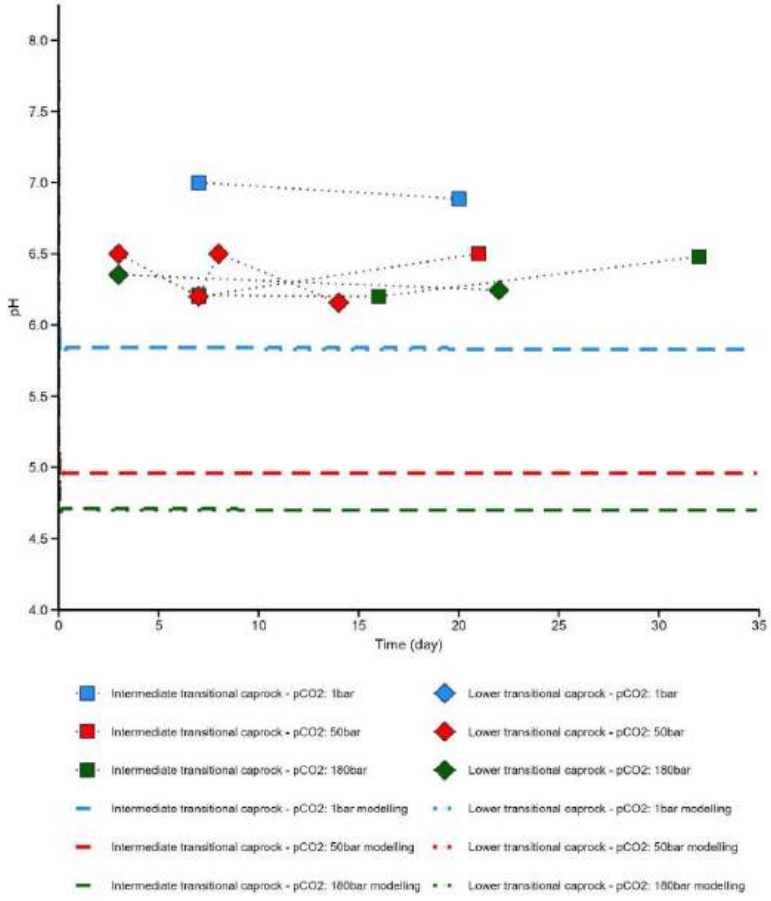

Figure 6-17: Modelled and measured pH of the fluid for the lower interval of the transitional caprock.

The modelled evolution of sodium, aluminum concentrations is broadly consistent with experimental observations (Figure 6-16). For Na, this agreement reflects its initially high concentration in the brine, the limited dissolution of plagioclase (albite), and the precipitation of interstratified illite/smectite (montmorillonite). The concentration of dissolved Al is influenced by multiple mineral phases. The Al concentration increases through the dissolution of chlorite, plagioclase, and K-feldspar, and is counterbalanced by the precipitation of illite, interstratified illite/smectite and kaolinite. The highest Al concentrations, measured mainly in the transitional caprock under the 180-bar pCO_2 condition, are relatively well reproduced by the numerical simulations (Figure 6-16).

In contrast, the model predicts a marked decrease in dissolved K driven by the dissolution of K-feldspar and the simultaneous precipitation of illite. Experimentally, however, this decreasing trend is observed only in a subset of samples and with a significantly lower magnitude than predicted. This discrepancy suggests that the geochemical model captures only part of the processes governing K mobility within the transitional caprock and that additional mineral–fluid interactions may need to be considered.

The silicon concentration measured experimentally remains extremely stable compared with the range predicted by the numerical models (Figure 6-16). The silica-bearing phases in the mineral assemblage include a wide set of minerals, encompassing both clay minerals and clastic silicates. The peak in dissolved Si predicted by the models during the first days of the experiment reflects the combined dissolution of K-feldspar, chlorite and – only for the intermediate transitional caprock –

The PilotSTRATEGY project has received funding from the European Union's Horizon 2020 research and innovation programme under grant agreement No. 101022664

plagioclase. As the solution gradually approaches equilibrium with respect to K-feldspar and plagioclase, its high undersaturation relative to chlorite leads to rapid and pronounced dissolution of this mineral – enhanced by the imposed pCO_2 – despite the slow kinetic constraints applied in the models. The absence of plagioclase in the intermediate transitional caprock further accentuates the disequilibrium of the fluid with respect to chlorite solubility, resulting in an even faster dissolution rate (Figure 6-16).

Once equilibrium with chlorite is reached, dissolved Si concentrations tend to stabilise in the 1-bar pCO_2 scenario, whereas in the 50- and 180-bar pCO_2 scenarios, the system evolves toward net Si uptake through the slow precipitation of clay minerals. An increase in dissolved Si is however predicted after approximately 10 days of simulation for the 50-bar pCO_2 scenario in the intermediate transitional caprock, resulting from dawsonite dissolution, which promotes enhanced chlorite dissolution.

Overall, these trends underscore the dominant role of chlorite dissolution as the main source of dissolved Si in the simulated conceptual model. However, XRD-Rietveld data show that the proportion of chlorite in the mineral assemblage varies considerably across samples and does not consistently indicate major dissolution of this phase (PilotSTRATEGY Deliverable D2.9; Kilpatrick et al., 2025). This suggests that a minor silicate phase, either present in low abundance and not detected by XRD-Rietveld or already occurring in the mineral assemblage, may also contribute to the evolution of Si in solution. In the conceptual model, quartz precipitation was not permitted, as Quartz precipitation requires very high nucleation energies, meaning that substantial supersaturation is often necessary before nucleation can effectively occur. Considering the high pressure and temperature conditions of the experiments, and that the fluid is supersaturated with respect to this mineral (saturation indices: +0.7), partial quartz precipitation is likely. The evolution of quartz proportions observed in the XRD-Rietveld analyses tends to support this interpretation over the duration of the experimental period (PilotSTRATEGY Deliverable D2.9; Kilpatrick et al., 2025).

Taken together, the comparison between experimental observations and numerical simulations highlights both the strengths and limitations of the conceptual model developed for the carbonate-rich transitional caprock. While several first-order trends—such as carbonate buffering, dolomite precipitation, and the behaviour of Na and Al—are reasonably reproduced, discrepancies persist for Ca, Mg, Fe, K, and Si under elevated pCO_2 conditions. These mismatches reflect uncertainties related to pH control, mineral-specific kinetics, and the potential role of minor or undetected silicate phases. Overall, the results show that although the model provides a coherent framework for interpreting CO_2-driven water–rock interactions, further refinement of the reactive mineral assemblage (e.g. role of quartz) and kinetic parameters (for chlorite) may be required to improve its predictive reliability.

6.4 Discussion

The combined numerical–experimental investigation provides valuable insights into the geochemical behaviour of the Dogger reservoir formations and overlying transitional caprock under CO_2-rich conditions. The modelling results consistently emphasize the central role of carbonate minerals – particularly calcite, with contribution of dolomite and ankerite – in regulating acidity generated by CO_2 dissolution. These phases govern the early fluid–rock interactions, undergoing rapid dissolution during pressurization and subsequently reprecipitating during heating and longer-term equilibration. This sequence reflects both their intrinsic reactivity and the capacity of carbonate-rich systems to buffer

The PilotSTRATEGY project has received funding from the European Union's Horizon 2020 research and innovation programme under grant agreement No. 101022664

pH perturbations. Accessory silicates and clay minerals further modulate these reactions, imparting formation-specific signatures to the geochemical evolution.

Taken together, the geochemical conceptual models indicate that, under elevated pCO_2 conditions, the reservoir sequence is dominated by the dissolution and subsequent (re)precipitation of carbonate minerals, the transformation of sulphate-bearing phases (gypsum–anhydrite), and the precipitation of kaolinite – where it forms part of the initial mineral assemblage. In contrast, the reactivity of the transitional caprock, whose initial brine is strongly out of thermodynamical equilibrium with the host minerals, is governed primarily by clay minerals (particularly chlorite, with additional contributions from illite and mixed-layer illite–smectite), along with carbonate phases – including the potential neoformation of dawsonite – and sulphate minerals. Together, these mineral groups exert the strongest control on the geochemical evolution of the transitional caprock within the simulated CO_2-rich environment.

Despite this conceptual consistency, several discrepancies between simulated and experimental results highlight limitations in the current modelling framework. Most notably, the expected increase in Ca, Mg, and Fe concentrations with rising pCO_2 is not observed experimentally. This discrepancy was assigned to post-sampling CO_2 degassing, which would promote rapid carbonate reprecipitation during or immediately after fluid recovery. As a result, only the 1-bar experiments, in which degassing effects are minimized, are satisfactorily reproduced by the numerical model. These observations underscore the sensitivity of carbonate equilibria to even minor sampling artefacts, complicating the validation of modelled reaction pathways.

Mineralogical uncertainties also arise from potential sample alteration during storage. The presence of gypsum, rather than the more thermodynamically stable anhydrite, likely reflects post-retrieval transformation rather than true reservoir mineralogy. While such alteration appears limited in extent for scenario controlled by equilibrium with respect to anhydrite (reprecipitation for elevated pCO_2), it may significantly bias the interpretation of experimental results. This illustrates the importance of sample quality and preservation when attempting to validate geochemical models from experimental results.

Trends for Na and Al concentrations are broadly consistent with simulations and reflect, for the latter, dissolution–precipitation processes involving kaolinite in the reservoir and albite, chlorite, illite, and interstratified clay minerals in the transitional caprock. However, the evolution of K and Si concentrations is partially or poorly captured. In the transitional caprock, the model predicts a marked decline in dissolved K due to illite precipitation, yet this signal appears only weakly in the experiments. Similarly, dissolved Si remains remarkably stable despite model predictions of early-stage increases linked to feldspar, chlorite, and plagioclase dissolution. These mismatches highlight gaps in the reactive mineral assemblage considered – particularly with respect to K- and Si-bearing phases – and reveal the challenge of simulating silicate dissolution kinetics at the short timescales of laboratory experiments. The potential involvement of minor or undetected silicate phases, as well as the exclusion of quartz precipitation despite thermodynamic supersaturation, may further contribute to these discrepancies.

Overall, the comparison between experimental observations and numerical simulations highlights both the strengths and limitations of the site-specific modelling approach. Accounting for the full mineralogical variability of the reservoir and transitional caprock improves the representativeness of the simulations and provides a coherent framework for interpreting CO_2-driven reactions. In the

The PilotSTRATEGY project has received funding from the European Union's Horizon 2020 research and innovation programme under grant agreement No. 101022664

Dogger reservoir, where calcite overwhelmingly dominates the mineral assemblage, the system responds rapidly and exhibits similar behaviour across all limestone formations for each imposed pCO_2 scenario. In contrast, the calcite-rich transitional caprock shows more heterogeneous responses, reflected in variable extents of mineral dissolution or precipitation and in differing timescales to reach equilibrium. This variability stems from the uneven distribution of accessory minerals – such as chlorite, illite, smectite, plagioclase, and minor silicates – which react at distinct rates and contribute differently to fluid–rock interactions. Consequently, spatial differences in mineral reactivity, reactive surface area, and kinetic sensitivity to pH and pCO_2 generate more complex geochemical pathways – i.e. not readily identifiable solely from experimental data – in the transitional caprock compared with the comparatively more uniform limestone reservoir formations.

Discrepancies in dissolved species, uncertainties in pH, and kinetic constraints all indicate that the model captures only part of the complexity of water–rock interactions under CO_2-rich conditions. Addressing these limitations will require refining reactive surface areas, accounting for *ex-situ* precipitation during sampling, and improving the representation of minor or kinetically slow phases. Despite these challenges, the study offers a strong foundation for anticipating the geochemical evolution of the Dogger system during CO_2 injection. It highlights the critical role of mineralogical heterogeneity, the need for careful experimental validation, and, last but not least, the value of integrating modelling and laboratory data to build realistic predictions of reservoir and caprock behaviour.

The PilotSTRATEGY project has received funding from the European Union's Horizon 2020 research and innovation programme under grant agreement No. 101022664

7. Conclusions

The modelled experiments highlighted the generally low levels of reactivity between the clastic rock samples and brines carrying dissolved CO_2. There was minimal dissolution of (alumino-)silicates and other minerals and little evidence for secondary precipitation to a degree which might have a meaningful impact on rock properties (i.e. porosity and permeability).

In the carbonate rocks, as may be expected, dissolution of primary carbonate minerals was observed, though with significant re-precipitation expected at an early and late stage in the French experiments – i.e. during temperature increase and final depressurisation, respectively.

In all cases modelling reliably predicted that the only reactions of significance on the timescale of the experiments were between the CO_2 saturated brine and the carbonate (where present) and gypsum (which is highly soluble regardless of pH) mineral phases. Thus, significant and rapid dissolution of the calcite present in the Spanish and Portuguese caprocks and the French samples was predicted, leading to large releases of Ca in the initial time-steps of all models. Notably all models overpredicted Ca release compared to that observed within the experiments. It may be that reactive surface area was more limited that assumed. Degassing of the reaction solutions shall have occurred during fluid sampling and probably contributed to discrepancies between experimental and modelled pH and calcium concentrations – the latter possibly due to calcite re-precipitation prior to the chemical analysis of the solutions.

In terms of the primary minerals in the clastic reservoirs, the match between modelled and experimental results are variable. Model results appear to accurately predict the gradual release of Al and K from the feldspar present in the Spanish reservoir sample, for example, while silica release was significantly underpredicted in this model and that of the Portuguese reservoir experiment. Similarly, for the models of the Spanish caprock and Portuguese reservoir rock, Al release matched relatively poorly to the measured results from the experiments. In the lower interval of the transitional caprock for the French site, then the models over-predict Mg but underpredict K concentrations.

The discrepancies between the modelled and measured results reflect issues common with the kinetic modelling of all mixed mineral bulk-rock systems. A major issue is a lack of understanding of mineral reactive surface areas within the system and how they change over the course of time. While assumptions can be made based on geometry (as in the case of the Portuguese modelling here) or likely bulk surface area (as for the French and Spanish models), in the case of mixed mineral systems, where different phases may have a wide range of specific surface areas, such approaches are unlikely to be particularly satisfactory. Hence, model assumptions produce a close approach to reality in some cases (e.g. Al and K release from feldspars in the case of the Spanish reservoir rock) but in others they may be wide of the mark (e.g. in accurately predicting Si release). As this work demonstrates, such discrepancies are also due to the compositional complexity of such systems, where mineral phases are almost never the pure end-members often as model assemblages and effects such as incongruent dissolution, adsorption and desorption processes and the reactivity of trace phases (e.g. dolomite) or impurities are very difficult to account for.

This work highlights the utility of geochemical modelling in the prediction of major reaction, both in terms of magnitude and direction, for mineral assemblages subject to conditions relevant to geological sequestration of CO_2, where rapid dissolution of carbonates and longer-term dissolution of some aluminosilicate phases were represented, with reasonable accuracy, within model outputs.

The PilotSTRATEGY project has received funding from the European Union's Horizon 2020 research and innovation programme under grant agreement No. 101022664

Care should be taken in extrapolating detailed results from modelling where, for example, simplifying assumptions on surface area or mineral composition may impact the results. Discrepancies in dissolved species, uncertainties in pH, and kinetic constraints all indicate that the models capture only part of the complexity of water–rock interactions under CO_2-rich conditions.

The PilotSTRATEGY project has received funding from the European Union's Horizon 2020 research and innovation programme under grant agreement No. 101022664

8. References

Kilpatrick, A., S. Stephant, S. Abad, F. Mathurin, P. Afonso, J. Mediatio, and P. Moita. 2025. Pilotstrategy Deliverable D2.9: Report of Geochemical Results for Three Areas. Pilotstrategy Project: H2020- Topic LC-SC3-NZE-6-2020 - RIA.

Lasaga, A.C. 1984. Chemical Kinetics of Water-Rock Interactions. *Journal of Geophysical Research* 89 (B6): 4009.

Marty, N.C.M., Claret, F., Lassin, A., Tremosa, J., Blanc, P., Madé, B., Giffaut, E., Cochepin, B., Tournassat, C., 2015. A database of dissolution and precipitation rates for clay-rocks minerals. Applied Geochemistry 55, 108–118. https://doi.org/10.1016/j.apgeochem.2014.10.012

Parkhurst, D.L., Appelo, C.A.J., 2013. Description of Input and Examples for PHREEQC Version 3—A Computer Program for Speciation, Batch-Reaction, One-Dimensional Transport, and Inverse Geochemical Calculations, in: Techniques and Methods 6–A43. U.S. Geological Survey, Denver, Colorado.

Blanc, P., Lassin, A., Piantone, P., Azaroual, M., Jacquemet, N., Fabbri, A., Gaucher, E.C., 2012. Thermoddem: A geochemical database focused on low temperature water/rock interactions and waste materials. Applied Geochemistry 27, 2107–2116. https://doi.org/10.1016/j.apgeochem.2012.06.002

Palandri, J.L., Kharaka, Y.K., 2004. A Compilation of Rate Parameters of Water-Mineral Interaction Kinetics for Application to Geochemical Modeling, REPORT (OF 2004-1068). U.S. GEOLOGICAL SURVEY, Menlo Park, California (USA).

Peng, D.-Y., Robinson, D.B., 1976. A New Two-Constant Equation of State. Industrial & Engineering Chemistry Fundamentals 15, 59–64. https://doi.org/10.1021/i160057a011

Pham, V.T.H., Lu, P., Aagaard, P., Zhu, C., Hellevang, H., 2011. On the potential of CO2–water–rock interactions for CO2 storage using a modified kinetic model. International Journal of Greenhouse Gas Control 5, 1002–1015. https://doi.org/10.1016/j.ijggc.2010.12.002

Xu, T., Sonnenthal, E., Spycher, N., Pruess, K., 2006. TOUGHREACT—A simulation program for non-isothermal multiphase reactive geochemical transport in variably saturated geologic media: Applications to geothermal injectivity and CO2 geological sequestration. Computers & Geosciences 32, 145–165. https://doi.org/10.1016/j.cageo.2005.06.014

The PilotSTRATEGY project has received funding from the European Union's Horizon 2020 research and innovation programme under grant agreement No. 101022664